ISBN 978-82-326-5728-5 (printed ver.)
ISBN 978-82-326-6386-6 (electronic ver.)
ISSN 1503-8181 (printed ver.)
ISSN 2703-8084 (electronic ver.)

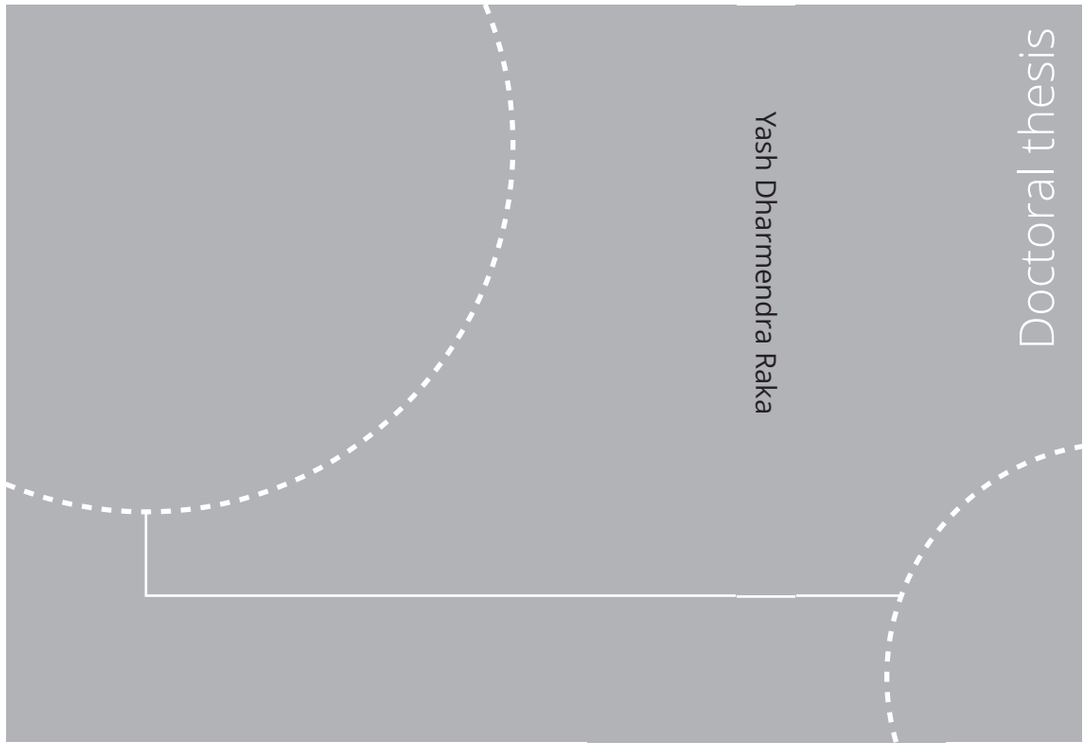

Doctoral theses at NTNU, 2021:169

Yash Dharmendra Raka

Waste heat to Hydrogen using Reverse Electrodialysis

NTNU
Norwegian University of Science and Technology
Thesis for the degree of Philosophiae Doctor
Faculty of Engineering
Department of Energy and Process Engineering

NTNU
Norwegian University of Science and Technology

Doctoral theses at NTNU, 2021:169

NTNU

NTNU
Norwegian University of Science and Technology

Yash Dharmendra Raka

Waste heat to Hydrogen using Reverse Electrodialysis

Thesis for the degree of Philosophiae Doctor

Trondheim, May 2021

Norwegian University of Science and Technology
Faculty of Engineering
Department of Energy and Process Engineering

NTNU
Norwegian University of
Science and Technology

NTNU
Norwegian University of Science and Technology

Thesis for the degree of Philosophiae Doctor

Faculty of Engineering
Department of Energy and Process Engineering

ISBN 978-82-326-5728-5 (printed ver.)
ISBN 978-82-326-6386-6 (electronic ver.)
ISSN 1503-8181 (printed ver.)
ISSN 2703-8084 (electronic ver.)

Doctoral theses at NTNU, 22021:169

Printed by Skipnes Kommunikasjon AS

Acknowledgement

The research work was carried out at the RED-ED lab at the Department of Energy and Process Engineering from 2017 to 2020. I want to thank NTNU and ENERSENSE for financial support during this period.

I want to thank my supervisor Prof.Odne Stokke Burheim, for giving me an opportunity to work on an exciting topic and his scientific feedback, especially during the experiments. His multi-faceted and pedagogical approach made me contemplate ideas and grow as an independent researcher. I want to thank Assoc. Prof. Håvard Karoliussen for his guidance on the electrochemical theory and experiments and his eye for detail. I want to thank Assoc.Prof. Kristian Myklebust Lien for instigating an industrial point of view and shared practical examples/facts that helped me develop the techno-economic study. Although I did not publish the work, I want to extend my thanks to Prof. Olivier Bernard. His significant help in creating a multi-objective memetic algorithm.

I want to thank Dr Kjersti Wergeland Krakhella for helping me settle in Trondheim with experiments and brainstorming sessions. I want to thank Dr Robert Bock for his contribution to writing articles that lifted the quality of the articles, conclusive discussions on theory and help during experiments. Simon Birger Byremo Solberg, I want to thank you for supporting me with permselectivity investigations and assisting in irreversible thermodynamics derivations. Pauline Zimmermann, I want to thank you for your help with RED stack measurements. Discussions with you and Önders Tekinalp were always instigating. I want to give special thanks to Bjørn Volseth for his help in realising the experimental setups and all the lab activities. My research would not be complete if not for students Asle Handro Nybakk, Hammad Farooq, Martin Nord Flote and Michael Aaron Fried on ASPEN HYSYS/Plus modelling, permselectivity and membrane resistance measurements. The questions raised by you all helped me develop a better understanding of the topics.

I want to thank my colleagues Alaa, Ailo, Asanthi, Astrid, Behnam, Ebrahim, Ellen, Eline, Faranak, Felix, Hujjatul, Ian, Ida, Jacob, Jakub, Koteswara, Lena, Markus, Marjorie, Silje, Zohreh for all the small talks, coffee breaks and social gatherings. It helped my stay be fun and engaging. I also want to thank all the social groups and friends in Trondheim and other places worldwide for philosophical discussions, sports and social gatherings. It helped me take my mind off during stressful times.

My sincere and most profound thanks to my family mother- Ujwala, sister- Shreya and father- Dharmendra for their never-ending support and love.

Prose

What is Truth?

What we see, listen or say is that true? Are their meanings true?
What is this thing whose search has bothered and divided many philosophers?

When I see, there are many aspects,
When I listen there are many stories,
When I say, there are many questions.

If I want to know, where shall I search, what can I do, how can I understand, what are the methods?
If I think the truth is in-depth, then the conclusion is influenced by it.
If I think the truth is in the diversity, then I get lost in its turbulence.

Why is the truth so complex?
What can I do that I understand? That I can use it, that I use it as a basis to lead my life.

We are surrounded by talks, confused in thoughts, influenced by stories.
We are sinking in the external gratification, in the misunderstandings.
We believe in something, devote ourselves to someone and create truth.
It is true to us and those who resonate with it.

Many people, with many thoughts,
Many thoughts with many meanings,
Many meanings have many bases,
Many bases have many associated experiences,
Many experiences influence by circumstances,
One's intelligence and surroundings influence these circumstances.
If I believe this is true, then what is false?

We live in a constantly changing environment.
When I feel I understand, I get tangled with my reference, what to trust and what to believe.
When I get calm, I understand that this is a matter of time; only age can resolve this.

If I assume this as truth, then life is like a search; this search has many ideologies, which has many perspectives, many perspectives have many conclusions that change with time.
In the end, these are our choices, every choice has a consequence, and these consequences make us.
I have been entangled with my choices, and three years have passed by, and the search for my truth continues.

Abstract

In current times the research across the globe is focused on carbon-free energy sources that can drive the economy in future. One of the promising ways to achieve this is to have demand-based sustainable energy storage powered by renewable energy sources. The use of excess renewable energy to produce chemicals or storing energy in the form of chemicals is the point of focus. This shows that we are transitioning towards power to chemical-based future energy system. Hydrogen is one such chemical. However, renewable energy sources such as solar and wind are intermittent. Sectors such as chemical industries, transportation are found to have potential. More than 40% of the total industrial energy use is being wasted by dumping it in the surrounding. We propose a salinity gradient-based energy system known as Reverse electrodialysis (RED) to solve these problems. Here, the driving force is concentration difference across an ion exchange membrane that causes a flow of ions in a specific direction. This flux of ions can be converted either into electrical current or produce gas such as hydrogen depending on the appropriate choice of electrode-electrolyte system. The RED system does not produce any toxic waste when in operation; it can be up-scaled to Mega-Watts size. Closed-loop RED systems use Mechanical or thermal energy to reuse the solutions exiting from the system. This heat can be at a temperature lower than 373 K. Thus leading to a stand-alone system independent of the geographical constraints for the source of the feed solutions.

A thermolytic salt- ammonium bicarbonate can use the low-grade waste heat (less than 373 K) to restore the concentration to initial. A thermodynamic model developed provides insight into the different parameters such as operating conditions- concentration of feed solutions, temperature; system parameters such as inter-membrane distance or channel thickness; residence time of feed solutions in the RED stack; and membrane properties such as permselectivity and area-specific membrane resistance. The system's performance is evaluated based on hydrogen production rate normalised over membrane area, waste heat required to produce unit kilograms of hydrogen and cost incurred to produce one kilogram of hydrogen if the system is to be operated for 20 years levelised cost of hydrogen (LCH).

The concentration of concentrate solution increases the hydrogen production rate and reduces the levelised cost of hydrogen. The theoretical maximum concentration of concentrate solution is 2.6 M, whereas, in practice, it is 2 M at room temperature. There is an optimal dilute solution concentration; any deviation decreases the hydrogen production rate and increases the levelised cost of hydrogen. However, with the increase in the concentration of feed solutions, the waste heat required to restore the concentration increases. This increase in the waste heat required increases the levelised cost of hydrogen. Hence to achieve low LCH, there is an optimum value of dilute solution concentration. This optimum was found to be $\pm$ 0.1 M. The increase in operating temperature increases the open circuit potential, increases ionic mobility, i.e. solution conductivity and thus the hydrogen production and lowers the LCH.

Assuming negligible resistance due to the electrical double layer and diffusion boundary layer, the increase in the inter-membrane distance or channel thickness decrease the hydrogen production rate due to increased channel ohmic resistance. The increase in the inter-membrane distance decreases waste heat required per unit volume due to the reduced salt flux through the membrane but increases the total waste heat required due to the increased amount of volume flowing through the channel. An increase in residence time decreases pressure drop and thus the pumping power required. The amount of salt diffusing through the membrane increases, which increases the waste heat per unit volume. However, as the volume flow rate decreases, the total heat required to restore the concentrations decreases.

The economic study suggests that in the present scenario, capital expenses (CAPEX) and waste heat required contributes to more than 75% of the LCH. Regeneration system and membranes contribute more than 80% to the CAPEX. Hence it is essential to optimise regeneration system and membranes to achieve market competitive LCH. In the present and future scenario for a euro increase in the membrane cost, the LCH increases by 0.055 and 0.01 € $kg_{H_2}^{-1}$. And for a 0.001 € kWh^{-1} increase in the cost of waste heat, the LCH increases by 4.02 and 1.78 € $kg_{H_2}^{-1}$.

Membrane properties such as permselectivity and membrane resistance of ten commercial membranes were studied. In general, the anion exchange membranes (AEM) showed lower conductivity at different concentration and elevated temperatures when compared to the cation exchange membrane (CEM). The membranes with high conductivity (CMF- CEM; APS-AEM) and low area-specific membrane resistance (CSO- CEM; FAS- AEM) were compared based on hydrogen production rate, specific waste heat required, energy efficiency and LCH. The highest performance was achieved with a stack made of FAS and CSO, producing hydrogen at $8.48 \cdot 10^{-7}$ kg $m_{mem}^{-2} s^{-1}$ with a waste heat requirement of 344 kWh kg^{-1} hydrogen. This yielded an operating energy efficiency of 9.7% and a levelised cost of 7.80 € $kg_{H_2}^{-1}$. Permselectivity of the best performing membranes was studied at different concentrations; the AEM- FAS had lower permselectivity values than CEM- CSO. The concentration of ammonium bicarbonate solutions in the salt bridge influences the junction potential measurements without any clear trend. The estimated values for hydrogen production rate, thermodynamic efficiency, specific waste heat and the levelised cost of hydrogen for RED stack with CSO/FAS are $8.05 \cdot 10^{-7}$ kg $m^{-2} s^{-1}$, 9.1%, 365.87 kWh $kg_{H_2}^{-1}$, 10.132 € kg^{-1} H_2 respectively. Finally, membrane area-specific resistance lower than $1 \cdot 10^{-4}$ Ωm^{-2} and permselectivity higher than 0.9 at membrane cost lower than 10 € m^{-2} and waste heat cost of 0.005 € kWh^{-1} will make ammonium bicarbonate RED competitive with the current renewable source-based hydrogen-producing technologies.

List of publications

The following publications are included in this thesis:

(I) "**Opportunities and challenges for thermally driven hydrogen production using reverse electrodialysis system**",

Y D. Raka, H Karoliussen, K M. Lien and O S. Burheim

Journal of International Hydrogen Energy, 2020.

Y Raka: Developed the thermodynamic and economic model, analysed the results, presented it in graphical form. Wrote the manuscript with contributions from weekly supervision meetings.
H Karoliussen, K M. Lien and O.S. Burheim: Contributed to the idea of economic study, formulated concept of combining low-grade waste heat with Ammonium bicarbonate RED system as heat engine, contributed with scientific feedback, proofreading and manuscript development.

(II) "**Low-Grade Waste Heat to Hydrogen**"

Y D. Raka, R Bock, J J. Lamb, B G. Pollet and O S. Burheim,

Micro-optics and energy: sensors for energy devices.

Y Raka: Developed the model, analysed the results, presented it in graphical form and wrote the manuscript with contributions from weekly supervision meetings.
R Bock: Contributed to discussions of the modelling, editing and proofreading the manuscript.
J Lamb: Contributed to editing and proofreading the manuscript.
B Pollet: Contributed to proofreading the manuscript.
O Burheim: Formulate the idea of combining low-grade waste heat with Ammonium bicarbonate RED as heat engine and had supervisory meetings for discussion, and. Contributed with scientific feedback.

(III) "**The Influence of Concentration and Temperature on the Membrane Resistance of Ion Exchange Membranes and the Levelised Cost of Hydrogen from Reverse Electrodialysis with Ammonium Bicarbonate**".

Y D. Raka, R Bock, Ø Wilhelmsen, H Karoliussen, and O S. Burheim

Membranes, 2021

Y D. Raka: Measured membrane resistance, developed the model, analysed the results, presented it in graphical form and written the manuscript with contributions from supervisors.
Robert Bock: Contributed to discussions of the results, editing and proofreading the manuscript.
Ø Wilhelmsen: Contributed to editing and proofreading of manuscript.

Odne Stokke Burheim: Provided guidance in analysis of results and scientific feedback.

(IV) "**Permselectivity of IEMs for ammonium bicarbonate- influence of junction potentials and influence of permselectivity on the levelised cost of hydrogen**"
Y D. Raka, S B B Solberg, R Bock, Ø Wilhelmsen, H Karoliussen, and O S. Burheim
Manuscript
Y D. Raka: Measured measured membrane potential, analysed the results, estimated the permselectivity, presented it in graphical form and has written the manuscript with contributions from colleagues and supervisors.
S B B Solberg: Developed the non-equilibrium thermodynamic model for permselectivity, discussions of the results, and helped in experiments.
Robert Bock: Contributed to discussions of the results and proofreading the manuscript.
Ø Wilhelmsen: Contributed to development of non-equilibrium thermodynamic model for permselectivity, discussions of the results, editing and proofreading of manuscript.
H Karoliussen: Theoretical and experimental relevance of junction potentials.
Odne Stokke Burheim: Provided guidance in the experimental procedure, analysis of results and scientific feedback.

Contents

List of Abbreviations

AEM	Anion exchange membrane
CAPEX	Capital expenses
CCS	Carbon capture and storage
CEM	Cation exchange membrane
CG	Coal gasification
CPE	Constant phase element
CV	Cyclic voltammetry
DJE	Double junction electrode
Don	Donnan potential
ED	Electrodialysis
EIS	Electrochemical impedance spectroscopy
GHG	Green house gases
HER	Hydrogen evolution reaction
IEA	International energy agency
IEC	Ion exchange capacity
IEM	Ion exchange membrane
LCA	Life-cycle analysis
LCH	Levelised cost of hydrogen
LCoE	Levelised cost of energy
LJP	Liquid junction potential
OER	Oxygen evolution reaction
OCV	Open-circuit voltage
OPEX	Operation and maintenance expenses

RED	Reverse electrodialysis
SJE	Single junction electrode
SD	Swelling degree
SGE	Salinity gradient energy
SHE	Standard hydrogen electrode
SMR	Steam methane reforming

Part I

Thesis

This part is divided into five chapters. The first chapter gives an introduction to future energy systems with hydrogen as one of the sources. It also provides a brief explanation of waste heat potential and how a closed-loop reverse electrodialysis system can utilise it to produce hydrogen. The aim of the research and research questions are also described in the chapter. The second chapter elaborates on the theory and principles of reverse electrodialysis. The third chapter gives a brief on the methodology used to conduct the research and then summarises results, an overall conclusion and a few suggestions for further work. It should be noted that most of the information provided in this part is given in the papers.

1 Introduction

This chapter encapsulates the motivation to carry out the research followed by the research work's aim, divided into four research questions that focus on the complexity and specific feasible tasks.

1.1 Decarbonising industry with green hydrogen

According to the International energy agency (IEA), supplying hydrogen to industrial users is now a significant business worldwide where the demand for hydrogen has grown more than threefold since 1975 and continues to rise [1]. In 2019, the demand for pure hydrogen was 70 million tons (Mt). According to the recent study by Hydrogen Council, 18% of the global energy demand (equal to 78 EJ) can be supplied by hydrogen in 2050 [2]. Hydrogen is a critical chain between hydrogen consuming industries such as ammonia and ethanol production plants and some crucial sectors such as electricity grid, gas grid, transportation, residential, agriculture and energy storage as shown in Figure 1.1[3]. Hydrogen can be efficiently converted into electricity [4], [5].

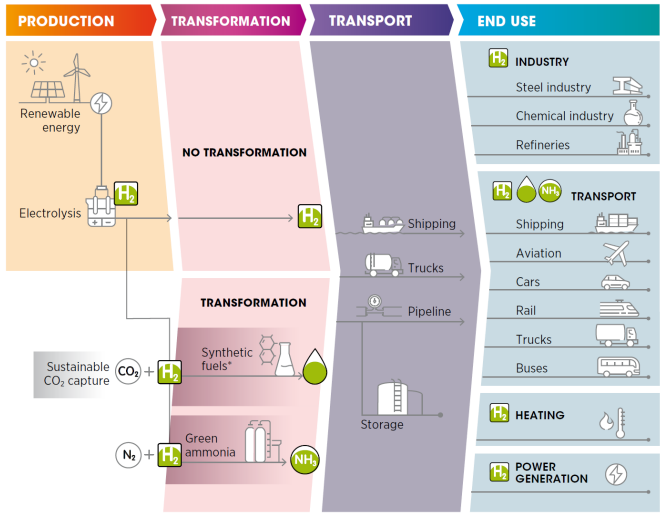

Fig. 1.1: Green hydrogen production, conversion and end uses across the energy system [6]

Hydrogen can be produced from renewable materials such as biomass and water. A significant portion is supplied from fossil fuels, with 6% from global natural gas and 2% from global

coal going to hydrogen production [1]. The only 0.3% of by-product hydrogen or around 5% of total hydrogen produced is coming from renewable sources [1], [6]. This has resulted in CO_2 emissions of around 830 million tonnes from the production of hydrogen. This is equivalent to the CO_2 emissions of the United Kingdom and Indonesia combined [1]. In energy terms, the total annual hydrogen demand worldwide is around 330 million tonnes of oil equivalent (Mtoe), more significant than Germany's primary energy supply. According to the energy technology prospective report of IEA in 2015, to limit the increase of global temperature within 2 K, CO_2 emissions related to energy and industrial processes should be decreased by approximately 60% [1].

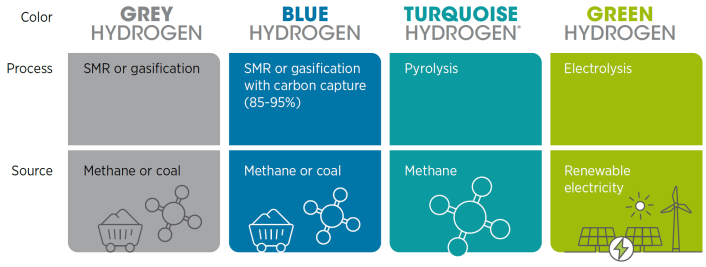

Fig. 1.2: Different shades of hydrogen based on their source or method of production[6]

Some solutions for reducing environmental impacts are carbon capture and storage (CCS), chemical looping carbon capture [7], [8]. As hydrogen produced via different routes have different CO_2 emissions, referring to the method with a colour code is now a nomenclature as shown in Figure 1.2. Although carbon capture can save environmental cost, it cannot be a long-term solution for sustainable development in energy. One of the alternatives for carbon-free sources is hydrogen production from renewable energy sources and can be considered one of the sustainable solutions to climate change. Some key strategies recommended by IEA for scaling up of hydrogen economy is that adequate solutions are required to overcome investment risks of the new customers, and further development and commercialisation studies are required for better cost-effectiveness.

1.2 Waste heat from industries as energy source

In general, 'industrial waste heat' can be regarded as the energy generated in industrial processes but not put into any practical use. This energy is lost, wasted or dumped into the environment. Waste heat from industries on a global scale amounts for more than 40% of the total energy use [9]. The industrial waste heat potential in the EU has been estimated to be 304 TWh per year [10]. Utilising this waste heat provides economic and environmental benefits as in 2013, it was estimated about 370 million USD for reducing carbon dioxide equivalent emissions from waste heat from industries in the UK [11]. The EU addressed this issue with a policy that recommends reducing greenhouse gases (GHG) emissions by 40% and improving energy efficiency by 27% in the transportation and industrial sectors by 2030. Also, hydrogen in the transportation sector was identified as an alternative solution that caters to energy efficiency and CO_2 emissions.

The quality of waste heat depends on its temperature, and the selection of suitable waste heat recovery technology depends on the quality or grade of waste heat. The high-grade waste heat of temperature above 373 K has been reused within the processes and across industries. The most waste heat of less than 373 K is still discarded into the atmosphere [12], [13]. A part of the waste heat cannot be tapped due to the second law of thermodynamics; the recovery yield of extractable waste heat depends primarily on the system design and operation. A considerable amount of low-grade waste heat (temperatures between 373 K and 323 K) is available worldwide, for example, 833 TWh yr^{-1} in the USA [14]. However, this heat cannot be reintegrated entirely on-site or be used for district heating. Some of the few technologies that operate below 373 K to utilise this energy are Organic Rankine Cycle (ORC) and thermoelectric generators. ORC has an intrinsic limitation of efficiency where the efficient operating temperature range for the power plants using this cycle is above 373 K [15]. Further, disadvantages of using ORC is environmentally harmful refrigerants (in some cases) and limitations of downsizing [15]. While the thermo-electrochemical cell has no moving part, they suffer from low thermal efficiency or low power production [16], [17]. From the second law of thermodynamics, any energy converter that operates between two temperatures cannot exceed Carnot efficiency η_c given as,

$$\eta_c = 1 - \frac{T_c}{T_h}$$

T_c, T_h are sink and source at low temperature and high temperature. This means that maximum energy conversion efficiency cannot exceed 7% for a heat engine operating between 293 and 313 K.

1.3 Aim of the study

To date, none of the thermoelectric conversion technologies utilising low-grade waste heat has demonstrated conversion of heat to hydrogen at temperatures below 373 K with efficiencies and costs adhering to industrial standards. We propose an energy-efficient ammonium bicarbonate reverse electrodialysis (AmB RED) system that utilises the low-grade waste heat (333 K - 413 K) to produce hydrogen. Reverse electrodialysis (RED) stack is an electrochemical device that converts chemical energy into electrical energy or chemical energy in the form of H_2 gas using a concentration gradient across an ion-selective membrane. RED is one of the few renewable technologies which is capable of directly producing hydrogen from waste heat. This study aims to perform a feasibility study of a thermally driven ammonium bicarbonate based reverse electrodialysis system for hydrogen production. This study is divided into four parts based on the following research questions,

1. Assuming that the technology is ready for commercialisation, what are the critical economic parameters that limit the diffusion of the thermally driven AmB RED hydrogen producing system and what are specific values of the economic driver that will make this technology market competitive and minimum cost of per Kg of hydrogen produced one can achieve?

2. What factors influence the technical feasibility of hydrogen production from the thermally driven AmB RED system, and how these parameters affect the cost of hydrogen produced?

3. It was found from the previous studies that membranes play a crucial role in the techno-economic feasibility of the system. However, there is a little investigation done in studying the influence of operating conditions such as concentration and temperature on the membrane resistance for ammonium bicarbonate solution. How do the concentration and temperature affect the membrane conductivity of 10 commercial ion-exchange membranes, affecting the hydrogen production rate and the cost of producing hydrogen?

4. In the literature, there are very few studies on membrane permselectivity measurement for ammonium bicarbonate salt. However, these measurements suffer from junction potential and require tedious corrections and may not necessarily be exact. Can a method be developed to measure the permselectivity of IEM soaked in ammonium bicarbonate solution? What experimental factors influences this measurement? Can a theoretical model be developed to estimate permselectivity?

2 Background

This chapter outlines the theoretical information on reverse electrodialysis (RED), its components such as salt solution, ion exchange membranes, thermodynamics of salinity gradient-based processes, salt solutions and membrane transport processes. Further, it summarises relevant research in ammonium bicarbonate based reverse electrodialysis (AmB RED) systems, hydrogen-producing RED systems, and thermally driven RED systems. This is followed by gaps in the present literature that has led to this research.

2.1 Reverse electrodialysis (RED)

Salinity gradient-based energy system (SGE), also known as 'Blue Energy', is generated by converting the chemical potential difference between two salt solutions with different concentrations into electrical, chemical or mechanical energy [18], [19]. Reverse electrodialysis (RED) is one such technology. RED is a membrane-based technology that can directly convert chemical potential into electricity or gas evolution by controlling the mixing of two different salinity solutions with ion-exchange membranes (IEM). A RED stack, as shown in the figure 2.1 consists of two electrodes together with alternately stacked anion exchange membrane (AEM) and cation exchange membrane (CEM) separated by spacers. These spacers are sealed with gaskets to avoid leakage. When high concentration solution (HC) and low concentration solution (LC) are fed into the stack, cations in the HC will migrate through the CEMs while anions migrate through the AEMs into LC due to the concentration gradient. This creates a flux of ions in either direction. This ionic flux is converted into either an electronic flux or gas evolution at the electrodes in the electrode rinse compartment via redox reactions. Thus generating electric current supplying an external load or producing gas.

RED is a sustainable energy source with no toxic gas emissions when in operation, and river and seawater are feed solutions (chlorine gas evolution may take place). It has unlimited access to fuel supply in the vicinity of the sites where sea and river water meet. The potential power released by mixing seawater and river water, which has an estimated maximum global potential of 2 TW [19]. Although the gross global potential energy from such resource is estimated to be more than 27 PWh yr^{-1}, the extractable part of which is approximately 2 PWh yr^{-1} [20]. This is more than 10% of the total global potential of renewable energy resources [20]. Also, considering that the energy requirement of electrolysers between 53-70 kWh kg^{-1}, efficient utilisation of the available SGE would produce up to 38 Mt yr^{-1} of hydrogen [21]. These estimates depend on factors, such as salinity levels, flow rate, temperature, efficiency, fouling behaviour, ecological and legal constraints [20]. The accessibility to these natural resources limits its locational options. There is only one pilot-scale installation - 50 kW at Afsluitdijk in the northern province of the Netherlands, to the

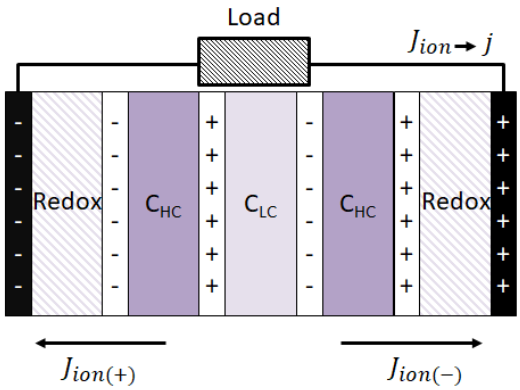

Fig. 2.1: Schematic is showing the working principle of reverse electrodialysis (RED). The $J_{(ion)}$ are the ionic fluxes that are converted into electric current (j) by redox couple and electrodes (denoted by '+' or '-' signs) at the end. At one end, reduction and at the other oxidation occurs, thus maintaining the electroneutrality. The electrical circuit is completed by connecting electrodes to an external load.

best of our knowledge. One of the barriers to commercialising RED systems is the high maintenance cost of the IEMs, which need to be replaced with new ones or recovered when affected by different types of fouling. These disadvantages can be overcome by using an artificial saline solution that ensures the availability of large amounts of Gibbs free energy of mixing, low energy consumption in the regeneration unit to restore the original concentration levels of feed solutions, and utilising waste heat at low temperature. The different salinity solutions provide a driving force by separating the increased solute from the diluted side and reintroducing it in the concentrated side without any fresh solution supply. The closed-loop system mitigates the geographical limitations since there is no need for a continuous supply of fresh seawater and river water, thus preventing the danger of membrane fouling and saving pre-treatment costs. Novel SGE applications based on closed-loop systems using excess waste heat could also enable the utilisation of 304 TWh yr^{-1} [10]. In contrast to intermittent wind and solar energy sources, SGE can be exploited continuously 24 h per day and 365 days a year. Recently it was demonstrated that reverse electrodialysis could be used to harness as the voltage source needed to enable hydrogen gas production [22]. In a RED system, with seawater and river water as feed solutions that are pumped between the membranes in a stack that can contain $\sim$ 20 or more membrane pairs can generate a potential $\sim$ 0.1 to 0.2 V per membrane pair that is sufficient to split water [22]–[24].

2.1.1 Thermodynamic potential of salinity gradients

The Gibbs free energy is defined as,

$$G = \sum_i \mu_i n_i \tag{2.1}$$

where n is the number of moles of each component, expressed in terms of molar concentration c (mol m^{-3}) and total volume V [m^3] as,

$$n_i = c_i V \tag{2.2}$$

The Gibbs energy of mixing (ΔG_{mix}) is released when two solutions of different salinity are mixed. For the i-th component in a solution, the chemical potential μ_i [J mol^{-1}], i.e. its partial molar Gibbs energy, is defined as

$$\mu_i = \mu_i^o + v_i \Delta p + |z_i| F \Delta\varphi + RT\, ln\gamma_i x_i \tag{2.3}$$

where v is the partial molar volume [$m^3 mol^{-1}$], Δp the pressure difference [Pa], z the valence [equiv.mol^{-1}], F the Faraday constant [96,485 C $equiv.^{-1}$], $\Delta\varphi$ the electrical potential difference [V], R the gas constant [8.314 J $mol^{-1}K^{-1}$], T the absolute temperature [K], γ the activity coefficient and x is the mole fraction. In a system with constant pressure and in the absence of an electrical field, equation 2.3 simplifies to:

$$\mu_i = \mu_i^o + RT\, ln\gamma_i x_i \tag{2.4}$$

Therefore, ΔG_{SGE} is calculated from the difference between the Gibbs free energy of the mixed solution (G_{mix} and the Gibbs free energy of the initial solutions (G_c and G_d) with subscripts 'c', 'd' and 'mix' referring to the concentrate solution, dilute solution, and to the mixed salt at the outlet,

$$\Delta G_{SGE} = G_{mix} - (G_c + G_d) \tag{2.5}$$

$$\Delta G_{SGE} = RT \sum_i \left\{ [c_i ln(\gamma_i c_i)]_{mix} - \left[\left(\frac{1-f}{f}\right) c_i ln(\gamma_i c_i)\right]_c - \left[\left(\frac{1}{f}\right) c_i ln(\gamma_i c_i)\right]_d \right\} \tag{2.6}$$

where f is the volume fraction of dilute feed solution to the total feed solution.

2.1.2 Thermodynamics of electrolytic solutions

The chemical compounds that are dissociated into ions in solid, liquid or dissolved form are called electrolytes. An electrolyte, when in contact with a polar solvent such as water, a solvation process occurs. The solvent molecules, dipoles, interact with the ions, orienting themselves in the direction of the electric field and reducing the electrostatic force of the electrolyte lattice. The solvation process causes the electrolyte to separate into cations, and anions uniformly disperse in the solvent. With the increase in solute concentration, these ion-ion and ion-solvent interactions influence the behaviour of the solvent and solute in an electrolyte solution resulting in a deviation from the ideal case. The means of activity coefficients for ions and solvent accounts for these deviations thermodynamically. The chemical potential of individual ionic species,μ_i, is given by,

$$\mu_i = \mu_i^o + RT\, ln\, a_i \tag{2.7}$$

where μ_i^o is the chemical potential of the i^{th} ion in the standard state, [J mol^{-1}], a_i is the activity of the i^{th} ion in the solution, T is the absolute temperature, [K], and R is the

universal gas constant, [J mol^{-1}K^{-1}]. Thus, the chemical potential for a generic electrolyte (MX) is given by:

$$\mu_{MX} = \mu^o_{MX} + \nu\, RT\, ln(m_{\pm}\gamma_{\pm}) \tag{2.8}$$

It is not strictly possible to measure individual ion activity coefficients with exact thermodynamic measurements. Moreover, the assumptions for individual ion activity are debatable. Hence, we use the mean ion activity $\gamma_{\pm} = (\gamma_+ \cdot \gamma_-)^{\frac{1}{\nu_{\pm}}}$, where mean stoichiometric coefficient $\nu_{\pm}$ is sum of individual ion stoichiometric coefficient ν_+ and ν_-. The μ^o_{MX} is a combination of the chemical potentials of the two ions in the standard state, [J mol^{-1}], ν is the number of ions generated by the complete dissociation of the salt, $m_{\pm}$, [mol kg^{-1}] and $\gamma_{\pm}$ are the geometric averages of molality and activity coefficient of the two ions in the case of monovalent salts. The reference state for the solute is that of infinite dilution in the solvent, i.e. $\gamma_{\pm} \rightarrow 1$ as $m_{\pm} \rightarrow 0$. For a solvent, the chemical potential is defined as,

$$\mu_s = \mu^o_s + RT\, ln\,(a_s) \tag{2.9}$$

in which a_s is the solvent activity and μ^o_s is the solvent chemical potential in the standard state, [J mol^{-1}]. For the solvent, the normal reference state is used, i.e. that of the pure liquid at the same temperature and pressure of the mixture. Assuming the pressure effects are negligible and therefore neglecting Poynting correction factors. The solvent activity in electrolyte solutions is given by the ratio of the solution fugacity (f_s) [bar] and pure water fugacity (f^o_s) [bar] at the saturation temperature. This relation links the measurable properties such as vapour pressure to the activity of the solvent and the osmotic coefficient Φ, which in turn characterises the deviation of a solvent from ideal behaviour. The following expression gives the relation between the osmotic coefficient and the activity coefficient,

$$\Phi = \frac{-1000 \ln\, a_s}{mw_s \sum_i \nu_i m_i} \tag{2.10}$$

where mw_s is the molar mass of the solvent [g mol^{-1}], m_i is the electrolyte molality in the solution [mol kg^{-1}], ν_i is the number of each i^{th} ions generated by the complete dissociation of the salt. The osmotic coefficient and the activity coefficient are related to the Gibbs-Duhem equation. The relationship is given in the following expression:

$$-\ln\gamma_{\pm} = \int_{m=0}^{m} (1-\Phi) d\ln m \tag{2.11}$$

While there are various models estimating activity coefficients for various salts, there is limited research on estimating activity coefficients of ammonium bicarbonate at various concentrations and temperatures. The Pitzer's model was used to fit the measured values of ion-interaction parameters or virial coefficients for ammonium bicarbonate solution. Hence, we discuss the Pitzer's model. The Pitzer's model estimates the activity coefficients for solute and solvent. The model includes the long-range interactions between the charges described by the Debye-Huckel term, while the short-range interactions are modelled using an empirical virial expansion. The osmotic and salt activity coefficients can be calculated from Equation 2.13, 2.12, as they are consistent with the Gibbs-Duhem relationship.

$$\ln(\gamma) = -|z_M z_M| f^{\gamma} + 2m\frac{v_M v_X}{v} B^{\gamma}_{MX} + 3m^2 \frac{(v_M v_X)^{3/2}}{v} C^{\gamma}_{MX} \tag{2.12}$$

$$\Phi = 1 - |z_M z_M| A_\Phi \left(\frac{I^{0.5}}{1 + bI^{0.5}} \right) + 2m \frac{v_M v_X}{v} B^\gamma_{MX} + 2m^2 \frac{(v_M v_X)^{3/2}}{v} C^\gamma_{MX} \tag{2.13}$$

Where m_0=1 mol kg^{-1} is the standard molality, b=1.2 kg$^{1/2}$mol$^{-1/2}$ is a constant for all solutes; α is a numerical constant equal to 2 for monovalent ions [25]–[27]; I is the ionic strength; A_Φ, is the Debye-Huckel parameter for the osmotic coefficient; z_M and z_X are the charges of cation and anion; β^0_{MX} and C^γ_{MX} are the ion-interaction parameters or virial coefficients. Ion-interaction parameters or virial coefficients are related to the short-range interaction between the ions, thus being particularly important when the salt concentration is high. The virial coefficients are a function of the electrolyte type, the temperature and the pressure. The correlations to evaluate the interaction parameters were found in the literature for a temperature 298K, and pressure of 1 atm [25]–[27].

$$f^\gamma = -0.392 \left(\frac{I^{0.5}}{1 + bI^{0.5}} + \frac{2}{b} \ln \left(1 + bI^{0.5} \right) \right) \tag{2.14}$$

$$B^\gamma_{MX} = 2\beta^0_{MX} + \frac{2\beta^0_{MX}}{\alpha^2 I} \left(1 - e^{-\alpha I^{0.5}} \left(1 + \alpha I^{0.5} - \frac{\alpha^2 I}{2} \right) \right) \tag{2.15}$$

The virial coefficients for ammonium bicarbonate, NH_4HCO_3, solutions at 298 K are $C^\gamma_{MX} = \frac{3}{2} C^\Phi_{MX},\ \alpha = 2,\ b = 1.2\ ,\ \beta^0 = -0.038,\ \beta^1 = 0.07$

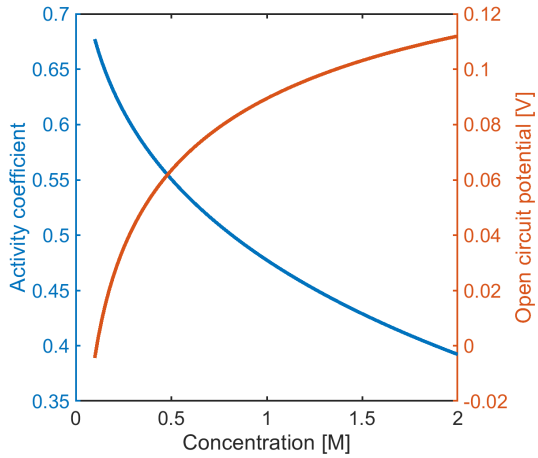

Fig. 2.2: The graph depicts activity coefficient and membrane potential as a function of concentration. The dilute solution concentration was kept constant at 0.1 M and concentrate solution concentration was varied from 0.1 M to 2 M (maximum in practice).

The properties of electrolyte solutions strongly influence the performance of all electrochemical processes. Hence, the selection of salt for a RED application is crucial. According to Tamburini et al. and Micari et al., a suitable salt for thermally drive RED applications should have [15], [28]:

1. High solubility in water. Solubility in water defines a clear physical threshold to the maximum concentration exploitable for salinity gradient, thus increasing the driving force for the RED process.

2. High equivalent conductivity of the aqueous solution. The equivalent conductivity has a strong impact on stack resistance, most likely the highest contribution to the overall internal resistance [23].

3. Large activity coefficients ratio. The generated electromotive force within the RED unit is strongly dependent on the ratio between high concentrate and low concentrate solution activities, as shown in Figure 2.2. Some salts can present a very beneficial behaviour in terms of activity vs concentration, which tends to enhance the activity ratio and, thus, the electrochemical potential.

4. Low Boiling Point Elevation (BPE) and low enthalpy of vaporisation[1]. The BPE affects the temperature of the heat source required for decomposition and can limit the number of stages of a multi-stage evaporative process. The enthalpy of vaporisation influences the heat consumption of the evaporative unit.

2.1.3 Regeneration or separation system

Due to the concentration gradient across an IEM, salt is transferred from the concentrated to the dilute solution in the RED stack. In addition, the concentration gradient causes the solvent transport from the dilute to the concentrated solution due to osmotic pressure across the ionic exchange membrane. These processes cause different salt concentration of the solutions exiting the RED stack than the feed solutions. The regeneration or separation stage restores the exiting solutions to the initial concentrations. This can be achieved by extracting either the solvent or the solute from the exiting solutions. There are two different ways to restore the concentrations, as outlined in the process flow diagrams in Fig 2.3. In the solvent extraction process, the amount of salt transferred in the RED stack from the concentrated to the dilute solution is re-balanced by adding stream 1 to 2 followed by the necessary solvent excess extraction. The two exiting streams are the solute-rich stream, 5 and a solute-free stream, 4. Stream 6 reduces the input flow rate to the regeneration stage, resulting in a decrease in heating requirement.

In the salt extraction process, the amount of salt transferred in the RED stack from the concentrate solution to the diluted one is extracted from the dilute stream 2 in the regeneration unit. The output streams 4 and 5 are solvent rich and solute rich streams. One of such methods uses thermolytic salts, for example, ammonium bicarbonate, decompose into the gaseous compounds NH_3 and CO_2 by increasing the temperature of the solution at and above 333 K. These gases are subsequently reabsorbed in the concentrate solution, thus restoring it to the initial concentration as shown in the Fig 2.4. Such thermolytic solutions have the potential to utilise a low-grade heat source in the temperature range of 323–333 K. Ammonium bicarbonate (NH_4HCO_3) salt is one of the promising thermolytic salt solutions.

[1] For closed-loop thermally driven regeneration system

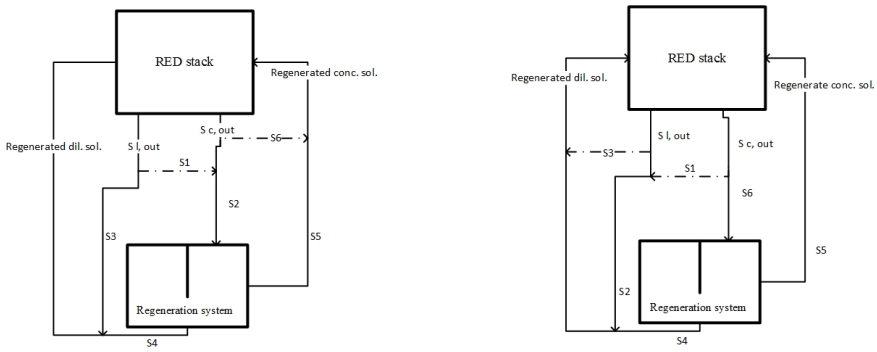

Fig. 2.3: Schematic of reverse electrodialysis (RED) with solvent extraction regeneration process(left) and solute extraction regeneration process (right) [29]

The low decomposition temperature of around 333 K at 1 atm, high solubility in water, and relatively low molecular weight make it a suitable choice for the thermolytic salt needed in this process.

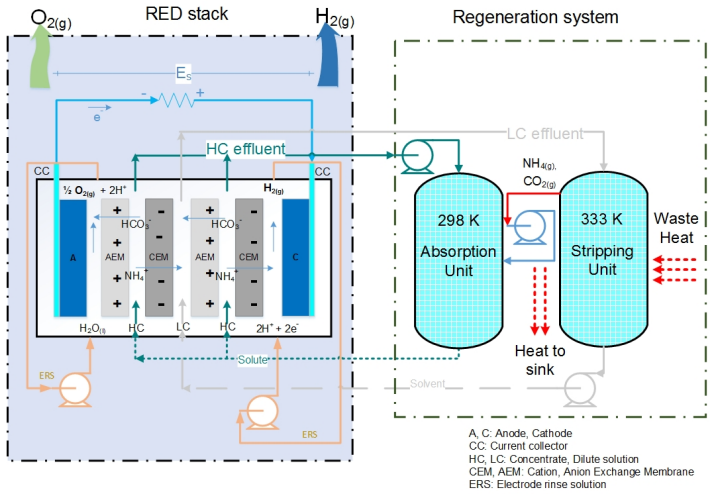

Fig. 2.4: Schematic of reverse electrodialysis (RED) system for ammonium bicarbonate salt with solute extraction regeneration system for H_2 production

Various salts solutions have temperature-dependent behaviour. Such salts solutions can be used in a thermal separation or regeneration process. It also provides an opportunity to utilise low-grade waste heat. In such salts, the properties such as solubility, osmotic pressure, decomposition temperature and heat are influenced by operating temperature. Thermolytic salts are chemical compounds that decompose into gaseous species when heated beyond a specific limit. The separation of such gases from the aqueous phase is expected to be easy [30], [31]. Some examples of thermolytic salts are ammonium sulphite, ammonium bicarbonate etc.

Ammonium bicarbonate was chosen because the solubility of the ammonium salts is high, the species have relatively low molecular weights, the solutes are almost completely removable (less than one ppm in case of ammonium bicarbonate solution), the thermal energy required for the separation and recycling of these solutes from a quantity of water is significantly less than the energy required to vaporise the water itself [32]. RED with feed solution as ammonium bicarbonate of concentration 1 M and 0.01 M can theoretically produce energy equivalent to 370 m of hydraulic head, much greater than that of the typical ocean and river water, 270 m [33]. The ammonium bicarbonate-water binary system is a particular case of the three-component complex reactive system CO_2-NH_3-H_2O. The reactions mentioned below are as follows carbamate formation from bicarbonate, dissociation of ammonia in water, dissociation of the bicarbonate ions, dissociation of carbon dioxide in water, dissociation of water and dissociation of ammonium bicarbonate [34], [35].

$$NH_3 + HCO_3^- \rightleftharpoons NH_2COO^- + H_2O \tag{2.16a}$$
$$NH_3 + H_2O \rightleftharpoons NH_4^+ + OH^- \tag{2.16b}$$
$$HCO_3^- \rightleftharpoons CO_3^{2-} + H^+ \tag{2.16c}$$
$$CO_2 + H_2O \rightleftharpoons HCO_3^- + H^+ \tag{2.16d}$$
$$H_2O \rightleftharpoons H^+ + OH^- \tag{2.16e}$$
$$NH_4HCO_3 \rightleftharpoons NH_4^+ + HCO_3^- \tag{2.16f}$$

It was indicated in the studies of all the species ammonium bicarbonate was the main component [34]–[37].

2.2 Ion exchange membrane (IEM)

The ion exchange membrane is a dense polymer having ionic groups. IEMs are primarily made of three components, the polymer matrix (backbone), the functional groups attached to the matrix (fixed charged group), and the mobile ions absorbed on the functional groups (exchangeable charges). IEMs conducts ions, meaning ions can transfer through the membrane together with water molecules. As the fixed charged groups are hydrated, these membranes are hydrophilic. The charged groups of the membrane act as a fixed carrier for various ionic materials. The fundamental principle of IEM based separation processes is the coupling of the transport of electrical charges with a mass transport, i.e. cations or anions are transported through a permselective membrane due to an externally applied or internally generated electrical potential gradient. There are many driving forces to transport ions and solvents through a membrane; this will be discussed in the following section.

There are two types of ion-exchange membranes; cation-exchange membranes (CEMs) have negatively charged groups such as -SO_3^-, -COO^-, -PO_3^{2-}, -PO_3H^-, -$C_6H_4O^-$, etc., fixed to the polymer matrix. Anion-exchange membranes (AEMs) have positively charged groups such as -NH_3^+, -NRH^{2+}, -$NR_2\ H^+$, -NR_3^+, -PR_3^+, -SR_2^+, etc., fixed to the polymer matrix. A CEM and an AEM permit transport of cations and anions, respectively, due to the oppositely charged functional group. In an IEM, the fixed charges are in an electrical equilibrium with the mobile ions in the interstices of the polymer. Figure 2.5 shows a schematic representation

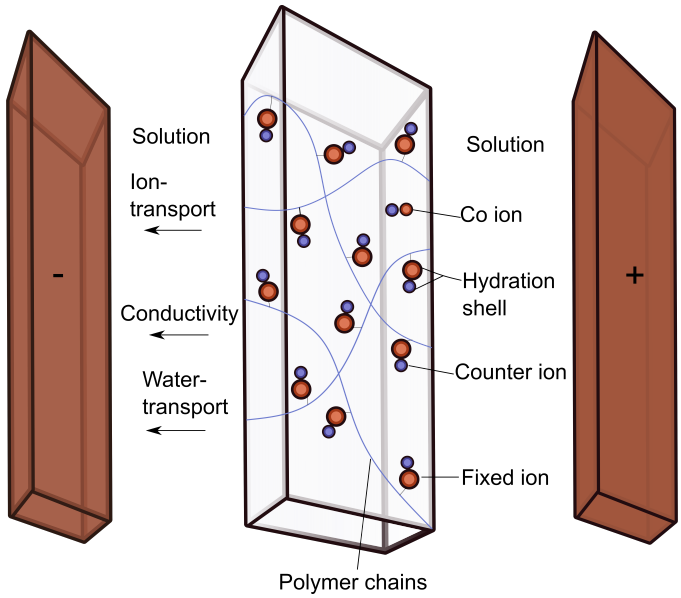

Fig. 2.5: Schematic of ion exchange membrane (IEM) polymer structure sandwiched between two electrodes.

of the polymer matrix of a CEM with fixed anions and mobile cations, also known as counter ions and the mobile anions are referred to as co ions. The co ions are excluded from the polymer matrix because their electrical charge is identical to that of the fixed ions; this phenomenon is called Donnan exclusion [38]. However, the extent of the co ions exclusion from an IEM depends on the membrane as well as on solution properties [39]. Therefore the selectivity of an IEM comes from the exclusion of co ions from the membrane phase. The properties of an IEM is determined by different parameters such as the density of the polymer network, the hydrophobic or hydrophilic character of the matrix polymer and the type and concentration of the charges in the polymer, and the morphology of the membrane itself [40].

2.2.1 Thermodynamics of transport processes

The three independent fluxes describe the mass transport in an electrolyte solution or in an ion-exchange membrane must be considered, that is, the fluxes of cations, the flux of anions, and the flux of the solvent. The driving forces acting in electrolyte solutions are gradients in the chemical, electrical, or electrochemical potential. In ion-exchange membrane separation processes, the ions of an electrolyte solution are transported due to an externally applied or by activity gradients induced electrical potential through a membrane from one electrolyte solution into another or to the surface of an electrode. For a system containing charged components the partial molar Gibbs free energy is given by the electrochemical potential,

$$d\tilde{\mu}_i = \mu_i + z_i F d\phi = V_i dp + RT d\,ln\,a_i + z_i F d\phi \tag{2.17}$$

where $\tilde{\mu}_i$ is the electrochemical potential and z_i is the charge number of the ion *i*, ϕ is the electrical potential and F is Faraday's constant.

Membrane potentials result from Donnan potentials arising from the discontinuity in the ion concentration at each membrane interface and diffusion potentials arising from the dissimilar mobility of anions and cations inside the membrane phase. The membrane potential for any given membrane is expressed by,

$$\phi^m = \phi^c_{Don} + \phi_{dif} - \phi^d_{Don} \tag{2.18}$$

Donnan potential is the potential difference between the membrane and the solution as a function of the activity of an ion i and the pressure in the solution and the membrane,

$$\phi_{Don} = \phi^m - \phi^s = \frac{1}{z_i F}(RT\, ln\, \frac{a^s_i}{a^m_i} + V_i \Delta\pi) \tag{2.19}$$

The diffusion potential is the change in free energy which is equal to the difference in chemical potential, μ_i, in the permeation of i having charge z_i through the membrane with transport number, t_i,

$$\phi_{dif} = -\frac{RT}{F}\sum_i \frac{t_{i,c} + t_{i,d}}{2z_i} ln \frac{\bar{a}_{i,c}}{\bar{a}_{i,d}} \tag{2.20}$$

The determination of the transport rate of different components in the membrane phase and the adjacent feed solutions results in performance evaluation of IEM based separation processes. The mobility and concentration of a component in a given environment and the driving force/s acting on the component govern the transport rate of the component. The Nernst Planck flux equation explains the transport phenomena in ion-exchange membranes and solution systems. When an ion i diffuses through the ion exchange membrane in a direction perpendicular to the membrane surface, the flux, J, is expressed by a product of the gradient of the chemical potential, $-(d\mu_i/dx)$,

$$J_{i,d} = \frac{D}{RT} C_i \left(\frac{-d\mu_i}{dx}\right) = D_i C_i \frac{d\, ln\, a_i}{dx} \tag{2.21}$$

where D_i is the diffusion coefficient of i, R the universal gas constant, T the absolute temperature, a_i activity of i. $a_i = m_i\gamma_i$, m_i, is the molal concentration of i; γ_i, activity coefficient of *i*. In addition, there exists a flux $J_{i,e}$ due to gradient in electrical potential $d\phi/dx$. Thus, the Nernst planck equation for total flux of ion *i* is given as,

$$J_i = J_{i,d} + J_{i,e} = -D_i \left(\frac{dm_i}{dx} + z_i m_i \frac{F}{RT}\frac{d\phi}{dx} + m_i \frac{d\, ln\, \gamma_i}{dx}\right) \tag{2.22}$$

A feed solution is an electrolytic solution where long-range electrostatic forces govern the interaction between components to a large extent with inherent macroscopic scale electroneutrality. The ionic fluxes in the solution dissolving two kinds of ions both ions influence each other irrespective of their charges. These ionic fluxes affect solvent fluxes. These phenomena mean that the fluxes and driving forces are dependent, and they are coupled

together. The Nernst–Planck equation does not concern with these coupled effects. All membrane processes are non-equilibrium processes, and the transport equation describing a particular membrane process must satisfy the principles of non-equilibrium thermodynamics. For the first principle, the rate of lost work $T\sigma$ should be a scalar product of all fluxes J_i and forces X_i,

$$T\sigma = \sum J_i X_i \tag{2.23}$$

where σ is the rate of entropy production per unit area. According to the second principle, if the system is close to equilibrium, linear relations between the thermodynamic forces and resulting fluxes exists,

$$J_i = \sum L_{ij} X_j \tag{2.24}$$

The final principle postulates the Onsager reciprocal relationship,

$$L_{ij} = L_{ji} \tag{2.25}$$

In an actual IEM based system, as shown in Figure 2.1, the electrolytic solutions are separated by an IEM. Assuming the following conditions,

1. The IEM forms a continuous boundary interface between the cell compartments.

2. There is no mass transfer between the closed system and the surroundings.

3. There is no consumption or production of material caused by a chemical reaction.

4. The system is isothermal.

The irreversible thermodynamics exhibit only approximated meaning where equilibrium states. General equations dissipation function

$$T\sigma = \sum_i J_i \bar{\mu}_i = I\Delta\phi + J\Delta P + \sum_i J_i \mu_i \tag{2.26}$$

where j, J and J_i are electric current, volume flow of a solution and a mass flux of component *i*, respectively. Coupling means that transport of mass will take place in a system when the gradient in the chemical potential, temperature or electric potential exists. The phenomenological equations in the ion exchange membrane system are,

$$j = \sum_i L_{ik}\Delta\mu_i + L_{EP}\Delta P + L_E\Delta\phi \tag{2.27a}$$

$$J = \sum_i L_{Pi}\Delta\mu_i + L_P\Delta P + L_{EP}\Delta\phi \tag{2.27b}$$

$$J_i = \sum_i L_{ik}\Delta\mu_i + L_{iP}\Delta P + L_{iE}\Delta\phi \tag{2.27c}$$

Phenomenological equation is

$$J_i = \sum_i (L_{ik}\Delta\mu_k + \nu L_{ik}\Delta P + z_k L_{ik}\Delta\phi) \tag{2.28}$$

where z_k and ν_k are an electric charge number and partial volume of component k. The membrane phenomena are expressed as follows based on the phenomenological equation,

1. Electric conductivity- when system is in mechanical equilibrium and there is no chemical potential developed we measure electrical conductivity. Substituting ΔP=0 and $\Delta\mu$=0 in equations 2.27, 2.28,

$$L_E = \left(\frac{j}{\Delta P}\right)_{\Delta P=0,\Delta\mu=0} = \frac{1}{E}\sum z_i J_i = \sum_i \sum_k L_i k z_i z_k \tag{2.29}$$

2. Electric transport number of component *i*- when system is in mechanical equilibrium and there is no chemical potential developed we measure transport number. Substituting ΔP=0 and $\Delta\mu = 0$ in equations 2.27, 2.28,

$$t_i = \left(\frac{z_i J_i}{\sum z_i J_i}\right)_{\Delta P=0,\Delta\mu=0} \tag{2.30}$$

One of the limitations or advantage of the framework of non-equilibrium thermodynamics for ion and water transport across an IEM is that the information on the membrane structure and transport mechanism is not used.

2.3 Liquid junction potential (LJP)

Liquid junction potential or diffusion potential is the potential differences formed in the contact zone of two different adjoining electrolytic solutions. The formation of such potential differences between different electrolytes is caused by differences in ionic mobilities, concentration and activities of dissolved ions. The LJP is related to Galvani potential. In practice, in place of model LJP calculations and corresponding emf corrections, the experimental elimination of the diffusion potential is conventionally applied. This can be achieved by introducing the so-called 'salt bridges' filled with concentrated solutions of salts, which satisfy the condition $t_+/z_+ = t_-/z_-$. A salt bridge is a device containing an electrolyte solution and placed between two electrodes or electrode compartments so that the electrolyte solution serves as the ionic conductor between the two electrodes. For a symmetric electrolyte, this means that anions and cations have very close diffusion coefficients, and the transport numbers of both ions are ~ 0.5. Some of the salt bridge requirements,

1. The electrolytic contact between the electrodes must be maintained.

2. The ohmic resistance *R* of the electrolyte bridge/s must be small enough so that the voltage drop *iR* is minimal or negligible.

3. The diffusion potentials at the boundary of different electrolytes must be as small as possible, and they must be as time-invariant.

4. The electrolyte of the reference electrode should not be contaminated by the electrolyte of the working electrode and vice versa.

These requirements are challenging to be achieved. One of the reasons for the discrepancy is to maintain a constant potential of the reference electrode. A high-input impedance measuring instruments are used so that the current flowing through the salt bridge is practically negligible. Also, concentrated solutions of potassium chloride offer the great advantage that the diffusion potentials are tiny because the effects of potassium cations and chloride anions almost cancel each other. Moreover, it is essential to arrange the hydrostatic pressure on both sides so that no pressure gradient will drive the liquids from one to the other side. The leakage of salt solutions from bridges to reference electrodes can be decreased by increased viscosity of the salt solutions with gelling agents. Gelling also contributes to decreased diffusion coefficients of the salt ions and thus to diminished liquid junction potentials [41]. The decreased ion mobility in gels results from geometric obstructions, and in the case of poly-electrolyte gels, also from electrostatic obstruction [41]. Agar is a mixture of agarose and agaropectin. Typically the salt solution contains 2–5 % (w/v) agar. Agar gels have a concentration-dependent pore structure (in the order of 100 nm pore size). The gel is prepared by gently heating the agar with the salt solution, and the liquid is allowed to cool down in the appropriate tubes. Solidification occurs between 313 K and 305 K. Agar gel is widely used in lab-made diaphragms, but they dry out, and microbes like to settle and grow on the gel.

2.4 Levelised cost of energy (LCoE)

One of the main criteria for selecting a particular technology over various available alternate technologies is economic competitiveness. The calculation of the unit cost of energy can provide a useful comparative measure between projects and technologies. The LCoE (cost per kWh) metric estimates the unit cost of energy over the lifetime of a project. This includes investment, operating and financing costs. LCoE metric is the ratio of the sum of the lifetime costs of the energy system under consideration to the lifetime energy production, in cost per unit energy. Conventionally, LCoE includes the plant-level costs and does not take into account effects at the system level, i.e. additional investments in transmission and distribution grids or additional reconfigurations of the electricity systems [42]–[44]. The LCoE formula defined by Business, Energy and Industrial Strategy, UK Government department is,

$$LCoE = \sum_{t=1}^{n} \frac{C_t + O_t + V_t}{(1+d)^t} / \sum_{t=1}^{n} \frac{E_t}{(1+d)^t} \tag{2.31}$$

where *t* is the plant lifetime, the period ranging from year 1 to year *n*, n the final year of operation, Ct the capital costs including cost associated with decommissioning in period *t*,

Tab. 2.1: Comparison of levelised cost of hydrogen for various conventional (SMR, CG) and non conventional technologies (Electrolysis). Here SMR is steam methane reforming; CCS is carbon capture and storage; CG is coal gasification.

Production method	**LCH, €/kg$_{H_2}$**	**Ref**
SMR	1.52 - 2.53	[47]
	1.01 - 1.52	[48]
	0.90 - 1.80	[1]
SMR with CCS	1.45 - 1.77	[49]
	1.34 - 2.67	[1]
CG with CCS	1.64 - 2.01	[49]
	2.00	[1]
Electrolysis	3.06 - 3.74	[49]
	5.00 - 5.50	[48]
Renewable electrolysis	2.23 - 5.34	[1]

O_t the fixed operating cost in period *t*, V_t the variable operating cost which includes fuel cost, carbon costs, and sometimes taxes, etc. in period *t*, E_t the electricity generated in period *t*, *d* is the discount rate. The main disadvantage of the LCoE method is it gives a future estimation that may lead to uncertain results. Despite its flaws the LCoE method provides a holistic universal method to evaluate and compare different investment opportunities[43], [45], [46]. Levelised Cost of Hydrogen (LCH, price per Kg of H_2) method is based on LCoE method. It is a break-even metric that calculates the ratio of lifetime cost to lifetime hydrogen production of a facility. The LCH may also include the levelised hydrogen production costs by component and the levelised cost of hydrogen compression, storage, and dispensing.

$$LCH = \frac{C_{cap,a} + C_{f\,om,a} + C_{v\,om,a}}{E_{H_{2,a}}} \tag{2.32}$$

where C_{inv} is the investment cost, The operational and maintenance (O and M) costs were divided between fixed $C_{f\,om,a}$ and variable expenses $C_{v\,om,a}$. The fixed expenses include equipment maintenance cost, service contract cost, the annualised replacement cost. The variable costs include the annual electricity cost and the annual water cost. $E_{H_{2,a}}$ amount of produced hydrogen (kg H_2). Various technologies produce hydrogen at a commercial scale. Most of the hydrogen production is from fossil fuel sources by steam methane reforming and coal gasification. Electrolysis is an alternate method to produce hydrogen. It is driven by electricity either produced from conventional power plants or renewable sources such as solar or wind. Table 2.1 gives a brief overview of current hydrogen-producing technologies. It shows that hydrogen produced from steam methane reforming (SMR) is the most cost-efficient.

2.5 Literature review

Neff was the first to develop ammonium bicarbonate solution as thermally regenerated drawing agent to remove water from a salt-water stream. He described it as 'Solvent extractor' in his patent[50]. McCutheon et.al. developed a forward osmosis process that uses ammonium bicarbonate concentrated solution to extract water through a semipermeable osmotic membrane, where the drawing solution can be regenerated using heat at 333 K in a distillation/stripping column [51]. McGinnis et. al. did simplified energetic analysis indicating the requirements for the regeneration step in Aspen Hysys. Here they studied regeneration schemes single and multi-distillation. At low temperatures the single column requires lower energy; while at temperatures over 313 K, the use of multiple columns was found to yield a greater thermal efficiency [31].

Luo et al. performed initial RED experiments using NH_4HCO_3 with varying operating conditions such as flow rate and feed solution concentration. They showed that the internal resistance and open circuit potential decrease with an increase in the dilute solution concentration. Further, an increase in flow rate increases the open circuit potential while decreasing the internal resistance as well [52]. Hatzell et al. demonstrated the influence of spacers and channel alignment on the internal resistance and the power density. They found that reorienting the flow through the channels decreased the internal resistance due to decreased bubble coverage by 13%; reducing channel length increased the limiting current density and the power density by 23% and 14% respectively, and spacer-less stacks had lower ohmic resistance than those with spacers but at low flow rates [53]. Zhu et al. compared NaCl and NH_4HCO_3 salts and found that at the same concentration ratios the energy recovery and power density are lower for NH_4HCO_3 than for NaCl mainly due to the low conductivity (low ion activity) [54]. Kwon et al. studied parameters such as the concentration difference, the membrane type, the inlet flow rate, and the compartment thickness. Their results indicate that the open circuit potential highly depends on the concentration difference across an IEM, and the maximum power density increases with increasing inlet flow rate and decreasing the intermembrane distance [55]. Bevacqua et al. performed a parametric study evaluating parameters such as dilute solution concentration and feed velocity. They observed that for feed velocities higher than 1 $cm\,s^{-1}$ the gross power density reduces to a negative power output owing to losses due to a more significant pressure drop [56]. Bevacqua et al. developed a lumped parameter model for the RED unit and an ASPEN Plus model to assess the thermal duty of the stripping column. They performed sensitivity analysis to study the effect of feed solution concentrations and velocities. The predicted a maximum power density of about 9 $W\,m^{-2}$ of cell pair for the RED unit, and a maximum exergetic efficiency of about 22 % was found for the heat to electricity process [35]. Kwon et al. developed a theoretical RED model. They computed the membrane potential using the Planck- Henderson equation based on conductivity measurements. They studied effect of concentration ratio, permselectivity, flow rate and intermembrane distance. They found maximum net power density of 0.84 $W\,m^{-2}$ for a concentration ratio of 200 (2 M/0.01 M), inter-membrane distance of $1{\cdot}10^{-4}$m, a feed solution flow rate of $3{\cdot}10^{-6}m\,min^{-1}$[57].

Hatzell et al. did the first study for hydrogen production using RED. They studied different cathode reactions (hydrogen evolution reaction (HER) and oxygen reduction reaction

(ORR)) and catalysts from NH_4HCO_3 RED. They found that the potential for direct hydrogen production at limiting current density using a HER cathode gives the highest energy, 1.5 times (most in the form of H_2) the energy produced by cathodes with ORR. In contrast, the ORR cathode produces more electricity. Further, indirect hydrogen production (i.e. coupling RED and electrolysis) resulted in one-third energy to that of direct hydrogen production [22]. Nazemi et al. developed a thermodynamic model to evaluate how much electricity and hydrogen gas can be extracted from the natural mixing of river and seawater. The results indicate that the maximum current density and hydrogen production is achieved with five cell pairs, while the maximum electrical power density was reached with 20 cell pairs [24]. Chen et al. demonstrated the use of acidic catholyte and alkaline anolyte for hydrogen and oxygen production in a RED stack. They found that the current density (concentration difference) and the electrode rinse solution's concentration (hydrogen evolution over-potential) has a strong influence on hydrogen production [58]. All these studies have been summarized in the Table 2.2.

Tab. 2.2: Ammonium Bicarbonate Reverse Electrodialysis systems (AmB RED) and Hydrogen Production from RED

Type	Concentration		Membrane								Electrolyte-Electrode	E	P	Ref
	c_c (M)	c_d (M)	Name	α	R_{mem} (Ωm^{-2})	Area (cm^2)	δ_{mem} (μm)	δ_{ch} (μm)	N_p	v Feed (ml min^{-1})	Redox (ml min^{-1})		(V)	(W m^{-2})	
Experimental: Electricity	1.5	0.003 to 0.15	Selemion CMV and AMV	1	na	10.5 × 7.5	130	500	20	150-1200	5	0.1 M $K_4Fe(CN)_6$ and $K_3Fe(CN)_6$ (50:50). Titanium plates coated with Ru-Ir.	3.7	0.33	[52]
	0.6-1.5	0.005 - 0.02	Neosepta CMX and AMX Excellion I-100 and I-200	na	na	7 x 7	na	200 - 800		1-20	50	0.05 M $K_4Fe(CN)_6$ and $K_3Fe(CN)_6$. Ru-Ir coated titanium electrodes. 0.3 M NH_4HCO_3. Ru-Ir coated titanium electrodes	1	0.62	[55]
	2	0.01 - 0.1	Fujifilm RP1 80050-04, 80045-01 Nafion at electrode	na	na	10 x 10	120	270	10	0.5-2 cm s^{-1}	225	0.1 M $K_4Fe(CN)_6$ and $K_3Fe(CN)_6$ Ru-Ir oxide- coated Ti electrode. 1 M NH_4HCO_3. Ru-Ir oxide- coated Ti electrodes.	1.56	2.42	[56]
	1.1	0.011	Selemion CMV and AMV	na	na	2 x 1	na	1100	1	1- 18 mm s^{-1}		Pt mesh	0.155	0.15	[53]
	1.5 and 0.6	0.015 and 0.006	PC-SK and SA	na	na	8 x 8	na	500	10	100		Ti mesh coated with Pt–Ir		0.32	[59]
Hydrogen	1.5					207	250	20	10 to 20	400	100	Ti mesh coated with Pt/Ir. Pt/C on carbon cloth- ORR and HER. Pt/Ir on Ti or MoB/C on carbon cloth for only HER.		118 Wh m^{-3}	[22]
	1.5 to 5	0.008 to 0.5	CJMC-1 CJMA-1			9 x 21	160 to 200	750		na	75	0.2 to 2 M HCl and 0.5 NaOH	2.91	0.72 ml $cm^{-2}h^{-1}$	[60]
Theoretical: Electrical	0.05 - 2	0.01	CMV/AMV	0.88-0.95 0.86-0.96		49		100 - 1000		0.1 to 20		0.05 M $K_4Fe(CN)_6$, $K_3Fe(CN)_6$ - 0.3 M NH_4HCO_3. Ti coated with Ir and Ru	1.1	0.84	[61]
	0.5-2.6	0.01-0.1	Fujifilm	0.754	$2 \cdot 10^{-4}$ $(c_d)^{-0.236}$ $4 \cdot 10^{-5}$ $(c_d)^{-0.236}$	50 x 50		270	1000	0.5-5 cm s^{-1}			1.8	7.5	[35]
	1 to 2.5	0.01 to 2		0.9	0.5	10 x 10		270	10	0.1-3 cm s^{-1}					
	0.5 to 2	0.01 to 0.1		0.85 and 0.95	$6 \cdot 10^{-4}$ to $1.5 \cdot 10^{-4}$	50 x 50			1000	0.5-2					
Hydrogen	0.6	0.0015		1	3	0.635		150	5 to 20					1.72 mol $cm^{-2}h^{-1}$	[24]

Tab. 2.3: Summary of techno-economic studies on reverse electrodialysis (RED).

Author	Year	Capacity (MW)	Plant life (yr)	Cmem (€m^{-2})	tmem (yr)	P (Wm^{-2})	LCOE (€kWh^{-1})	Type
Turek [62]	2007	-	-	100 [2,3]	10	0.46	6.79 [2]	River/Sea
Post [63]	2010	200	40	2	7	2	0.08	River/Sea
Daniilidis [64]	2014	200	25	50	7	2.2	0.72	River/Sea
Weiner [65]	2014	-	20	750 [2,3]	-	1.2	6.33 [2]	River/Sea
Bevacqua [35]	2017	100	20	50	20	4.78	0.3	AmB
Hu [66]	2018	-	20	750	-	4.5	8.19	
Micari [28]	2018	1	30	1-30	-		0.4	RED-HE
Giacalone [67]	2019	0.001-1000	-	4, 15	10	>1-19	0.27-0.33	River/Sea
Papapetrou [68]	2019	0.5-50	30	1-30	10	0.8 - 33	1.36-3.69	RED-HE
Raka [69]	2019	1500 kg_{H_2}	20	3,4,150	4,7,10	0.7-3.7	1.71-153 $kg^{-1}_{H_2}$	RED-HE-H_2

In literature there have been several studies estimating levelised cost of electricity (LCoE) for RED technology. Table 2.3 summarises these studies indicating diversity in parameters such as cost of membrane, membrane life, power density and LCoE.

[2]Currency in $

[3]Cost includes membranes, gasket, spacers, electrodes and end plate

3 Methodology

This chapter illustrates in detail the method to measure membrane potential, junction potential and membrane resistance. It includes the procedure for membrane equilibration, salt bridges preparation, electrode preparation, and mathematical estimation of permselectivity and membrane resistance.

Tab. 3.1: Overview of the membranes examined in this work. The membrane resistance and permselectivity values extracted from manufacturer´s data sheet are tested in 0.5 M NaCl at 298 K, and 0.5 M/0.1 M NaCl at 298 K, respectively. Here '*' is the data extracted from manufacturers data sheet.

IEM	Type	Thickness (μm)	Fixed charge group	Material	Counter-ion	Permselectivity	Resistance ($\times 10^{-4}\Omega$ m^2)	IEC (meq g^{-1})	SD (wt%)	Ref
FKE	CEM	28-33	-SO_3^-	-	H^+	0.97-0.99	1.6-2.46	1.35-1.36	12-27	[70]
FKSPET	CEM	74-87	-SO_3^-	-	H^+	>0.95	2.5	1-1.25	-	*
FAS	AEM	27-33	-	-	Br^-	0.89-0.90	1.03-2	1.1-1.85	8-19	[70], [71]
FASPET	AEM	72-85	-	-	Br^-	>0.90	<3	1-1.5	-	*
DSV	AEM	95-121	-		Cl^-	0.90	2.3	1.89	28	[70]
AMV	AEM	110-150	-$N(CH_3)_3^+$	PS/DVB/CMS	Cl^-	0.87-0.96	2.8-3.15	1.78-1.9	17-19.8	[70]–[72]
CMV	CEM	101-150	-	PS/DVB	Na^+	0.91-0.99	1.03-1.1	2-2.4	20-30	[70]–[72]
CSO	CEM	100	-	PS/DVB	Na^+	0.92-0.97	2.29-3	1.04	16	[72]
CMF	CEM	440	-	-	H^+	> 0.95	2.5	-	-	*
APS	AEM	138-150	-$N(CH_3)_3^+$	PS/DVB/CMS	SO_4^{2-}	0.88	0.68-0.7	0.29	147	[70], [72]

Tab. 3.2: Input parameters for thermodynamic model for Ammonium Bicarbonate-Based Reverse Electrodialysis

Parameter	Present	Future	Unit
Concentrate solution	2.6	2.6	M
Dilute solution	0.05	0.099	M
Permselectivity	0.8	0.95	
Membrane life	4	10	Years
Membrane resistance	$4.1{\cdot}10^{-4}$	$6.9{\cdot}10^{-4}$	Wm^{-2}
Cost of regeneration system	3400	3000	$€\,\mathrm{kwh}^{-1}\mathrm{m}^{-3}$
Cost of waste heat	0.01	0.005	$€\,\mathrm{kwh}^{-1}$

3.1 Permselectivity

3.1.1 Apparent permselectivity measurement

Membrane equilibration: Membranes were cut in a rectangular shape with varying size. Each of these membranes was soaked in a bottle with approximately 250 ml of ammonium bicarbonate solution (Merck, Germany, EMPROVE, 99 - 101%) at a specific concentration for at least 72 hrs without refreshing the solution. For brevity, we term this concentration as equilibration concentration (Eq.conc.). The membranes were kept at temperature 295 ± 2 K.

The experimental setup is shown in figure 3.1. The equilibrated membranes were directly sandwiched between rubber gaskets with diameter $35 \cdot 10^{-3}$ m. Therefore, the effective membrane size was $3.84 \cdot 10^{-4}\,\mathrm{m}^2$. The room temperature measurements were performed in the glass bulbs (each 200 ml) with magnetic stirrers to avoid concentration polarisation near membranes. The membrane potential E_m^m was measured with the reference electrodes when a steady-state was reached. The junction potential from the salt bridge and electrode bias potential were measured as well. The procedure for the same is explained in the subsection 3.1.2 below. The reference electrodes used in this study were double junction B2220 (Ag/AgCl) from SI Analytics, Germany. These electrodes were filled with 4 M KCl solution for more stable measurements than a single-junction electrode. The potentiostat used was a Gamry 5000E interface. The two salt bridges were prepared with 4 M KCl and 2-4% agar. The potentiostat was connected to the reference electrodes, which were dipped in 400 ml beakers filled with 4 M KCl. The potential across these electrodes with the salt bridge was measured as the membrane potential. The cell diagram of the presented setup is given below.

$$\mathrm{Ag} \mid \mathrm{AgCl} \mid \mathrm{KCl}_{aq} \,||\, \mathrm{HC}\,,\, \mathrm{NH_4HCO_{3,aq}} \mid \mathrm{IEM} \mid \mathrm{LC}\,,\, \mathrm{NH_4HCO_{3,aq}} \,||\, \mathrm{KCl}_{aq} \mid \mathrm{AgCl} \mid \mathrm{Ag}$$

The membrane potential was recorded every second for 30 mins. The measurement was followed by two 10 mins readings and a delay of 1 min between each measurement to confirm constant potential. The three concentration ratios we tested were 0.5/0.1, 1/0.1 and 2/0.1 mol L^{-1}. For high-temperature analysis at 313 K, a flow cell setup was used with

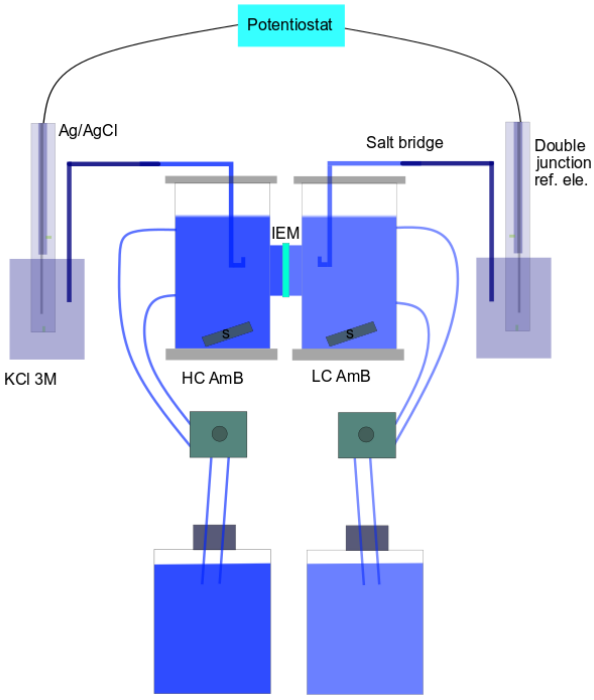

Fig. 3.1: Permselectivity measurement setup. The membrane potential is measured across the two double junction Ag/AgCl reference electrodes filled with 3 M KCl solution. These electrodes are dipped in 3 M KCl solution. The two agar salt bridges connects electrodes with the bulk solution in the cylindrical cell. Two Peristaltic pumps recirculate concentrate (0.5 M / 1 M / 2 M) and dilute solutions (0.1 M) at 100 ml min^{-1}. The top of the cells are covered with paraffin film.

magnetic stirrers and continuous recirculation of fresh solution. Four thermocouples were used to measure the temperature of the salt solution in the storage bottle and the flow cell compartments. The temperature was measured using a K-type thermocouple. The measurements were performed after the salt solution temperature in the flow cell reached 313 ± 2 K. A typical temperature gradient of 2 K was observed between the storage bottle and the flow cell compartments.

3.1.2 Junction potential measurement

The charge separation occurs due to the difference in the mobility of ions when solutions of different concentrations come in contact resulting in the formation of a transition region. The potential drop across this transition region is called diffusion potential or liquid junction potential. According to Kingsbury et al., the liquid junction potential arising from the difference in the concentration of filling in the electrodes and bulk solution contributes

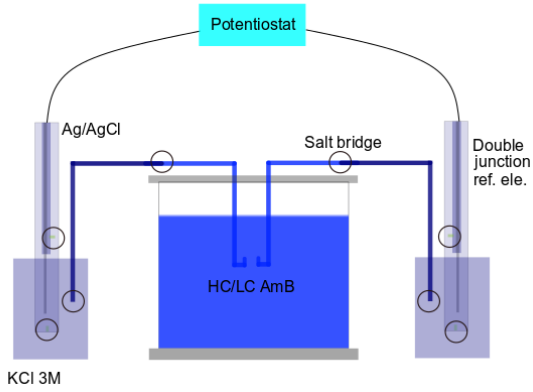

Fig. 3.2: Static junction potential measurement setup. The junction potential is measured across the two double junction Ag/AgCl reference electrodes filled with 3 M / 3.5 M / saturated KCl solution. These electrodes are dipped in 3 M / 3.5 M /saturated KCl solution. The two agar salt bridges connect electrodes with the bulk solution in the cylindrical cell. The circles highlight various liquid junctions that give rise to junction potential. These junction potentials are due to tip potential from the porous glass frit or platinum wire or agar with KCl and agar with AmB solution

to non-physical values of permselectivity [73]. The measured potential ΔE_m^m consists of the membrane potential [V], the reference electrode potential ΔE_{ref} [V] and the junction potential ΔE_j [V] [73]. While the use of bare Ag/AgCl electrodes would reduce the influence of junction potential, these bare electrodes are not stable for long term measurements. The use of salt bridges may lead to a lower contribution from the configuration of the reference electrodes, but still, it will add a systematic error to the membrane potential measurements.

$$\Delta E_m^m = \Delta E_{mes}^m - \Delta E_{ref} - \Delta E_j \tag{3.1}$$

here ΔE_m^m [V] is the membrane potential due to activity difference, ΔE_{mes}^m [V] is the measured membrane potential, ΔE_{ref} [V] is the bias potential between two reference electrodes due to differences in the filling solution concentration and ΔE_j [V] is the junction potential between filling solution and the bulk solution in the cell (for c_{fil} [M]$\neq$ c_{bulk} [M]). In this article, we define ΔE_{ref} as bias potential between two reference electrodes and ΔE_j as the junction potential in the salt bridge between agar and ammonium bicarbonate solution. Figure 3.3 shows the differences in ion mobility giving rise to liquid junction potentials in the agar filled AmB solution in the salt bridge. With KCl and AmB filling solutions in reference electrode and salt bridge respectively, the cation $\left(NH_4^+\right)$ diffuses through the junction faster than the anion, making the filling solution in the salt bridge negative with respect to the bulk solution.

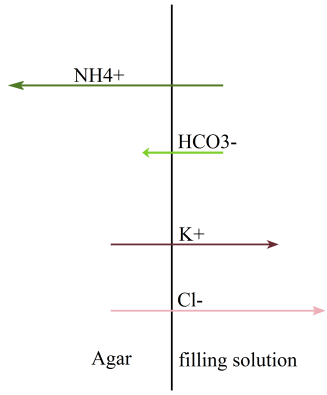

Fig. 3.3: The liquid junction potential arising from differences in ion mobility. The arrows denote the direction and the length of arrows denotes the value of mobility

We propose this approach of use of the salt bridge for open circuit potential measurement. The liquid junction potential was measured independent of the membrane permselectivity measurement. The experimental procedure replicating the selectivity measurement procedure is as follows, the salt bridges were stored overnight in saturated KCl. Four salt bridges were filled with AmB solution with two high concentration (HC) and two low concentration (LC). The LC was fixed to 0.1 M AmB while the HC was varied as 0.5 M, 1 M and 2 M. The open-circuit potentials (OCP) were measured as shown in the figure 3.2, using Gamry potentiostat. To see the influence of change in concentration in the salt bridge on junction potentials, after getting steady-state readings, the concentrations in the salt bridges were switched, i.e. HC to LC and vice versa. OCP was measured again until a steady-state is reached. Then the concentrations were switched back to the initial, and each measurement was performed for 600 seconds at least three times. The experiments were repeated until the difference between the initial and the final measurements were less than 0.2 mV. The value corresponds to junction potential contribution to the permselectivity measurement less than 1%. These measurements were used to correct for the junction potentials influencing the permselectivity measurement.

3.2 Membrane ionic conductivity

3.2.1 Membrane equilibration

The experimental setup for direct measurement of membrane resistivities is depicted in Fig. 3.4. We shall next describe the details of how the experiments were carried out. First, membranes were cut in a circular shape with a diameter of $2 \cdot 10^{-2}$ m. Each of these membranes were soaked in a bottle with approximately 200 ml of ammonium bicarbonate solution (Merck, Germany, EMPROVE, 99 - 101%) in an equilibration concentration (0.1 M, 0.5 M, 1 M, 2 M) for at least 48 hrs without refreshing the solution. The membranes

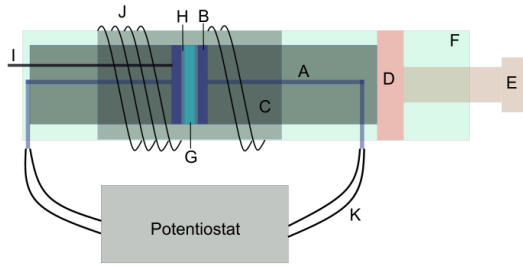

Fig. 3.4: Experimental setup for direct membrane resistance measurement using two electrodes and electrochemical impedance spectroscopy. Here A. Platinum wire, B. Platinum disc electrode, C. Ceramic casing, D. Stopper, E. Tightening screw, F. Metal casing, G. IEM, H. Solution thin film, I. K-type thermocouple, J. Heating coil, K. Cables

were kept at a temperature of 295 ± 2 K and 313 ± 1 K for room and elevated temperature measurements, respectively. The counter ions listed in the Table 3.1 were exchanged with ammonium ions for cation exchange membranes and bicarbonate ions for anion exchange membranes.

3.2.2 Electrode preparation

The membrane resistance was measured using Platinum disc electrodes. The disc electrodes were polarised for uniform surface using cyclic voltammetry using the reversible hydrogen electrodes (RHE) prepared in the lab. (RHE) were prepared in a glass tube with a $0.5 \cdot 10^{-3}$ m diameter platinum wire. An air tight glass flask of 1200 ml filled with 200 ml of 99 % concentrated H_2SO_4 diluted in 1000 ml of DI water was used to prepare RHE and disc electrodes using chronoamperometry and cyclic voltammetry. A glass tube was filled with the same solution and then a two-electrode setup was used to produce hydrogen with chronoamperometry using a Gamry 5000E interface. The experimental settings for this procedure are provided in Table 3.3.

Tab. 3.3: Parameters for the chronoamperometry procedure.

Parameter	Value	Unit
Electrode Area	$3.14 \cdot 10^{-4}$	m^2
Pre-step Voltage	0 vs E_{ref}	V
Pre-step Delay Time	0.5	s
Step 1 Voltage	-2.5	V
Step 1 Time	200	s
Step 2 Voltage	0.1	V
Step 2 Time	5	s
Max Current	200	mA
Limit I	$2 \cdot 10^{-2}$	$mA\,m^{-2}$
Equil. Time	5	s

The chronoamperometry was performed until the tube was 50% filled with H_2 gas. The disc electrodes used to measure membrane resistance were made of platinum with an active area of $3.14 \cdot 10^{-4}\,m^2$ and a thickness of $1 \cdot 10^{-3}\,m$. These electrodes were polarised using CV under the conditions provided in Table 3.4.

Tab. 3.4: Parameters for the cyclic voltammetry procedure.

Parameter	Values	Units
Initial potential	0	V
Final potential	0	V
Scan limit	1.6	V
Scan rate	20	mVs^{-1}
Step size	0.5	mV
Cycles	60	
Max current	20	mA

The CVs were performed with a three-electrode setup with the RHE (explained above) as the reference. 10 - 15 cycles were performed to have a stable voltammogram which corresponds to a uniform surface. Insulated platinum/copper wires were used to connect the platinum disc electrodes to the potentiostat. The disc electrodes were enclosed in a ceramic hollow cylinder and kept in a thick rectangular metal box. A screw was used to clamp the ceramic cylinder and metal box. A clamping torque of 2 Nm was set for all experiments.

3.2.3 Electrochemical Impedance Spectroscopy

Electrochemical impedance spectroscopy was used to measure the ohmic resistance of the membranes. A set of three measurements were performed for a stack of 1, 3 and 5 membrane layers. The settings for the measurements are provided in Table 3.5.

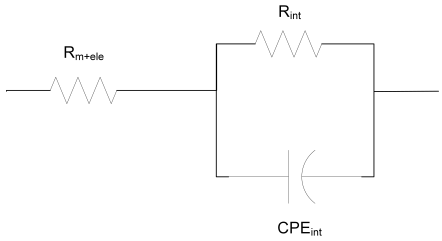

Fig. 3.5: Equivalent circuit used for the fitting of EIS measurements. The resistance (R_{int}) and constant phase element (C_{int}) represent the interface between electrode and solution layer on the IEM (i.e solution-electrode interface). The ohmic resistance of the IEM and the electrode is represented by R_{m+ele}

Furthermore, a blank cell measurement was performed after every set. In the case of a high-temperature measurement, the setup was kept in a heating oven. For boosting the

Tab. 3.5: Parameters for the electrochemical impedance spectroscopy procedure.

Parameter	Value	Unit
Initial frequency	10^6	Hz
Final frequency	10	Hz
Points/decade	15	-
AC Voltage	10	mV
Area	$3.14 \cdot 10^{-4}$	m^2
Init. Delay	60	s

temperature of the membrane and disc electrodes, an external heating coil was wound along the length on the hollow ceramic cylinder as shown in Fig. 3.4. One of the electrodes was connected to a thermocouple (type K) to measure the temperature of the disc electrode. The measurements were analysed using an equivalent circuit model. The Ohmic resistance of the membrane plus the electrodes were then estimated. These resistances were plotted as functions of the membrane thickness. The intercept was treated as the ohmic resistance of the blank cell.

4 Results and discussions

4.1 Publications I and II

In these studies we evaluate the influence of each parameter in terms of hydrogen production rate ($\dot{m}$) ($kg_{H_2}\,m^{-2}\,s^{-1}$), waste heat required for restoring the salt concentration (q_{th}) $kWh\,kg_{H_2}^{-1}$, and levelised cost of hydrogen (LCH) $€\,kg_{H_2}^{-1}$.

In general, an increase in production rate increases the total H_2 produced in the plant throughout its lifetime, which decreases the LCH. An increase in production rate can be achieved by increasing current density, which indirectly relates to the concentration ratio. High concentration ratios are achieved with high solubility of salt under the assumption that the electrical conductivity of the solution and membrane permselectivity remain the same. The production rate is a function of peak density, which in turn depends on the Nernst potential. This Nernst potential relates to the ratios of concentration or activity coefficients which are salt properties. The salts with higher OCP, higher solubility limit and lower resistance can produce H_2 at an increased production rate. Further, the use of an optimal combination of electrolytic solutions, electrode material, and geometric configuration can decrease the cell overpotential and increase the overall stack potential, which will improve the H_2 production rate. In the following subsections, we discuss a few parameters that significantly influence the H_2 production rate and waste heat required for restoring the salt concentration.

4.1.1 Feed Solution Concentration

At dilute solution concentrations below 0.1 M with a fixed concentration of concentrate, the concentration ratio (c_c/c_d) is high, but due to the high (ohmic) membrane and channel resistances, the electrochemical potential is low. The low electrochemical potential and high ohmic resistance result in a low current density. As the current density is directly proportional to the H_2 production rate, the latter decreases as well. The H_2 production rate increases until dilute solution concentrations 0.1 M and then decreases as shown in Figure 4.1. This decrease is due to a low concentration ratio (c_c/c_d). For the specified geometry and operating conditions of the RED cell, a maximum is observed at c_c 2.6 M and c_d 0.1 M, and 2.6 M and 0.2 M for present and future scenario, respectively. For an increase in the concentration of the concentrated solution, the H_2 production increases. Also, the concentration of dilute solution at which the maximum H_2 production is observed increases with an increase in the concentration of the concentrated solution.

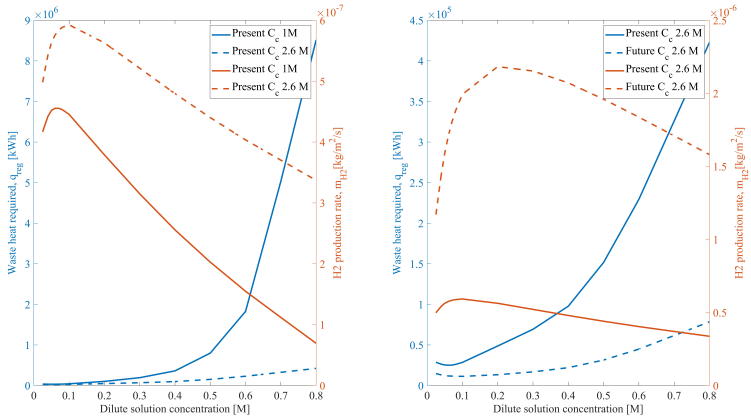

Fig. 4.1: Waste heat required and H_2 production rate as a function of both dilute and concentrated feed solutions (left). Waste heat required and H_2 production rate as a function of both dilute feed solution for present and future scenario (right).

An opposite trend is observed for the waste heat required for restoring the salt concentrations (Q_{reg}) as shown in Figure 4.1. For the specified geometry and operating conditions of the RED cell, an increase in the concentration of the dilute solution increases the waste heat required per unit volume to restore an increased amount of salt. At concentrations above c_d 0.07 M and 0.1 M (for present and future scenario), the increase in dilute solution concentration increases the current density due to the decreased (ohmic) membrane and channel resistances. However, as the concentration ratio decreases, the electrochemical potential decreases; this increases the number of cell pairs needed and increases the volumetric flow rate. The increase in volumetric flow rate causes an increase in the required waste heat. Finding the optimum between the H_2 production rate and waste heat required is essential for a reduced LCH. This optimum is usually found at a concentration of dilute solution less than the concentration at maximum H_2 production as waste heat required dominates the LCH. When comparing the scenarios, the H_2 production rate increases by one order of magnitude, and the waste heat required reduces by one order of magnitude. This is due to high permselectivity and low membrane resistance. Further, the concentration of the dilute solution at which maximum H_2 production rate is observed shifts towards higher concentrations.

4.1.2 Cell Geometry: Residence Time and Channel Thickness

With an increase in residence time, the feed solution velocity and volume flow rate decreases (at t_{res} 50 s the feed solution flow velocity is $1.6{\cdot}10^{-3}\,\mathrm{m\,s^{-1}}$). This decreases the pressure drop across the inlet and the outlet of the RED stack. This results in a decrease in the pumping power needed. Nevertheless, the increase in residence time increases the amount of salt diffusing through the membrane, which increases the waste heat per unit volume. However, as the volume flow rate decreases, the total heat required to restore the concentrations decreases, as shown in Figure 4.2. As we operate at peak power current density, the influence

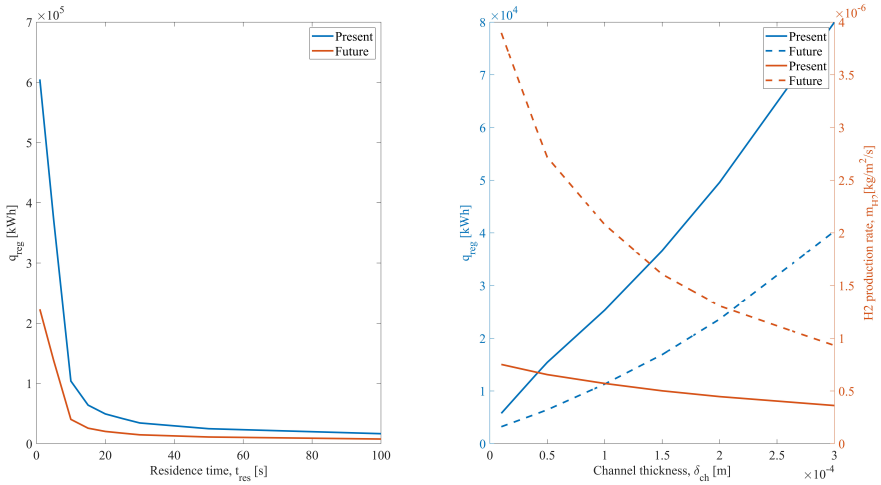

Fig. 4.2: Waste heat required and H_2 production rate as a function of residence time (left) and channel thickness (right).

of the resistance from the diffusion boundary layer and the electrical double layer on current density and electrochemical potential is neglected. Hence, the H_2 production rate is not affected by residence time. However, with an increase in residence time, these resistances will tend to dominate, and the H_2 production rate would decrease.

An increase in the channel thickness increases the ohmic resistance of the channels, decreasing the actual unit cell potential. The decrease in open circuit potential decreases the peak power current density, decreasing the H_2 production rate and the salt flux. Hence, the waste heat per unit volume of dilute solution required also decreases. However, the increase in channel thickness causes an increase in feed solution volume flowing through the channel. This causes an increase in the total waste heat required to regenerate the ammonium bicarbonate solutions. This increase in the heat requirement nullifies the decrease in waste heat per unit volume due to the decrease in salt flux. Thus, the net effect observed is an increase in the total heat required, as shown in Figure 4.2. Moreover, the increase in channel thickness increases the feed solution flow rate. The increase in flow rate increases the amount of water per gram of salt transported; thus, J_{osm} increases. Hence, the total heat required to recover the same amount of salt increases.

4.1.3 Economic Comparison: capital expenses and levelised cost of hydrogen

A scenario analysis was done for present and future scenario in terms of cost composition as shown in Figure 4.3. In the case of the present scenario, the CAPEX composition is dominated by 55% for the regeneration system and 28% for the membranes and RED stack. In the case of the future scenario, the regeneration system contributes the most with 77% . The share of

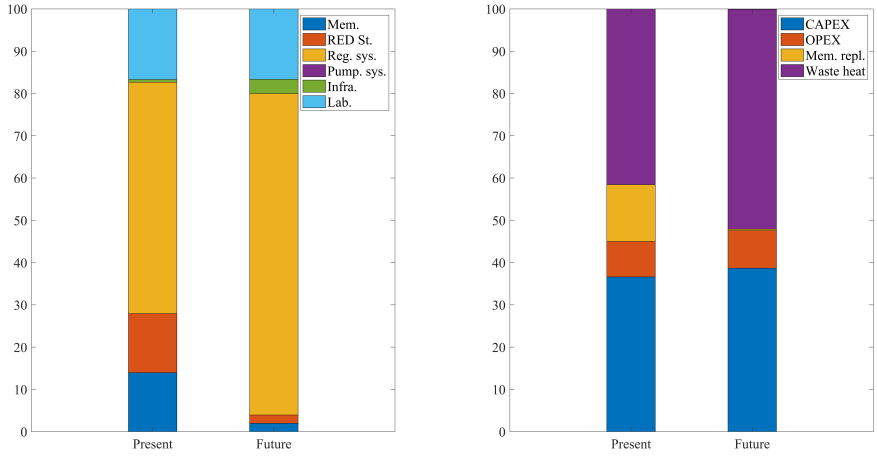

Fig. 4.3: Comparison of component contribution to CAPEX for present and future scenario (left) and comparison of cost composition of LCH for present and future scenario (right).

CAPEX for the regeneration system is high because of the high-volume flow rate of the dilute solution and the high amount of heat required per unit volume of the dilute solution.

In LCH composition for the present scenario, the costs associated with waste heat and CAPEX contribute most with 42% and 37%, respectively. The major contributor to CAPEX is the regeneration system. Hence, the regeneration system must be optimised to reduce its contribution to LCH further.

4.1.4 Economic Analysis: Membrane Cost, Lifetime and Waste Heat Cost

The membrane cost and the cost of waste heat have a linear relation with the LCH as shown in Figure 4.4. For every euro, the membrane cost increases the LCH increases by 0.055 € $kg_{H_2}^{-1}$ and 0.01 € $kg_{H_2}^{-1}$ for present and future scenario, respectively. In the case of the cost of waste heat, for every 0.001 € kWh^{-1} increase, the LCH increases by 4.02 and 1.78 € $kg_{H_2}^{-1}$. The membrane life increases from 3 years to 10 years, the LCH decreases approximately by 40% of the initial value for input values stated in Publication I. Membrane life of more than four years has no significant influence on the LCH Publication II. The minimum predicted cost of the membrane was calculated using the learning rate of 25 mm Nafion membrane for a production rate of $60{\cdot}10^8$ m^2 per year. The minimum membrane cost was found to be 1.69 $V\,m^{-2}$. For ammonium bicarbonate RED system, the membrane cost, C_{mem}, must drop below 2.86 and 22.3 $V\,m^{-2}$ for membrane lifetime t_{mem} of 4 and 10 years at a production rate of 1.19 and 3.71 $mol\,m^{-2}\,h^{-1}$, respectively, to compete with other clean energy technologies.

The membrane resistance and permselectivity have linear and non-linear relation with LCH. While the increase in membrane resistance increases LCH, an increase in permselectivity

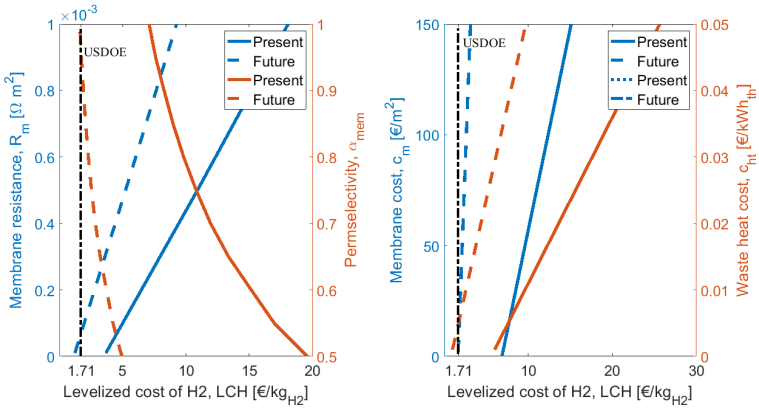

Fig. 4.4: Influence of membrane resistance on waste heat required and H_2 production for present and future scenarios (left). Influence of permselectivity on waste heat required and H_2 production rate (right).

decreases LCH. In a future scenario, at permselectivity as high as 0.95 and membrane resistance as low as 0.1 Ωm^2 the LCH can reach the US DOE target for other thermodynamic and economic parameters are kept constant.

4.2 Publications III

From the previous work in publication II, it is clear that membrane resistance plays a vital role in determining the performance of the RED system. This study evaluates the membrane resistances and studies its influence on hydrogen production rate, specific waste heat, and LCH. The membrane area resistances were estimated using equivalent circuit modelling of the data from the impedance measurement using a simple equivalent circuit as shown in Fig. 3.5. The resistance in series (R_{m+ele}) is associated with the ohmic resistance from the membrane and the electrode. A blank cell measurement was performed to estimate the electrode resistance. This value was subtracted from R_{m+ele} to estimate the membrane resistance values. In the following section, the measured values for R_{mem} will be reported and discussed.

4.2.1 Influence of thickness on membrane resistance and membrane resistance at elevated temperature

The membrane resistance is not only a material property, and it is a ratio between the membrane thickness and its conductivity. With increasing membrane thickness, the length of the transport pathway increases, and the membrane resistance increases proportionally. For all of the IEMs considered in this study, we observe a linear relationship between membrane resistance and membrane thickness. This has been shown for AEMs at 295 ± 2 K and 313 ± 1 K in publication III Figs. 5 and 7, and for the CEMs at the same temperatures in

Figs. 6 and 8. The membrane resistance is here found to increase with increasing thickness. Linear regression was used to fit the resistance as a function of thickness, and the coefficients of these polynomials and their uncertainties are provided in the publication III Appendix Tables A(1-4). Though the linear equation describes the effect of thickness on the resistance reasonably well, we observe a high double standard deviation in the resistivity (the slope of the equation). This is likely to be associated with the high variation in the IEM thickness, which is difficult to measure for swollen membranes, especially for the APS type (AEM). The increase in resistance due to an increase in thickness is because an ion has to traverse further through the tortuous path inside of the membrane. Even though the AEMs are thinner compared to CEMs, in general, the CEM have lower resistances compared to the AEM. This may be due to the mobility of NH_4^+ ions, which is very high compared to the mobility of HCO_3^- ions, as shown in Table. 4.1.

Tab. 4.1: Properties of the ions considered in this study

Ion	**NH_4^+**	**HCO_3^-**
Hydrated radius [nm]	0.331	0.439
Charge density [mC cm^{-3}]	1.05	0.45
Average polarizability [a.u]	7.91	23.7
Ionic mobility [$cm^2V^{-1}s^{-1}$]	$7.71 \cdot 10^{-4}$	$4.59 \cdot 10^{-4}$

The Fumasep membranes with reinforcement, FASPET and FKSPET, have higher resistances compared to FAS and FKE. The increased resistance can be explained by the increased thickness (polyester reinforcement). FAS and FASPET follow a similar trend in the resistance as a function of the thickness. It is difficult to evaluate the membranes based on their thickness normalised membrane conductivity or membrane's ohmic resistance, as they give a different prioritisation of which membranes should be preferred. Although a thinner membrane may show lower conductivity at different concentrations, the measured membrane resistance of the thinner membranes can be lower than the thicker membranes with the highest conductivity. This is because of the physical properties of the membrane, such as water content, fixed charge density etc.

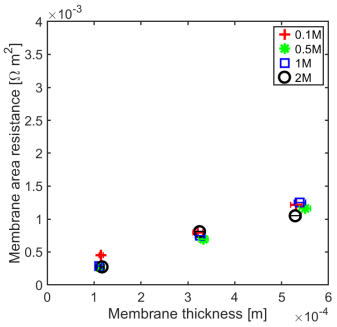

(a) DSV at 298 K

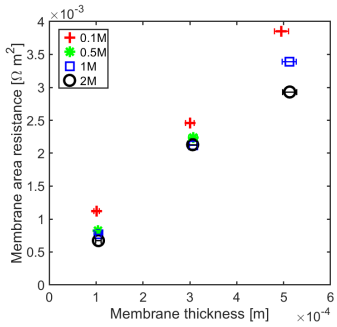

(b) AMV at 298 K

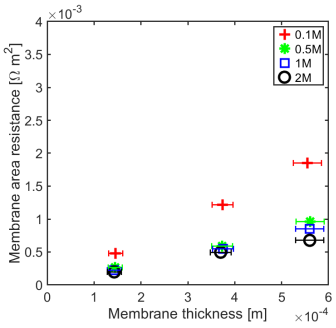

(c) APS at 298 K

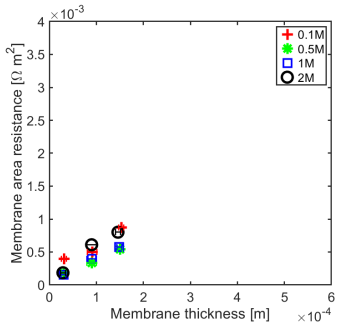

(d) FAS at 298 K

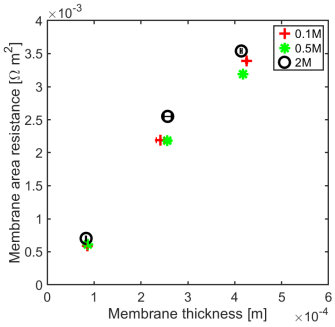

(e) FASPET at 298 K

Fig. 4.5: Anion exchange membrane (AEM) resistance as a function of thickness for different concentrations at 298 K.

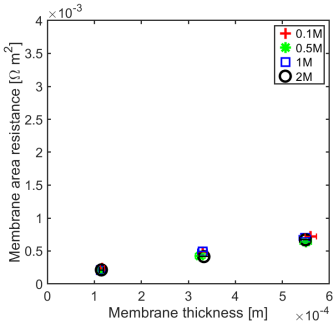

(a) DSV at 313 K

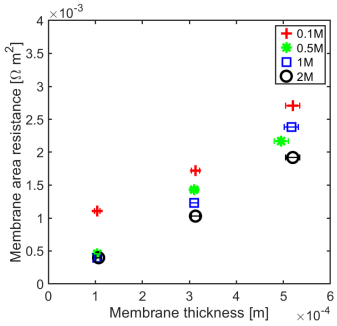

(b) AMV at 313 K

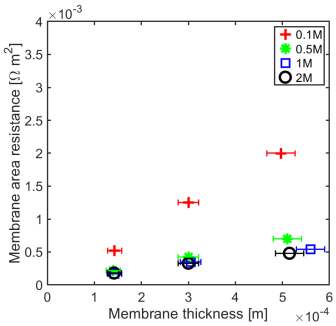

(c) APS at 313 K

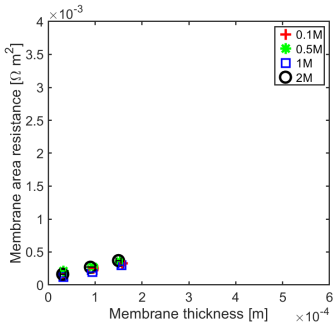

(d) FAS at 313 K

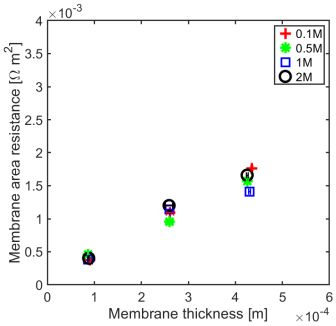

(e) FASPET at 313 K

Fig. 4.6: AEM resistance as a function of thickness for different concentrations at 313 K.

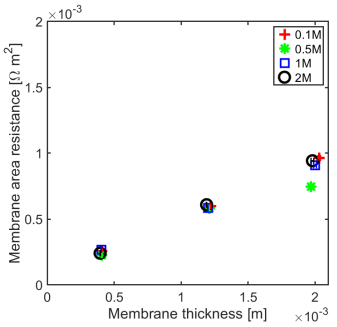

(a) CMF at 298 K

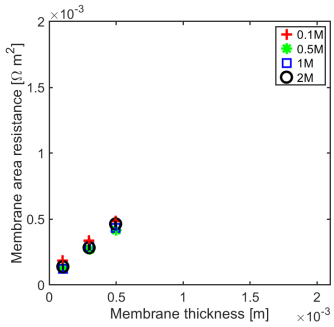

(b) CMV at 298 K

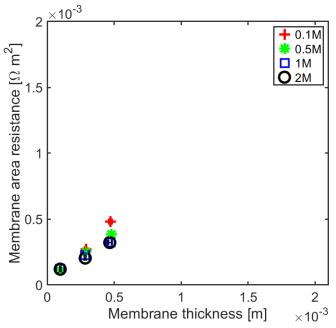

(c) CSO at 298 K

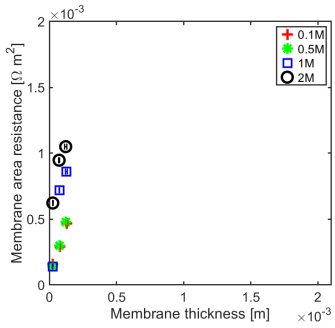

(d) FKE at 298 K

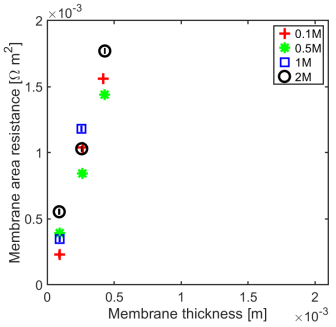

(e) FKSPET at 298 K

Fig. 4.7: Cation exchange membrane (CEM) resistance as a function of thickness for different concentrations at 298 K.

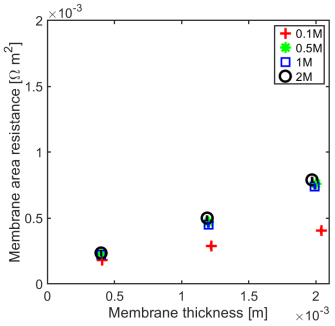

(a) CMF at 313 K

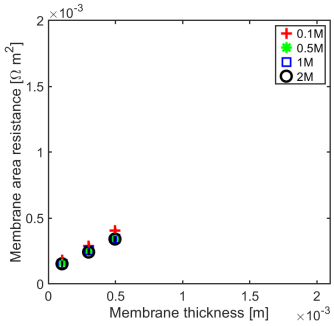

(b) CMV at 313 K

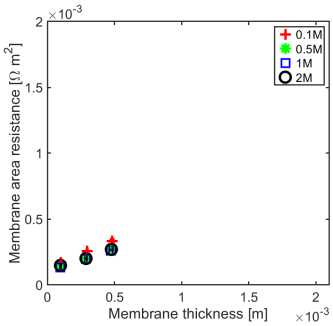

(c) CSO at 313 K

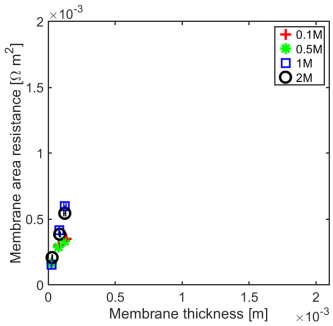

(d) FKE at 313 K

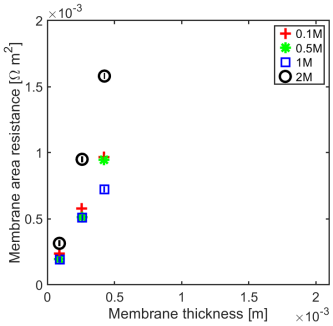

(e) FKSPET at 313 K

Fig. 4.8: CEM resistance as a function of thickness for different concentrations at 313 K.

In general, the membrane resistance decreases with increasing temperature. This is due to the increase in ionic mobility through the membrane, which increases with temperature.

4.2.2 Influence of concentration on membrane conductivity

Fig. 4.9 shows how the conductivities of the different AEMs and CEMs change with concentration. The first conclusion that can be made based on these results is that the conductivities of the CEMs are typically significantly higher than those of the AEMs. The mobility ratio of ammonium ions to bicarbonate ions is 1.67, which may explain higher conductivity in the CEM membrane than AEM.

The electrolyte concentration influences the various IEMs differently. In the CEMs, CMF and CSO exhibit the highest conductivities of all the membranes at both temperatures examined. For the AEMs, APS and DSV have the highest conductivities at both temperatures. APS and CSO display a clear trend, where the conductivity increases with increasing concentration.

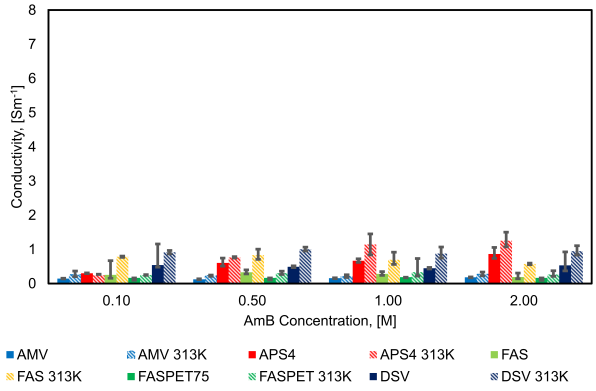

(a) AEM

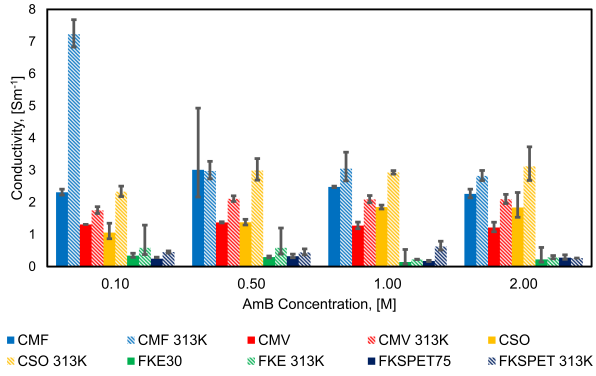

(b) CEM

Fig. 4.9: Effect of the solution concentration on the IEM conductivity

AMV, DSV and FKE have the lowest conductivities at 0.5 M and 1 M, respectively, and the conductivities increase/remain constant with further increase in concentration. This may be due to loss of water through the IEM or shrinkage, causing loss of conduction paths. In FAS, FASPET and CMV, the conductivity decreases with an increase in a concentration above 0.5 M, and it is lowest at 2 M. CMF shows almost constant conductivity with an increase in concentration. The exact values of the mean conductivities of the membranes are reported in publication III, appendix Tables a5 and a6.

4.2.3 Influence of membrane resistance on hydrogen production rate and specific waste heat required

After the membrane characteristics have been determined experimentally, it is of interest to study how they influence the performance of a RED stack for the generation of hydrogen by use of waste heat. Based on the measured values, we find a lower ohmic resistance for the membranes gives a higher hydrogen production rate and lower waste heat required per kg of hydrogen. The article compares the hydrogen production rate and specific waste heat required for membranes with the highest conductivity (APS and CMF) with the least resistance (FAS and CSO). The highest conductivity was found for a stack made with APS and CMF for 2 M/0.1 M feed solutions concentration. The hydrogen production rate and specific waste heat required based on APS and CMF membranes were found to be $6.51 \cdot 10^{-7}\,\mathrm{kg\,m^{-2}s^{-1}}$ and $419\,\mathrm{kWh\,kg_{H_2}^{-1}}$ respectively. For a stack made of FAS and CSO membranes as AEM and CEM with the least area-specific resistance ($\Omega\ \mathrm{m^2}$) for 2 M/0.1 M feed solutions concentration at room temperature, the corresponding hydrogen production rate and specific waste heat required is $8.48 \cdot 10^{-7}\,\mathrm{kg\,m^{-2}s^{-1}}$ and $344\,\mathrm{kWh\,kg_{H_2}^{-1}}$. The hydrogen production from a RED stack with NaCl solution operating at seawater/river water concentration- 0.6 M/0.0015 M was theoretically estimated to be $9.64 \cdot 10^{-7}\,\mathrm{kg\,m^{-2}s^{-1}}$ and artificial NaCl solution with concentrations 4 M/0.017 M was experimentally found to be $4.94 \cdot 10^{-8}\,\mathrm{kg\,m_{ele}^{-2}s^{-1}}$ [24], [60].

Compared with the proposed system, the reasons for the low hydrogen production rate can be low permselectivity, high area-specific membrane resistance, high overpotentials and the effect of activity coefficients. In comparison, the conventional electrolysis such as alkaline electrolysers operating at atmospheric conditions the hydrogen production rate was found to be $2 \cdot 10^{-4}\,\mathrm{kg\,m^{-2}s^{-1}}$ [74], [75]. Hence, an increase in the membrane resistance decreases the electrochemical potential of the stack and thus, the resulting peak power current density decreases. This decrease in current density decreases the number of hydrogen moles produced due to the water's electrolysis. From the previous sections, it is clear that a thinner membrane can have low area-specific resistance but can be relatively less conducive, for example, FKE. On the other hand, a thicker membrane can have more resistance but can be relatively highly conductive, for example, CMF. The results signify that the membrane's thickness plays a vital role in improving the hydrogen production rate. In the thermodynamic model to calculate the peak power density produced, we consider area-specific resistance, and we emphasise ohmic resistance rather than conductivity. Therefore, a stack made of CMF/APS has a higher area-specific resistance than CSO/FAS and was not chosen as optimum. Furthermore, the decrease in the operating current density causes a decrease in the amount of salt transported through a membrane due to electro-migration and decreases the amount of water dragged along due to electro-osmosis. As the salt flux decreases, the concentration of dilute solution at the outlet decreases. The decrease in the dilute solution concentration decreases the waste heat required per unit volume of a dilute solution (q_{th} [$\mathrm{kWh\ m^{-3}}$]). However, the total waste heat required per kg of hydrogen produced increases as the volume of the dilute solution at reduced current densities increases due to an increased number of unit cells required to develop the potential in a stack required for electrolysis of water.

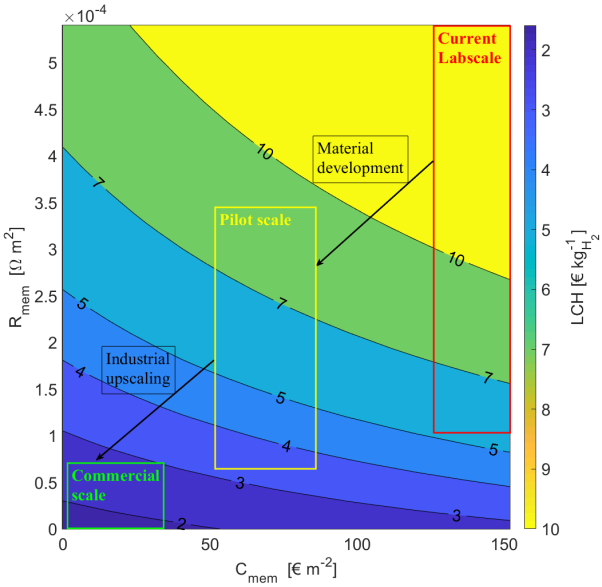

Fig. 4.10: LCH as a function of membrane resistance for different membrane cost. Here we assume the membrane resistances $R_{aem} = R_{cem}$. CSO and FAS permselectivities were measured and used as input. The membrane cost range assumed for lab, pilot and commercial scale is 130-150, 50-80 and less than 30 € m^{-2}, respectively. The cost of heating is assumed to be 0.005 € kWh^{-1} [69]. We assume for the pilot-scale that the material development will lead to cheaper and less resistive membranes, i.e. SPEEK or carbon-based membranes, and that for the commercial-scale, these membranes will be produced at a large scale ($60 \cdot 10^8$ m^2 per year) and reduced thickness (25 μm and maintaining the mechanical strength) which will, in turn, reduce the cost and resistance further [69], [76], [77].

4.2.4 Influence of membrane resistance on thermodynamic efficiency and levelised cost of hydrogen

An increase in the membrane resistance decreases the thermodynamic efficiency, η and increases the levelised cost of hydrogen (LCH), as shown in Fig 4.10. For a stack made of FAS and CSO membranes as AEM and CEM with the least area-specific resistance (Ω m^2) for 2 M/0.1 M feed solutions concentration at room temperature, the thermochemical conversion efficiency was found to be 9.7%, and the LCH was estimated to be 7.80 € $kg_{H_2}^{-1}$. The highest conductivity was found for a stack made with APS and CMF for 2 M/0.1 M feed solutions concentration. The corresponding thermodynamic efficiency and LCH estimated were 8.00% and 9.99 € $kg_{H_2}^{-1}$. The membranes with a lower resistance give a higher thermochemical conversion efficiency, lower waste heat required per kg of hydrogen and lower levelised cost of hydrogen. Thus, with an increase in membrane resistance, the thermochemical conversion efficiency decreases and the LCH increases significantly. The increase in membrane resistance

decreases the cell's performance by decreasing operating potential and peak power current density. Furthermore, with an increase in membrane resistance, the amount of heat required to restore the concentrations to original increases due to the increased amount of solution from the stack needed for the same amount of hydrogen production capacity. Therefore, a decrease in efficiency can be observed. In the case of LCH, the number of membranes required increases with an increase in the membrane resistance and hence the investment cost and membrane replacement cost increases. Moreover, an increase in the volume of the outlet solutions increases the capacity of the regeneration system, which in turn increases the cost. All these factors cause an increase in LCH.

4.3 Publication IV

From the previous work in publication II, it is clear that membrane permselectivity plays a vital role in determining the performance of the RED system. In this study, we evaluate the permselectivity of the least resistive membranes and study its influence on hydrogen production rate, specific waste heat and LCH. We measured open-circuit potentials of commercial IEM using two single-junction Ag/AgCl reference electrodes and estimated the transport numbers of salt and water for ammonium bicarbonate solution at different concentrations. We corrected the junction potentials due to salt bridges and bias from the reference electrodes. The results of the same are stated below. We assume averaged permselectivity of an IEM to estimate the hydrogen production rate, waste heat required, thermochemical conversion efficiency and levelised cost of hydrogen. Permselectivity at concentrations 2 M and 0.1 M were averaged.

4.3.1 Influence of concentration on membrane potential and permselectivity

As discussed in the background section, the concentration of bulk solution influences the measured membrane potential. From figure 4.11 we see that with an increase in bulk concentration, the membrane potential increases but the permselectivity decreases. This is due to the weakening of Donnan exclusion which allows transport of co-ions. With the increase in feed solution concentrations, the permselectivity decreases due to a decrease in the charge-exclusion ability of the membrane. The non-equilibrium thermodynamic model developed for the present system also shows that water transport decreases permselectivity. The number of moles of electrolyte and water transported reversibly with the electric current is known as transference coefficients [78]. Reversible conditions are, in this case, characterised by uniform chemical potential profiles. If we assume that the electrolyte and water transference coefficients are constant in the concentration range, then the reduction in permselectivity may be explained by the ratio of the chemical potential differentials for water and salt. The movement of salt creates electric energy down a concentration gradient. However, water is transported along with the salt in a process that reduces the net work output of the cell [79]. Thus the effect of the water transfer is higher if one or both of the electrolyte solutions are highly concentrated. This effect is shown as a contour plot of a range of concentrations in figure 4.13.

Tab. 4.2: Influence of concentration on Liquid junction potential and electrode bias

	$\mathbf{N}_j$	$\Delta\mathbf{E}_j^{SB}$	$\mathbf{E}_b^{ref}$
3M KCl	1	-	0.55±0.11
	2	-	0.92± 2.26
3.5M KCl	1	0.79±0.33	0.73±0.01
	2	0.84± 0.04	0.84±0.07
4M KCl	1	0.5±0.02	0.55±0.04
	2	-0.79±0.04	-0.83±0.07

The transference numbers are, in fact, dependent on concentrations and may also act in a way that decreases the permselectivity at higher concentrations [80]. Measured electric potentials and permselectivities for FAS and CSO are shown in figures 4.12 and 4.11. It was found that the permselectivity of the AEM is lower than the CEM. This must result from a lower transference number of salt for the AEM or a higher water transference number.

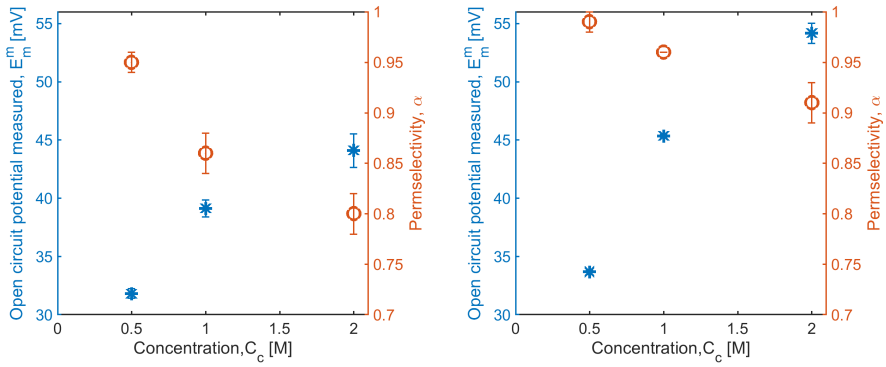

(a) AEM, FAS. **(b)** CEM, CSO.

Fig. 4.11: Concentration effect on permselectivities and measured electric potential of an AEM and a CEM. The dilute solution was kept at constant concentration of 0.1 M and the concentrate solution was varied 0.5 M, 1 M and 2 M.

4.3.2 Influence of liquid junction potentials and reference electrode bias

As discussed in the background section, it is not easy to calculate the exact LJP thermodynamically as it requires treatment of single-ion activity in the Planck- Henderson equation. We measured the LJP of salt bridges at different concentration we found no clear trend in measured LJP with the increase in concentration. It was also found that the measured bias between the reference electrodes influences the measurements. They may change their polarity when they are refilled, and other operating conditions are kept the same. The summary of the measured LJPs and bias potentials are depicted in 4.2.

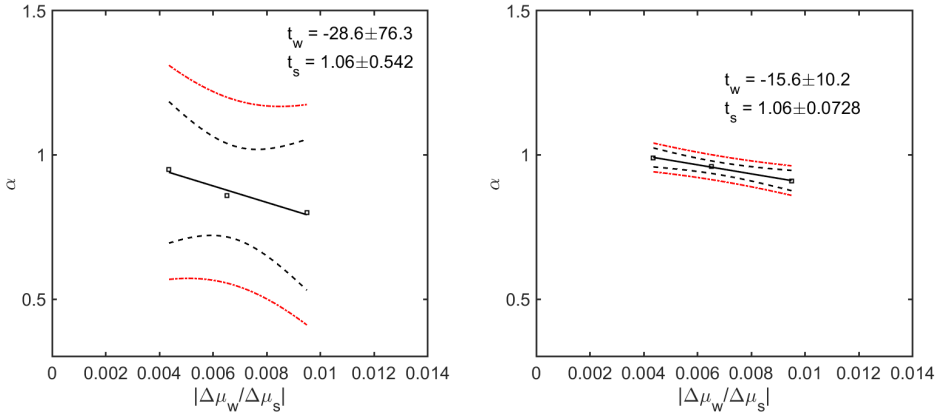

(a) AEM, FAS. **(b)** CEM, CSO.

Fig. 4.12: Concentration effect on permselectivities of an AEM and a CEM. The dilute solution was kept at constant concentration of 0.1 M and the concentrate solution was varied 0.5 M, 1 M and 2 M. The that t_w is typically reported in the literature with opposite signs because the water is transported in opposite directions for AEM and CEM.

4.3.3 The influence of permselectivity on hydrogen production and waste heat requirement

The increase in permselectivity increases the electrochemical potential of the IEM, increasing the operating voltage of the RED stack. This increases the current density, which increases the hydrogen production rate. The peak power density of a typical reverse electrodialysis system is directly proportional to the square of permselectivity. Similarly, the hydrogen production rate at peak power current density is directly proportional to the square of permselectivity. Therefore, an increase in permselectivity increases the hydrogen production rate. At concentrations 2 M/0.1 M, for a stack made of FAS and CSO having permselectivities of 0.8 and 0.91 respectively, the hydrogen production rate was estimated to be $8.05{\cdot}10^{-7}$ kg m^{-2}s^{-1} As the electrochemical potential of a cell pair increases, the number of cell pairs required

Tab. 4.3: Concentration effects on liquid junction potentials of salt bridge. Here SJE and DJE refers to single junction electrode and double junction electrode

AmB		**SJE**	**DJE**
0.5|0.1 M	E_j^{HC} - E_j^{LC} (mV)	0.972±0.06	2.512±0.15
	α	0.03	0.07
1|0.1 M	E_j^{HC} - E_j^{LC} (mV)	-0.937±0.04	-
	α	0.02	-
2|0.1 M	E_j^{HC} - E_j^{LC} (mV)	3.26±0.06	-0.703±0.05
	α	0.06	0.01

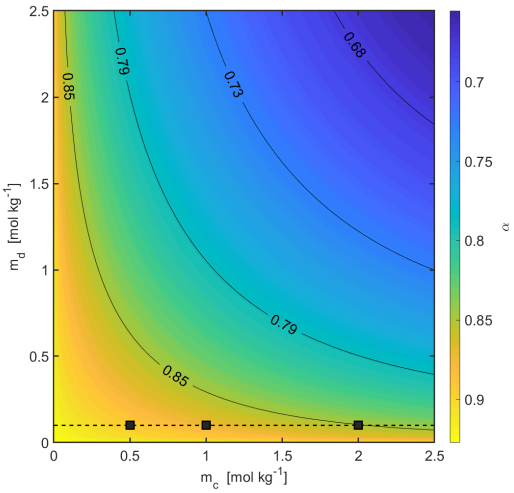

Fig. 4.13: Contour plot of a range of concentrations for m_c and m_d and the resulting permselectivity given $t_s = 0.93$ and $t_w = 8$. Transference numbers are taken from an experimental study by Zlotorowicz *et al.* [79].

to achieve the potential for water electrolysis decreases. This, in turn, relates to a smaller dilute solution volume. This relates to less total heat required. At concentrations 2 M/0.1 M, for a stack made of FAS and CSO having permselectivities of 0.8 and 0.91 respectively, the waste heat required was estimated to be 366 kWh $kg_{H_2}^{-1}$.

4.3.4 The influence of permselectivity on thermodynamic efficiency and levelised cost of hydrogen

As discussed in the previous subsection, permselectivity positively impacts the hydrogen production rate and reduces waste heat required. Cumulatively this increases the thermochemical conversion efficiency. The thermochemical conversion efficiency for a RED stack made of FAS and CSO was estimated to be 9.1%. An increase in permselectivity reduces the number of cell pairs required, reducing the waste heat required. A decrease in the amount of membrane needed and less total waste heat required corresponds to lowering the levelised cost of hydrogen as shown in the 4.14. The LCH for a RED stack made of FAS and CSO was estimated to be 10.132 € $kg_{H_2}^{-1}$.

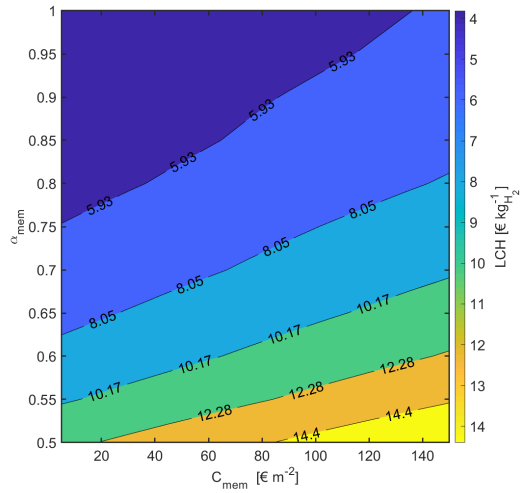

Fig. 4.14: LCH as a function of membrane permselectivity and membrane cost. Here, we assume the membrane resistances such that $\alpha_{aem}=\alpha_{cem}$.

5 Overall Conclusions

A thermodynamic model for reverse electrodialysis of ammonium bicarbonate to produce hydrogen was developed in the present work. An economic model to determine the levelised cost for the hydrogen production from a thermally driven reverse electrodialysis system was developed. Moreover, membrane properties such as permselectivity and membrane resistance were determined experimentally.

5.1 Publications I and II

In the thermodynamic model, we studied the influence of parameters such as the concentration of feed solutions, membrane properties- permselectivity and membrane resistance, cell geometry- channel thickness, residence time on hydrogen production and waste heat required per unit mass of hydrogen produced. A maximum observed for hydrogen production and a minimum observed for required waste heat that changes with feed solutions concentration. For the RED stack's specific geometry and operating conditions, the increase in concentration ratio increases open circuit potential and reduces the ohmic resistance of the IEMs in the stack, which increases the current density at peak power, which increases hydrogen production rate. When the dilute solution concentration increases beyond 0.1 M, the concentration ratio reduces (as the concentration of concentrate is kept constant 2.6 M), reducing the open circuit potential, the current density at peak power and hydrogen production rate. An opposite trend is observed for the waste heat required for restoring the salt concentration. An increase in the dilute solution's concentration increases the waste heat required per unit volume to restore an increased salt amount. However, as the concentration ratio decreases, the electrochemical potential decreases, so the number of cell pairs necessary to produce a specified amount of hydrogen increases and therefore, the volumetric flow rate increases. The increase in volumetric flow rate causes an increase in the required waste heat. With an increase in residence time, the feed solution velocity and volume flow rate decreases. This decreases the pressure drop across the inlet and the outlet of the RED stack. This results in a reduction of pumping power needed. As we operate at peak power current density, the influence of the resistance from the diffusion boundary layer and the electrical double layer on current density and electrochemical potential is neglected. Hence, the H_2 production rate is not affected by residence time. However, with an increase in residence time, these resistances will dominate, and the H_2 production rate would decrease. Nevertheless, the increase in residence time increases the amount of salt diffusing through the membrane, which increases the waste heat per unit volume; however, as the volume flow rate decreases, the total heat required to restore the concentrations decreases. An increase in channel thickness increases the channels' ohmic resistance, decreasing the actual unit cell potential. This, in turn, reduces the H_2 production rate and the salt flux. Hence, the waste heat per unit volume of dilute solution required also decreases. However, the increase in channel

thickness causes an increase in feed solution volume flowing through the channel. This causes an increase in the total waste heat required to regenerate the ammonium bicarbonate solutions. This increase in the heat requirement nullifies the decrease in waste heat per unit volume due to the salt flux reduction. Thus, the net effect observed is an increase in the total heat required. The increase in channel thickness increases the feed solution flow rate. The increased inflow rate increases the amount of water per gram of salt transported; thus, the osmotic water flux, J_{osm} increases. Hence, the total heat required to recover the same amount of salt increases. From the economic model, it was clear that membrane and regeneration system cost dominates the capital expenses contributing more than 70%. The capital expenses and waste heat contributes to more than 70% of the levelised cost of hydrogen. From scenario analysis, in future, the cost of the membrane can be reduced to 1.69 € m^{-2} with an increase in membrane production rate, a reduction in production and raw material cost, and a reduction in membrane thickness. AmB RED for H_2 production has economic potential at membrane cost of less than 4.5 € m^{-2}, and membrane life of 4 years or more. Finally, a thermally driven RED system with a regeneration system cost of less than 3000 € kWh^{-1} m^{-3} and a waste heat cost of less than 0.005 € kWh^{-1} can present an economically feasible for utilisation of low-grade waste heat for H_2 production. There are two scenarios with input parameters, as shown in Table 3.2.

For every euro, the membrane cost increases the LCH increases by 0.055 € $kg_{H_2}^{-1}$ and 0.01 € $kg_{H_2}^{-1}$ for present and future scenario, respectively. In the case of the cost of waste heat, for every 0.001 € kWh^{-1} increase, the LCH increases by 4.02 and 1.78 € $kg_{H_2}^{-1}$. Membrane life of more than four years has no significant influence on the LCH.

5.2 Publication III

Experimental studies were performed on ten commercial membranes to evaluate concentration and temperature effect on membrane conductivity or area-specific resistance. It was found that the area-specific membrane resistance increases linearly with thickness. It was found that cation exchange membranes (CEMs) have higher conductivities than anion exchange membranes (AEM) for nearly all of the concentrations examined (0.1 M, 0.5 M, 1 M and 2 M), and this may be due to the higher mobility of ammonium ions compared to bicarbonate ions. For use combined with reverse electrodialysis, the membranes with the least area-specific resistance were found for a stack consisting of the FAS type AEM and the CSO type of CEM.

Membrane conductivity increases the H_2 production because the electrochemical potential increases, which increase the current density at peak power. The increase in membrane resistance decreases the current density, which causes a reduction in the amount of salt transported through a membrane due to electromigration and reduces the amount of water dragged along due to electro-osmosis. As the amount of salt flux is low, there is a relatively more minor increase in the outlet dilute solution concentration. This decrease in dilute concentration causes a reduction in waste heat required per unit volume of a dilute solution (q_{th} kWh m^{-3}). Nevertheless, the total(waste) heat required per kg of H_2 produced increases

as the dilute solution's volume at reduced current densities increases due to an increased number of cell pairs in a stack necessary for water electrolysis.

A RED stack made of membranes that are highly conductive and low area-specific resistance were compared. In closed-loop ammonium bicarbonate reverse electrodialysis system that uses CMF/APS type of membranes in combination with waste heat to generate hydrogen, the hydrogen production rate and specific waste heat required based were estimated to be $6.51 \cdot 10^{-7}\,\mathrm{kg\,m^{-2}s^{-1}}$ and $413\,\mathrm{kWh\,kg_{H_2}^{-1}}$. This resulted in a thermodynamic efficiency of 8.00% and an estimated levelised cost of hydrogen of $9.99\,€\,\mathrm{kg_{H_2}^{-1}}$. Of the membranes examined in this work, the FAS type of AEM and the CSO type of CEM was found to have the least area-specific resistance. With a closed-loop reverse electrodialysis system with these membranes, the hydrogen production rate and specific waste heat required are estimated to be $8.48 \cdot 10^{-7}\,\mathrm{kg\,m^{-2}s^{-1}}$ and $344\,\mathrm{kWh\,kg_{H_2}^{-1}}$ respectively. This resulted in a thermodynamic efficiency of 9.7 % and an estimated levelised cost of the hydrogen of $7.80\,€\,\mathrm{kg_{H_2}^{-1}}$.

5.3 Publication IV

Experimental studies were performed on two membranes with the least area-specific resistance in ammonium bicarbonate solution to evaluate the concentration effect on membrane permselectivity. The proposed method to measure membrane potential using salt bridges made of agar and 4 M KCl using Ag/AgCl reference electrodes dipped in 4 M KCl developed low liquid junction potential. It was also found that the junction potentials from the salt bridge influences measured open circuit potential. We determine the permselectivity of cation exchange membrane CSO and anion exchange membrane FAS for concentrations 0.5 M/0.1 M, 1 M/0.1 M and 2 M/0.1 M. We observe that the membrane potential increases with an increase in the concentration of concentrate solution keeping dilute solution concentration constant. However, for both membranes, the permselectivity decreases with an increase in the concentration of concentrate solution. It was found that the CSO had higher permselectivity compared to FAS at all concentrations. This can be due to higher ion exchange capacity/ fixed charge density, as suggested in the literature. Further, there was no clear trend to evaluate the influence of ammonium bicarbonate concentration on liquid junction potential. The junction potential was found to introduce additional potential contributing to a maximum of 7% change in the permselectivity.

Membrane permselectivity increases the H_2 production because the electrochemical potential increases, which increase the current density at peak power. The decrease in permselectivity decreases the current density, which causes a reduction in the amount of salt transported through a membrane due to electromigration and reduces the amount of water dragged along due to electro-osmosis. As the amount of salt flux is low, the outlet dilutes solution concentration decreases. This decrease in dilute concentration causes a reduction in waste heat required per unit volume of a dilute solution (q_{th} $\mathrm{kWh\,m^{-3}}$). Nevertheless, the total(waste) heat required per kg of H_2 produced increases as the dilute solution's volume at reduced current densities increases due to a higher number of cell pairs in a stack. At concentrations 2 M and 0.1 M AmB we find the hydrogen production rate, thermochemical

efficiency, waste heat required, and levelised cost of hydrogen were estimated values are $8.05{\cdot}10^{-7}\,\mathrm{kg\,m^{-2}s^{-1}}$, 9.1%, $365.87\,\mathrm{kWh\,kg_{H_2}^{-1}}$, $10.132\,€\,\mathrm{kg_{H_2}^{-1}}$, respectively.

6 Further Work

The developed model had some shortcomings, and it was assumed that the resistance due to bubble formation at the electrodes, the resistance due to diffusion boundary layer and the double layer was negligible.

The regeneration model used the empirical relations for mass balances taken from literature developed for specific operating conditions. An ASPEN Plus model can be developed to have an engineered value and more control over operating conditions.

The economic model assumed the cost of endplates, gaskets, spacers and electrodes equal to the membranes. The up-scaling effect on the cost of these components as well as the regeneration system was not considered. An engineered cost model can be developed using the CAPCOST tool. In up-scaling, the raw material prices are functions of primary cost, purchase quantity or customer relationship. The input data from vendor inquiries prices for chemicals can be extracted from the PRODCOM database of the statistical office of the European Commission EUROSTAT.

The literature on life cycle assessment (LCA) of thermally driven reverse electrodialysis for a hydrogen production system is limited. Hence, developing a case study in SimaPro to compare the carbon emissions equivalent and other environmental impact parameters of this system in the context of low-grade waste heat to hydrogen production for industries such as waste incineration, cement and paper would provide more insight.

The membrane properties such as swelling degree, ion exchange capacity, co and counter ion concentration were not determined, which can help better understand the influence of concentration and temperature on permselectivity, membrane resistance and water and salt permeabilities.

The actual hydrogen production rate can be measured and compare with the model. The RED stack made of IEMs with high pemselectivity and low area-specific resistance for ammonium bicarbonate solution can be tested. The stack measurements can be performed under different operating conditions, such as a number of cell pairs in a stack that produce potential necessary for hydrogen evolution reaction, increased operating temperature, variation in flow rate of feed solutions.

Future efforts must be directed to evaluate the performance of potential salts that are highly conductive, highly soluble, and may require less heat for recovery, such as lithium bromide.

Part II

Publications

This part of the thesis contains the Four publications conducted during this PhD work:

1. Y D. Raka, H Karoliussen, K M. Lien and O S. Burheim, "Opportunities and challenges for thermally driven hydrogen production using reverse electrodialysis system", *International Journal of Hydrogen Energy, vol.45 (2020), 1212-1225*

2. Y D. Raka, R Bock, J J. Lamb, B G. Pollet and O S. Burheim, "Low-Grade Waste Heat to Hydrogen", *Micro-optics and energy: sensors for energy devices, Springer Nature (2020), 85-114*

3. Y D. Raka, R Bock, ØWilhelmsen, H Karoliussen, and O S. Burheim , "The Influence of Concentration and Temperature on the Membrane Resistance of Ion Exchange Membranes and the Levelised Cost of Hydrogen from Reverse Electrodialysis with Ammonium Bicarbonate", *Membranes (2021), 11, 135*

4. Y D. Raka, S B B Solberg, R Bock, ØWilhelmsen, H Karoliussen, and O S. Burheim , "Permselectivity of IEMs for ammonium bicarbonate- influence of junction potentials and reference electrodes", *manuscript*

INTERNATIONAL JOURNAL OF HYDROGEN ENERGY 45 (2020) 1212–1225

Available online at www.sciencedirect.com

ScienceDirect

journal homepage: www.elsevier.com/locate/he

Opportunities and challenges for thermally driven hydrogen production using reverse electrodialysis system

*Yash Dharmendra Raka, Håvard Karoliussen, Kristian Myklebust Lien, Odne Stokke Burheim**

Dep. of Energy and Process Engineering, Faculty of Engineering, Norwegian University of Science and Technology, NTNU, Norway

HIGHLIGHTS

- First study of levelized cost of hydrogen by ammonium bicarbonate reverse electrodialysis.
- For economic feasibility, max. membrane cost 20 €/m^2 and min. membrane life 7 years.
- Waste heat required varies from 480 to 105 kWh/kg_{H2}.
- In *Present scenario* membrane replacement cost dominates with 44% of total expenses.
- In *Future scenario* cost of heating dictates with 58% of total expenses.

ARTICLE INFO

Article history:
Received 21 December 2018
Received in revised form
11 May 2019
Accepted 13 May 2019
Available online 2 July 2019

Keywords:
Reverse electrodialysis (RED)
Ammonium bicarbonate (AmB)
Sustainable energy
Hydrogen production
Low grade waste heat to hydrogen
Levelized cost of hydrogen (LCH)

ABSTRACT

Ongoing and emerging renewable energy technologies mainly produce electric energy and intermittent power. As the energy economy relies on banking energy, there is a rising need for chemically stored energy. We propose heat driven reverse electrodialysis (RED) technology with ammonium bicarbonate (AmB) as salt for producing hydrogen. The study provides the authors' perspective on the commercial feasibility of AmB RED for low grade waste heat (333 K–413 K) to electricity conversion system. This is to our best of knowledge the only existing study to evaluate levelized cost of energy of a RED system for hydrogen production. The economic assessment includes a parametric study, and a scenario analysis of AmB RED system for hydrogen production. The impact of various parameters including membrane cost, membrane lifetime, cost of heating, inter-membrane distance and residence time are studied. The results from the economic study suggests, RED system with membrane cost less than 2.86 €/m^2, membrane life more than 7 years and a production rate of 1.19 mol/m^2/h or more are necessary for RED to be economically competitive with the current renewable technologies for hydrogen production. Further, salt solubility, residence time and inter-membrane distance were found to have impact on levelized cost of hydrogen, LCH. In the present state, use of ammonium bicarbonate in RED system for hydrogen production is uneconomical. This may be attributed to high membrane cost, low (0.72 mol/m^2/h) hydrogen production rate and large (1,281,436 m^2) membrane area requirements. There are three scenarios presented the *present scenario*, *market scenario* and *future scenario*. From the scenario analysis, it is clear that membrane cost and membrane life in *present scenario* controls the levelized cost of hydrogen. In *market scenario* and *future scenario* the hydrogen production rate (which depends on membrane properties, inter-

* *Corresponding author.*
E-mail address: odne.s.burheim@ntnu.no (O.S. Burheim).
https://doi.org/10.1016/j.ijhydene.2019.05.126

membrane distance etc.), the cost of regeneration system and the cost of heating controls the levelized cost of hydrogen. For a thermally driven RED system to be economically feasible, the membrane cost not more than 20 €/m^2; hydrogen production rate of 3.7 mol/m^2/h or higher and cost of heating not more than 0.03 €/kWh for low grade waste heat to hydrogen production.

Introduction

Many large-scale industries for e.g. manufacturing applications dissipate heat at relatively low temperature. In general, this heat is in overabundance, and often cannot be reintegrated entirely on-site or used for district heating. Thus, this heat is rejected to the surroundings [1]. Globally, waste heat in the industrial sector accounts for more than 40% of total energy use, meaning almost half of the energy consumed is wasted as heat to the environment [2]. In Norway, the waste heat potential was estimated to be 19 TWh/a in 2008 [3]. There are various sources of industrial waste heat as shown in the Table 1. Though there is a huge potential for waste heat recovery, the amount of heat varies with temperature as shown in Fig. 1.

The low-grade waste heat is an untapped energy resource generated in industrial plants due to lack of efficient and cost-effective recovery methods. About 300 thousand USD savings was accounted for carbon dioxide equivalent ($CO_{2,eq}$) emissions from waste heat from industries in UK [5]. In order to mitigate climate change, EU policy 2030 recommended a target to reduce GHG emissions by 40% and improve energy efficiency by 27% in the transportation and industrial sectors. Further, the use of hydrogen in the transportation sector was identified to be an alternative solution. We propose an energy efficient ammonium bicarbonate reverse electrodialysis (AmB-RED) system that utilizes the low grade waste heat (333 K–413 K) to produce hydrogen. Reverse electrodialysis (RED) stack is an electrochemical device that converts chemical energy into electrical energy using concentration gradient across an ion selective membrane. RED is one of the few renewable technologies which is capable of directly producing hydrogen from waste heat.

Cost and some technicalities are major barriers to market penetration of RED technology [6]. Literature survey indicates lack of studies evaluating challenges in market diffusion. The economic studies report that membrane accounts for almost 40–80% of total investment cost [7–10]. The literature study till date to the best of the authors' knowledge shows quite an uncertainty in estimated membranes costs ranging from 2 €/m^2 to 640 €/m^2 as shown in Table 2. Moreover, the membrane life was assumed to be in the range of 7–20 years. While some are optimistic assumptions and rest suppositions, an engineered estimate of membrane cost for levelized cost of energy (LCOE) for RED needs to be addressed.

In this article, we evaluate for the first time the economic feasibility of AmB RED system for hydrogen production with low grade waste heat of (313 K–413 K) as a source. A model with technical and economic aspects was developed to evaluate levelized cost of hydrogen (LCH). The model can be applied to decentralized hydrogen refuelling station. Critical parameters were identified, and their sensitivity was evaluated. We estimate the membrane price for the technology to be economically viable for hydrogen production. In this parametric study we account for five parameters. In the scenario analysis, we propose three scenarios estimating the values of the financial and performance indicators for present state, economically competitive to other clean energy technologies and an optimistic future scenario.

Table 1 – Industrial waste heat potential (TWh/a) from different sectors at various temperature range (their share [4]).

Sector	L.T < 373 K	M.T 373–572 K	H.T > 572 K
World	63%	16%	21%
Transportation	7.9 (46%)	–	9.3 (54%)
Industry	3.7 (42%)	1.8 (20%)	12.1 (38%)
Electricity	26.2 (88%)	3.6 (12%)	–
Residential	3.0 (36%)	5.4 (64%)	–
Commercial	2.3 (59%)	0.2 (5%)	1.4 (36%)

System description

A typical RED cell converts directly the electrochemical potential of salt into electrical energy. The electrochemical potential in the form of concentration gradient across an ion exchange membrane provides the driving force for ions to migrate from the high concentrate channel (HC) to the low concentrate channel (LC). By using alternate permselective membranes, the flow of ions is controlled. This ionic current is converted into electrical current at the electrodes by redox reactions. The ammonium bicarbonate based RED system is divided into a RED stack and a regeneration system as shown in Fig. 2. Similar to a typical reverse electrodialysis system, a concentrate and a dilute solution of ammonium bicarbonate are introduced into the cell in the respective channels. The concentration difference across a cation exchange membrane causes ammonium ions to flow from HC to LC. Similarly, bicarbonate ions flow from the HC to the LC across anion exchange membrane. Mixing of these solutions decreases the concentration of the HC effluent, while the LC increases. This LC effluent is introduced into the regeneration system. The regeneration system includes a stripping column and an absorption column. The low grade waste heat, at 313 K and

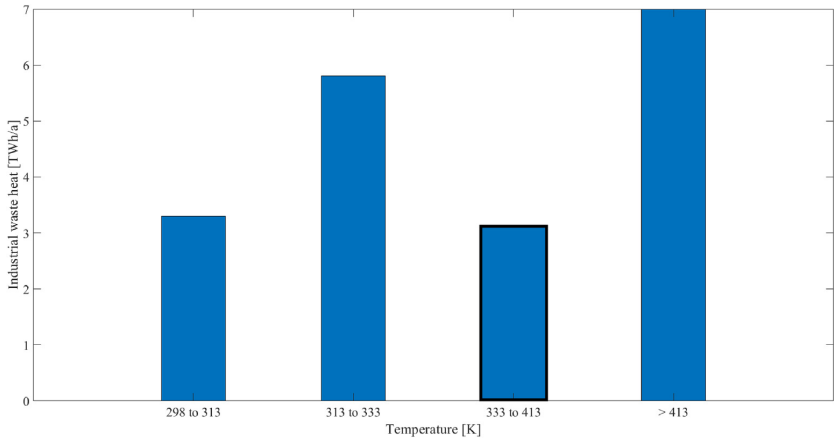

Fig. 1 – Industrial waste heat [TWh/a] in Norway as function of temperature [K].

Table 2 – Summary of previous economic studies on RED for electricity production.

Author	Year	Capacity MW	Lifetime years	C_{mem} €/m^2	t_{mem} years	P_{op} W/m^2	LCOE €/kWh
Turek [11]	2007	–	–	100[a,b]	10	0.46	6.79[a]
Post [9]	2010	200	40	2	7	2	0.08
Daniilidis [10]	2014	200	25	50	7	2.2	0.72
Weiner [7]	2015	–	20	750[a,b]	–	1.2	6.33[a]
Bevacqua [12]	2017	100	20	50	20	4.78	0.3

[a] Currency in $.
[b] Cost includes membranes, gasket, spacers, electrodes, end plate.

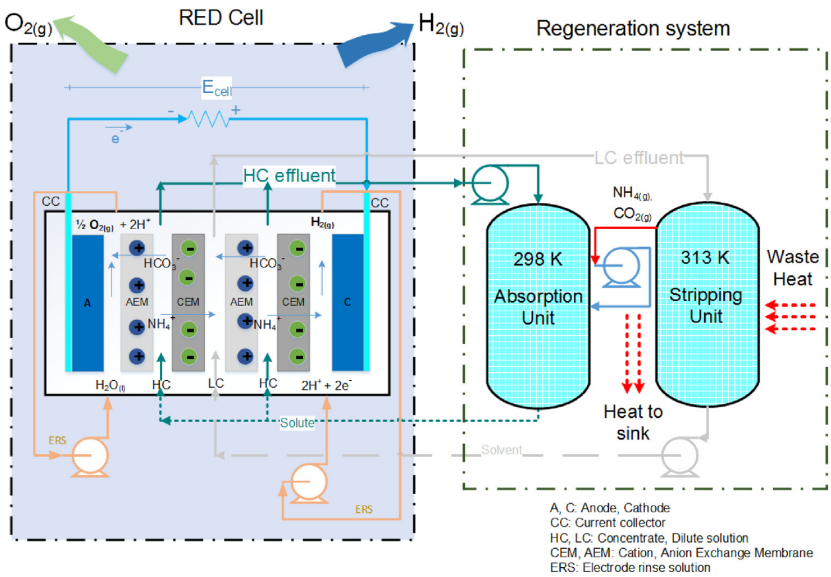

Fig. 2 – Schematic of Reverse Electro-Dialysis (RED) system based on ammonium bicarbonate salt with regeneration system for hydrogen production (For interpretation of the references to colour in this figure legend, the reader is referred to the Web version of this article).

1 atm, heats the LC effluent solution in the stripping column. This heat strips the solution into ammonia and carbon dioxide gases. The stripped gases absorb into the HC effluent in the absorption column at 298 K. The outlets of absorption and stripping column are reintroduced into the RED cell by mixing them with HC and LC inlets.

A typical RED stack consists of $K_4Fe(CN)_6/K_3Fe(CN)_6$ as electrode rinse solution (ERS) with inert electrodes such as Ti coated in Ir–Ru–O [13]. The alternative cost efficient carbon electrode with $FeCl_2/FeCl_3$ as ERS are not used widely due to low conductivity [13,14]. In AmB-RED system, we propose use of 1 M KOH as ERS with Nickel/nickel mesh as electrode for hydrogen evolution reaction (HER) and oxygen evolution reaction (OER) similar to alkaline water electrolyzers, respectively. The redox reactions at the respective electrodes are as follows.

Reactions at Anode:

$$H_2O_{(l)} \rightleftharpoons 2H^+_{(aq)} + \frac{1}{2}O_{2,(g)} + 2e^-$$

Reactions at Cathode:

$$2H^+_{(aq)} + 2e^- \rightleftharpoons H_{2,(g)}$$

Ammonium bicarbonate has low decomposition temperature of around 60 C at 1 atm that makes it an ideal candidate for low grade waste heat recovery [12,15–18]. Thermolytic salts such as ammonium bicarbonate can access control over solution concentrations. Increase in the salt concentrations increases the osmotic pressure differences which results in higher energy production. An ammonium bicarbonate based RED system can produce osmotic pressure heads equivalent to 380–510 m for higher concentrations (1–1.5 M), which is three to four times higher when compared to seawater-riverwater RED. In addition, use of ammonium bicarbonate salt in RED system avoids the geographic constraints such as coastal regions that are essential for sea/river based RED systems. This eliminates the need for energy intensive pretreatment processes. Further, high solubility in water, and relatively low molecular weight, makes it suitable for RED application. Ammonium bicarbonate production in terms of environmental concern, $CO_{2,eq}$ emissions, production of AmB can be net carbon negative [19]. Moreover, carbon capture can be realized in the oxyfuel process, where oxygen and steam are burnt with natural gas. Recovering the waste heat from such processes, not only as hydrogen but additional oxygen too makes AmB RED to hydrogen a carbon neutral economy. AmB has an additional advantage compared to NaCl solutions because its use reduces electrode overpotentials for both hydrogen evolution reaction (HER) and oxygen reduction reaction (ORR) [20]. Thus, AmB may make these reactions more favourable for energy production than previously achieved using river water and seawater in RED systems.

Methodology

Input data

The economic assessment was performed for a decentralized hydrogen production plant (refuelling station) of capacity 1500 kg/day [21]. Depending on the conversion efficiency, the waste heat required for such capacity varies from 1 MW to 8 MW. List of input parameters for techno-economic modelling are shown in the Table 3. The dimensions of RED stack are 1 m × 1 m x 2 m (l x w x h) per 10 kW (electric power) [10]. The technical parameters including model equations for membrane resistance and theoretical waste heat for ammonium bicarbonate decomposition are referred from literature [12,22]. It was difficult to extract market price of membranes, due to commercial sensitivity. Hence, the cost estimates were assessed based on the information from the literature (see Table 4).

Assumptions

In this method, inflation rate was moderate and similar to the interest rate. All economic assumptions were based on values taken from literature for European market. In the economic analysis, fuel, insurance and emissions cost, were considered. Ion exchange membranes (IEM) for RED specific applications follows the learning curve and economic trend as Nafion. The levelized cost of hydrogen (LCH) of 3.59 €/kg was considered for *market scenario* [21]. The operational cost associated to heating including equipment cost heat exchanger was assumed to be 0.01 €/kWh [23].

Table 3 – Input technical and economic data for proposed model.

Parameter	Symbols	Value	Unit
Concentrate solution conc.	c_{hc}	2.0	M
Dilute solution conc.	c_{lc}	0.06	M
Ideal gas constant	R	8.314	J/K/mol
Temperature	T	293	K
Faraday's constant	F	96,485	C/mol
Permselectivity of CEM/AEM	α	0.85	
Diffusivity coefficient (mem)	D_{AmB}	$2{\cdot}10^{-12}$	m^2/s
Inter-membrane distance	δ_{ch}	100	μm
Membrane thickness	δ_{mem}	125	μm
Number of membrane pair	N	10	
Residence time	t_{res}	1	s
Length of channel	l	0.1	m
Width of channel	w	0.1	m
Viscosity of water	μ	$9{\cdot}10^{-4}$	Pa-s
Porosity	ε	0.8	
Velocity of dilute sol.	v_{lc}	0.01	m/s
Membrane life time	t_{mem}	4	yr
Plant life time	t	20	yr
Operational hours per year	t_a	8000	h
Pump efficiency	η_{pump}	0.75	
Faradaic efficiency	η_F	0.95	
Production capacity	$\dot{m}^{cap}_{H_2}$	1500	kg/day
Pumping system cost	c_{pump}	300	€/kW
Membrane cost	C_{mem}	150	€/m^2
Waste heat price	c_{heat}	0.01	€/kWh
Discount factor	r	0.06	
Infrastructure price	c_{infra}	1123	€/m^2[a]
Regeneration system price	c_{regen}	3400	€/m^3/h[b]
Labour cost	C_{lab}	20%	(% of CAPEX)
RED stack	$C_{RED_{stack}}$	same as C_{mem}	€/m^2

[a] Land area.
[b] Vol. flow.

Table 4 – Effect of raw material cost and production volume on cost of membrane [28].

Membrane	Production rate m^2/a	C_{raw} \$/m^2	C_{prod} \$/m^2	Total cost \$/m^2	Thickness μ m
Nafion	2800	–	–	576	183
	250,000	35	100	–	183
	28,000,000	–	–	62	183
	10,000	–	–	250	25
	600,000,000	–	–	2.8	25
SPEEK	250,000	4.5	50	–	100
NFM	10,000	1 + 0.05	10	–	200 + 25

System model

The system model was subdivided into AmB-RED system, pumping system and regeneration system. In AmB-RED system, electrochemical equations were used to estimate hydrogen produced. Pumping system model deals with hydrodynamics in the cell and related losses. Regeneration system was modelled based on simple mass balances and thermal duty assumed from Bevacqua et al. [12].

AmB-RED system

The objective was to estimate the hydrogen production, and membrane area required. At first, the input data as shown in Table 3 were initialized. Parameters such as conductivity and activity coefficients were estimated. On this basis, cell voltage, resistances of membranes and channels were estimated followed by stack resistance, and stack voltage. Using these values, short circuit current density, peak power current density, and peak power stack voltage were determined. Finally, the moles of hydrogen produced and membrane area required were estimated. The proposed system was mathematically modelled using equations as follows,

- Conductivity of solutions (k): The equivalent conductivity of ammonium bicarbonate depends on concentration and molar conductance which depends on temperature. The conductivity was calculated at constant temperature 293 K using Jones-Dole equation,

$$k = \Lambda \cdot c_i \tag{1}$$

where $\Lambda = \Lambda_0 - \frac{A_\Lambda \cdot \Lambda_i \cdot c_i^{1/2}}{1+B_\Lambda \cdot c_i^{1/2}} - C_\Lambda \cdot c_i$. Here $A_\Lambda, B_\Lambda, C_\Lambda$ are model parameters used for fitting and referred from Bevacqua et al. [12], c_i is inlet concentration; Λ_0 molar equivalent conductivity of salt at infinite dilution. The conductivity is calculated in mS/cm for both feed solutions at 293 K.

- Activity coefficient of solutions (γ): The activity coefficients depend on molar salt concentration. The linear dependence of activity coefficients on concentration was estimated using ENTRL-RK thermodynamic package in Aspen Plus.

$$\gamma = g_1 \cdot c_i + g_2 \tag{2}$$

here c_i is expressed in mol/l, $g_1 = 0.1366$ l/mol and $g_2 = 1.0007$. These values were estimated at T = 293 K [12].

- Unit cell open circuit potential ($E_{u.c.}^{ocp}$): It is the membrane potential [V] for a cell pair (CEM, AEM) with no losses considered. The electrochemical potential difference across an IEM placed between two different concentration solutions can be described using modified Nernst equation,

$$E_{u.c.}^{ocp} = (\alpha_{cem} + \alpha_{aem}) \cdot \frac{R \cdot T}{F} \cdot ln\left(\frac{\gamma_{hc} \cdot c_{hc}}{\gamma_{lc} \cdot c_{lc}}\right) \tag{3}$$

α is permselectivity of IEMs measured at concentration c_{hc} and c_{lc} at constant temperature 293 K for specific membrane. Here we assume same α for both membranes. F is Faraday constant. T is room temperature. R is ideal gas constant.

- Area specific membrane resistance ($R_{aem/cem}$): It is the ohmic resistance [Ωm^2] of the membranes when immersed in the solution. It is expressed as function of concentration [12].

$$R_{cem} = R_{aem} = r_1 \cdot (c_{lc})^{-0.236} \tag{4}$$

R_{cem}, R_{aem} are area specific membrane resistances for cation and anion exchange membrane, c_{lc} is inlet concentration of low concentrate solution. r_1 is fitting parameter [Ωm^2/M]. It is estimated to be 0.0002 [Ωm^2/M] for *present* and *market* scenario and 0.00004 [Ωm^2/M] for *future* scenario [12]. As concentration lowers below 0.1 M, the contribution to resistance from low concentrate solution dominates.

- Channel ohmic resistance ($R_{lc/hc}$): The resistance (Ωm^2) due to the solution in the channel and spacer geometry. It depends on concentration, and is calculated using molar conductivity of the salt.

$$R_{lc} = \frac{\delta_{lc}}{\varepsilon \cdot k_{lc} \cdot c_{lc}} \quad R_{hc} = \frac{\delta_{hc}}{\varepsilon \cdot k_{hc} \cdot c_{hc}} \tag{5}$$

here δ_{ch} is intermembrane distance in μm, ε is the porosity of spacers, k_{lc} and k_{hc} are conductivities of feed solutions

- Unit cell resistance ($R_{u.c.}$): The cumulative sum of resistance of membranes and channels in a unit cell [Ωm^2].

$$R_{u.c.} = R_{cem} + R_{aem} + R_{lc} + R_{hc} \tag{6}$$

- Current density at peak power ($j_{u.c.}^{pp}$): The peak power current density occurs at potential half the open circuit potential. As the resistance remains constant the current density [A/m^2] at peak power is calculated using Ohm's law,

$$j_{u.c.}^{pp} = \frac{E_{u.c.}^{ocp}}{2 \cdot R_{cell}} \tag{7}$$

- Actual unit cell potential ($E_{u.c.}^{act}$): The potential across the RED unit cell drops due to ohmic resistances in the RED unit cell and is estimated as,

$$E_{u.c.}^{act} = E_{u.c.}^{ocp} - R_{u.c.} \cdot j_{u.c.}^{pp} \tag{8}$$

- Number of unit cells ($N_{u.c.}$): Alkaline electrolyzers operate above reversible potential 1.23 V. The anodic and cathodic overpotentials are estimated to be 300 mV at low current densities [24]. Hence, the required potential for water electrolysis is assumed to be 1.5 V. In order to meet this potential, unit cells are stacked together in series. The minimum number of unit cells to be stacked in series is calculated as,

$$N_{u.c.} = \frac{1.5}{E_{u.c.}^{act}} \tag{9}$$

- Stack open circuit potential (E_{stack}^{act}): The stack open circuit potential [V] drops upon connecting the RED device to external load. Thus the actual voltage across the terminals of the stack is given by,

$$E_{stack}^{act} = N \cdot E_{u.c.}^{act} \tag{10}$$

- RED stack resistance (R_{stack}): The total resistance including unit cells, N and electrodes in a stack.

$$R_{stack} = N \cdot R_{u.c.} + R_{ele} \tag{11}$$

here R_{ele} [Ωm^2] is resistance from electrodes in electrode rinse solution. This resistance value is assumed to be 0.01 Ωm^2 [12]. But, its contribution to the performance is not significant for large stacks.

- Hydrogen production rate ($\dot{n}_{H_2}$): The theoretical moles of hydrogen produced per unit time in the compartment with electrode-electrolyte rinse solution of RED stack.

$$\dot{n}_{H_2} = \frac{j_{u.c.}^{pp} \cdot 3600}{z \cdot F} \cdot \eta_F \tag{12}$$

here z = 2 is the ion valence per mole of hydrogen gas, η_F is Faradaic efficiency. η_F signifies that all current density generated is not utilized to make hydrogen, due to system related losses. In a RED system, the main source of loss in Faradaic efficiency is due to ionic short circuiting in feed and drain channels. This loss in Faradaic efficiency is 6% for well designed RED system in comparison with alkaline water electrolyzer where these losses range from 5 to 25% [20,25].

- Membrane area (A_{mem}^{tot}): The total membrane area [m^2] required to produce 1500 kg hydrogen a day ($\dot{m}_{H_2}^{cap} = 0.0174$ kg/s is the required production capacity).

$$A_{mem}^{tot} = \frac{I_{para.}^{pp} \cdot N_{u.c.}}{j_{u.c.}^{pp}} \tag{13}$$

$I_{para.}^{pp}$ is total current from the stacks in parallel. It is calculated as $I_{para.}^{pp} = \frac{\dot{m}_{H_2}^{cap} \cdot 1000 \cdot z \cdot F}{2.016 \cdot \eta_F}$. Where, $\dot{m}_{H_2}^{cap}$ is required hydrogen production capacity [kg/s] and molecular weight of hydrogen is 2.016 g/mol.

Pumping system

Experimentally, a pressure drop is observed over the inlet and outlet of feed water. Hence, to compensate this loss, pumping of feed solutions is essential. The important parameters such as flow rate, pressure drop and pumping power were calculated and are presented in this section.

- Flow rate (Q_{lc}): As suggested in the literature [22,26], the velocity of LC solution influences the double layer resistance and thus the power density. The flow rate [m^3/s] for low concentrate feed solution is estimated as,

$$Q_{lc} = N \cdot v_{lc} \cdot \delta_{ch} \cdot w \cdot \varepsilon \tag{14}$$

here ε is porosity of the spacer, v_{lc} velocity of feed solution in low concentrate channel [m/s], δ_{lc} intermembrane distance [m], w width of channel.

- Hydraulic diameter ($d_{h,lc}$): The spacer filaments obstruct the flow through the channel and this requires additional pumping power. To estimate the influence of spacer filaments, hydraulic diameter of spacer filled channel was determined using following equation,

$$d_{h,lc} = \frac{4\varepsilon}{\frac{2}{\delta_{ch}} + \left((1-\varepsilon) \cdot \frac{8}{\delta_{ch}}\right)} \tag{15}$$

- Pressure drop (Δp_{lc}): Assuming an ideal case of fully developed laminar flow, the pressure drop (Pa) was estimated using Darcy-Weisbach equation,

$$\Delta p_{lc} = \frac{12 \cdot \mu \cdot l^2}{0.25 \cdot d_h^2 \cdot t_{res}} \tag{16}$$

the μ is dynamic viscosity of water [Pa-s], t_{res} is the residence time [s], l length of channel.

- Pumping power (P_{pump}): The power [W/m^2] required to overcome the hydraulic resistance in pumping the feed solutions through the channels. This strongly depends on the spacer porosity, as it dictates hydraulic radius which influences pressure drop.

$$P_{pump} = \frac{\Delta p \cdot d_{h,lc} \cdot \varepsilon}{t_{res}} + \frac{\Delta p \cdot d_{h,hc} \cdot \varepsilon}{t_{res}} \tag{17}$$

- Reynolds number (*Re*): It is the ratio of inertial forces to viscous forces within a fluid. The Reynolds number for wide channel corrected for spacer porosity is defined as [27],

$$Re = \frac{\rho \cdot v_{lc} \cdot d_h}{\mu} \tag{18}$$

Mass balances

The concentration difference between the adjacent channels drives the salt flux from high concentrate to low concentrate channel.

- Salt flux (J_{salt}): The total solute transport.

$$J_{salt} = \frac{j^{pp}}{F} + 2 \cdot \frac{D_{AmB}\left(c_{hc}^{in} - c_{lc}^{in}\right)}{\delta_{mem}} \quad (19)$$

here δ_{mem} is the thickness of IEMs in operation [m], D_{AmB} diffusivity coefficient of ammonium bicarbonate in membrane [m^2/s]. The first term relates to coulombic (counter ion) transport, while the second term relates to co-ion transport. The factor 2 relates to number of membranes in a unit cell.

Waste heat/Regeneration system

The regeneration system compensates the amount of salt diffused through the IEM from high concentrate channel to low concentrate channel. The regeneration system includes air stripping column and absorption column. The air stripping column decomposes solution from dilute compartment outlet to ammonia gas and carbon dioxide gas at 333 K. The absorption column dissolves the decomposed gases at 298 K in the outlet of concentrate channel.

- Heat required for regeneration (q_{regen}): The total amount of thermal power required to strip Q_{lc} of ammonium bicarbonate salt from LC solution

$$q_{regen} = \dot{q}_{th} \cdot Q_{lc} \cdot 3600 \cdot A_{mem}^{tot} \quad (20)$$

q_{th} is the specific thermal duty [kWh/m^3] required to decompose ammonium bicarbonate solution into its components $NH_{4,(g)}$ and $CO_{2,(g)}$. The value was estimated using relation $q_{th} = a_1 \cdot e^{a_2 \cdot C_1} - a_3 \cdot C_2^{a_4} + a_5 \cdot C_1^{a_6} \cdot C_2^{a_7}$ from Bevacqua et al. [12] for inlet concentration to stripping column C_1 and outlet concentration C_2 from stripping column. Here a_1 to a_7 are fitting parameters that are function of C_1, refer to appendix Table 8.

Economic model

Levelized cost of hydrogen (LCH) method assesses the economic feasibility of the proposed process. This method considers annuity factor $\left(\frac{1}{(1+r)^t}\right)$ as shown in equation (21). This method is preferred as it is simple, and provides realistic results. These results of economic assessment of different technologies are easy to compare, transparent, and easy to understand. The disadvantage of using this method is that the distinction in variations in costs and benefits from one year to the next is not possible (same net benefit is applied to every year). Further, the time delay between investment and first year of regular operation are not considered.

$$LCH = \frac{\sum_{i=1}^{i=t} \frac{CAPEX + OPEX + C_{heat}}{(1+r)^t} + C_{mem.re}}{\sum_{i=1}^{i=t} \frac{m_{H_2}}{(1+r)^t}} \quad (21)$$

Capital cost (CAPEX)

The capital cost [€] of the plant was evaluated as CAPEX, using equation (22).

$$CAPEX = C_{mem} + C_{RED_{stack}} + C_{regen} + C_{pump} + C_{lab} + C_{infra} \quad (22)$$

The capital costs include all the expenses related to purchase and installation (labour and infrastructure) of systems such as RED stack (including membranes), pumping unit, regeneration unit. The labour cost includes civil work associated with site preparation, process equipment building, offsite services and is assumed to be 20% of capital cost. The cost of regeneration system was normalized to flow rate [m^3/h], and cost of pumping system was normalized to pumping power [kW]. The cost of membranes was normalized per unit membrane area. The cost of membrane was estimated as sum of the production cost and raw material cost. Using analytical approach to investigate the cost of Nafion membranes, Minke et al. [28] suggested that for constant thickness with increase in production rate by four orders of magnitude the total membrane cost decreases by almost one order of magnitude w.r.t the initial cost. With a decrease in thickness by almost 7 times and a further increase in membrane production rate by one order of magnitude, the total membrane cost reduces to one tenth of the present raw material cost [28]. Assuming a learning rate similar to that of Nafion membrane of 25 μm thickness, a minimum membrane cost was estimated. The production rate was assumed 60×10^8 m^2 as a RED application requires large membrane areas due to low membrane potential or power density [10].

- Cost of RED stack ($C_{REDstack}$): It includes cost of electrodes, gaskets, spacers and end plates. It is assumed to be the same cost as that of the membrane.
- Infrastructure cost (C_{infra}): It is the real estate cost and this was calculated using dimensions of RED cell, stack referred from Daniilidis et al. [10].
- Pumping system cost (C_{pump}): The pumping unit consists of two pumps. The cost associated with a pump is c_{pump} [€/kW]. The pumping unit compensates the pressure drop inside a RED stack, the total cost is normalized per unit stack.

$$C_{pump} = \frac{P_{pump} \cdot A_{mem}^{tot} \cdot c_{pump}}{1000} \quad (23)$$

- Regeneration system cost (C_{regen}): The specific investment cost for regeneration system is c_{regen} [€/m^3/h]. The total cost of the regeneration system is estimated for the required flow rate Q_{lc} from a RED stack.

$$C_{regen} = \frac{c_{regen} \cdot Q_{lc} \cdot A_{mem}^{tot} \cdot 3600}{2} \quad (24)$$

Operational and maintenance cost (OPEX)

OPEX [€] includes labour maintenance, service and repairs expenses which is assumed to be 2% of CAPEX. Direct and indirect operational costs such as chemical, emissions to air, supply of water, labour, taxes, administration, and insurance are not included.

$$OPEX = 0.02 \cdot CAPEX \quad (25)$$

here t is plant life time [years].

Membrane replacement cost ($C_{mem,\ re}$)

The ion exchange membranes have limited lifetime. Hence, these membranes have to be replaced at the end of their lifetime until plant lifetime. The cost associated to membrane replacement is calculated as,

$$C_{mem,re} = \sum_{n=1}^{n=f} \frac{C_{mem}}{(1+r)^{t_{mem}*n}} \quad (26)$$

where c_{mem} and t_{mem} are membrane costs [€/m^2] and membrane lifetime [years]. f is the factor that denotes the number of times replacement takes place ($f = t/t_{mem}$).

Waste heat price (C_{heat})

The regeneration system requires heat for producing $NH_{3,g}$ and $CO_{2,g}$ from the LC outlet solution. This heat required by the process can be sourced from various thermal energy intensive industries including cement, paper, biomass, waste incineration etc. Though it is said to be waste heat, a heat exchange system is required to provide the heat at specific temperature. Hence a cost c_{heat} is associated with it. This cost is assumed to be as low as 0.01 €/kWh.

$$C_{heat} = c_{heat} \cdot q_{regen} \cdot t_a \quad (27)$$

t_a is the total number of operational hours per year [h].

Profit

The sum of revenue earned by selling produced hydrogen and operational expenses incurred on annual basis.

$$\text{Profit} = \left(\sum_{i=1}^{i=t} \frac{m_{H_2} \cdot c_{H_2}}{(1+r)^t} \right) - \left(\sum_{i=1}^{i=t} \frac{\text{CAPEX} + \text{OPEX} + C_{heat}}{(1+r)^t} + C_{mem,re} \right) \quad (28)$$

where c_{H_2} is hydrogen selling price [€/kg_{H2}] and assumed to be 3.59 €/kg_{H2}[21].

Scenario case study

The study includes three scenarios based on the cost of membrane, the membrane life time and the hydrogen production rate. In all the scenarios for ammonium bicarbonate solution, the hydrogen production rate was calculated from the corresponding input data as shown in Table 5. In the *present scenario*, the cost and lifetime of membrane were fixed input and LCH was estimated. In the *market* competing *scenario*, the LCH was assumed the same as estimated by US DOE for hydrogen produced from renewable energy source. In the *market* and *future scenario*, the concentration of feed solutions were optimized to maximize hydrogen production for present properties of membranes refer Table 5 [12]. There are no profits made in *market* scenario, the membrane life was assumed to be 7 years and membrane cost was estimated. Finally, an optimistic *future scenario* was considered, wherein the profits of 10% were made on annual basis, with an increased membrane life of 10 years, and the membrane cost was estimated accordingly. In the *future scenario*, the hydrogen is produced at 3.71 mol/m^2/h with increased permselectivity of membranes 0.95 and Faradaic efficiency 0.95, as shown in Table 5. The channel length and width were assumed to be the same for all scenarios. The heating cost for all scenarios was assumed to be 0.01 €/kWh. The Table 6 summarizes all the input and estimated parameters.

Table 5 – Input parameters of AmB RED system for scenario study.

Parameter	present	market	future	Unit
Concentrate solution conc. (c_{hc})	2	2.6	2.6	M
Dilute solution conc. (c_{lc})	0.06	0.05	0.07	M
Permselectivity (α)	0.753	0.85	0.95	–
Inter-membrane distance (δ_{ch})	270	100	100	μm
Residence time (t_{res})	70	60	50	s
Membrane lifetime (t_{mem})	4	7	10	years
Faradaic efficiency (η_F)	0.95	0.95	0.99	–

Table 6 – List of input and output parameters for scenario study.

Scenario	Input	Output
present	C_{mem}, t_{mem}	$\dot{n}_{H_2}$, LCH, Profit
market	LCH, t_{mem}, Profit	$\dot{n}_{H_2}$, C_{mem}
future	Profit, t_{mem}	$\dot{n}_{H_2}$, C_{mem}, LCH

Results and discussion

Cost of membrane

Fig. 3a shows the influence of membrane cost on the LCH for AmB based RED system for hydrogen production at 0.72 mol/m^2/h production rate, and a membrane life, t_{mem} of 4 years. LCH is a linear function of membrane cost, C_{mem}. The LCH of AmB RED system decreases with decrease in membrane cost, C_{mem}. Fig. 3b compares LCH for ammonium bicarbonate RED system in the *market* and the *future* scenarios. The rate of decrease of LCH for *market scenario* is three times as high as *future scenario*, this shows that LCH was sensitive to membrane cost in *market scenario*. The intercepts in Fig. 3b shows the contribution of balance of plant cost to LCH at membrane cost, $C_{mem} = 0$ €/m^2, and, LCH at this intercepts are below the LCH target set by US DOE. Assessing all the costs in *present scenario*, it was found that the membrane cost influences the most, accounting for almost 40% of CAPEX. This is in agreement with the previous studies [9–11,29]. The minimum predicted cost of membrane was calculated using the learning rate as that of 25 μm Nafion membrane for production rate of 60×10^8 m^2/a. The minimum membrane cost was found to be 1.69 €/m^2. For ammonium bicarbonate RED system, the membrane cost, C_{mem}, must drop below 2.86 and 22.3 €/m^2 for membrane lifetime t_{mem} of 4 and 10 years at production rate of 1.19 and 3.71 mol/m^2/h, respectively, to compete with other clean energy technologies.

Hydrogen production rate

The LCH is predicted for different hydrogen production rates. With increase in production rate, the LCH decreases. With the present membrane cost (150 €/m^2) and membrane life of 4 years, the LCH decreased by almost 42% (72.49 €/kg) for increase in production rate from 0.72 mol/m^2/h to 1.19 mol/m^2/h. This increase in production was due to optimal concentration

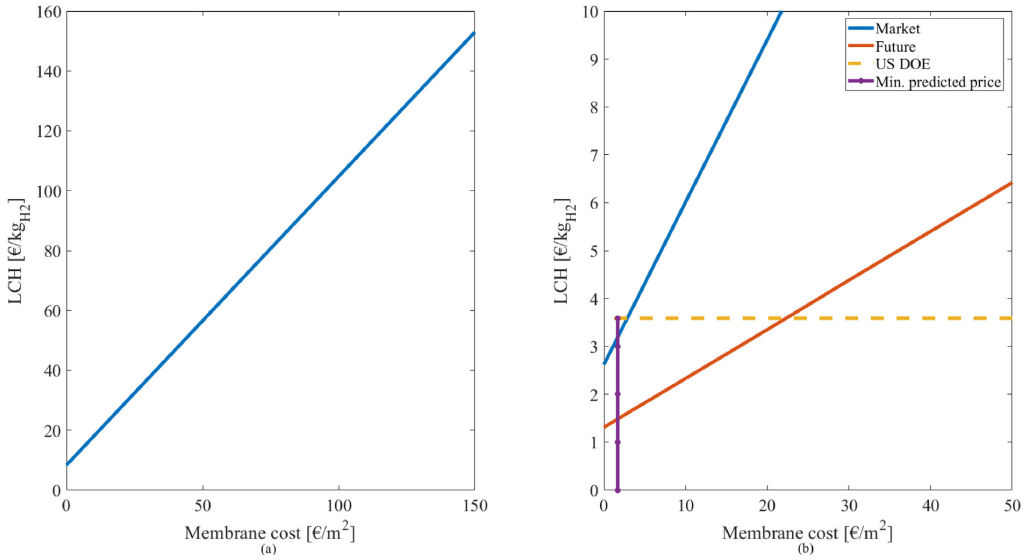

Fig. 3 – a. Influence of cost of membrane on LCH for a membrane lifetime of 4 years in case of *present scenario* (left). b. Comparison of *market*, *future* scenario with US DOE target price, for LCH as function of membrane cost (right).

of feed solutions. The LCH decreased to 23.7 €/kg for further increase in hydrogen production rate to 3.71 mol/m^2/h. This increase was a combined result of increase in permselectivity and Faradaic efficiency. The increase in production rate increases the total hydrogen produced in the plant lifetime. Therefore, LCH decreases. Increase in production rate is due to increase in current density, which indirectly relates to concentration ratio. High concentration ratios are achieved with high solubility of salt under the assumption that the electrical conductivity of the solution and permselectivity of membrane remains same. The production rate is a function of peak current density, which in turn depends on Nernst potential. As this Nernst potential relates to ratios of concentration or activity coefficients which are salt properties (solubility etc). The salts that can produce hydrogen at a production rate higher than that of AmB-RED system due to synergetic effect of higher OCP, higher solubility limit and lower resistance needs to be investigated experimentally. However, this is beyond the scope of this work. Hydrogen production rate can be increased by improving membrane properties such as permselectivity, conductance and reducing thickness while maintaining the mechanical strength. Further, the use of optimal combination of electrolytic solutions, electrode material and their geometric configuration can decrease cell overpotential and increase the overall stack potential, which in turn will improve the hydrogen production rate.

Lifetime of membrane

Fig. 4a describes the influence of membrane lifetime at a membrane cost of 150 €/m^2 for *present scenario*. With increase in membrane life, the LCH decreases substantially. As the membrane lifetime increases from 3 years to 10 years, the LCH decreases to almost 40% of the initial value in the *present scenario*. Fig. 4b shows asymptotic behaviour of t_{mem} required at a hydrogen production rate of 1.19 mol/m^2/h to 3.71 mol/m^2/h in order to meet a LCH of 3.59 €/kg. The increase in membrane life 7 years or more, show less significant impact on LCH in *present* and *market scenario*. Due to the operating conditions, the membrane properties such as permselectivity, membrane resistance etc. can be expected to deteriorate with time. As the performance of the system depends on the membrane properties, corresponding deterioration in the system performance will be observed. The higher the deteriorate rate, the quicker the membranes need to be replaced. For best performance, the system is operated at optimum conditions, and to maintain the performance, the membranes need to be replaced on timely basis. Increasing the frequency of replacing a membrane increases membrane replacement cost (contributes 44% of total expenses in *present scenario*). Thus, the overall trend implies that the lifetime of membrane (indirectly, the degradation rate) of these membranes plays a critical role in minimizing LCH. *market scenario* becomes economically feasible at membrane life of 7 years while 1 year for *future scenario*. This shows that increase in membrane life beyond 7 years has relatively low impact on LCH with the case parameters chosen in the study.

Inter-membrane distance

Increase in the inter-membrane distance decreases the actual unit cell potential. The decrease in open circuit potential decreases the peak power current density, which in turn decreases the salt flux. Hence, the theoretical heat required also decreases. On the contrary, the increase in inter-membrane distance cause, an increase in feed solution volume flowing through the channel. This, again, causes an increase in the theoretical heat required to regenerate the ammonium

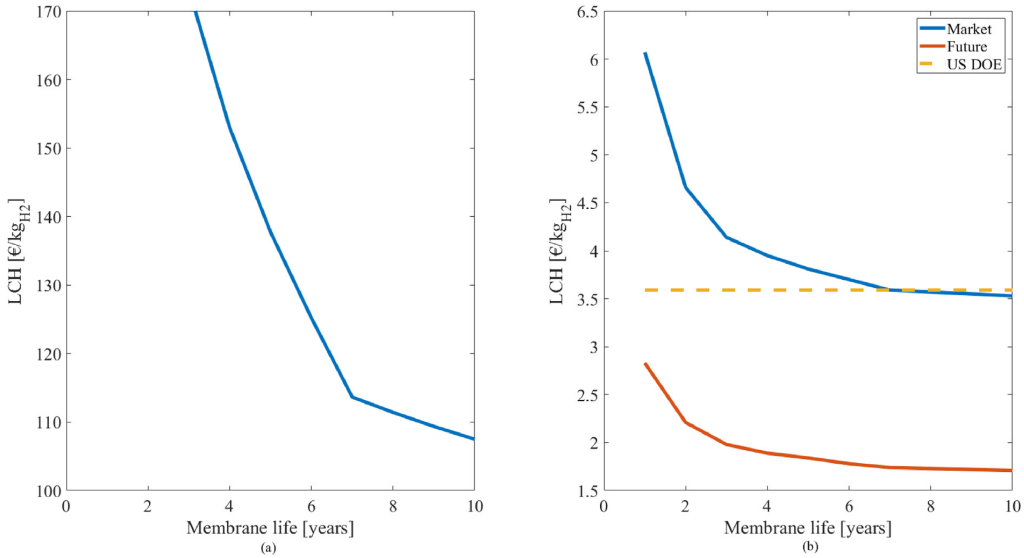

Fig. 4 – a. Influence of membrane life time on LCH for AmB RED *present scenario* (left). b. Comparison of *market* and *future* scenario for membrane lifetime on LCH (right) (For interpretation of the references to colour in this figure legend, the reader is referred to the Web version of this article).

bicarbonate solutions. This increase in the heat requirement nullifies the decrease in heat requirement due to decrease in salt flux. Thus, the net effect observed is an increase in the total heat required.

Moreover, as the increase in inter-membrane distance increases the feed solution flow rate. The increase in flow rate increases the amount of water per gram of salt. Thus, the total heat required to recover same amount of salt increases.

Increased inter-membrane distance has a negative impact on LCH, as shown in Fig. 5a and b The LCH decreases with decrease in inter-membrane distance. The increase in inter-membrane distance increases the channel resistance. This increase in resistance decreases the open circuit potential and increases number of membrane pairs required. This results in increase LCH. In case of the *market scenario*, the LCH varies almost linearly with change in inter-membrane distance. In the *market scenario* and the *future scenario* the maximum inter-membrane distance to match with the US DOE were found to be 100 μm, and 200 μm from Fig. 5b respectively.

Cost of heating

Fig. 6a and b, shows the influence of cost of heating for the *present*, *market and future scenario*. The cost of heating, c_{heat}, has a negative impact on LCH. With increase in c_{heat}, the LCH increases as shown in Fig. 6a and b. In the *market* and the *future scenario*, the cost of heating contributes as high as 58% to the total expenses. Hence, it is considered as a critical parameter. From Fig. 6b, the maximum cost of heating was found to be 0.01 and 0.03 €/kWh for *market scenario* and *future scenario* respectively. The intercept on y axis shows the LCH for case with no cost of heating. These values were found to be approximately 148.5, 2.2 and 0.7 €/kg$_{H_2}$ for the *present*, the *market* and the *future scenario* respectively.

Scenario analysis

Out of the three scenarios, LCH in *present scenario* was found to be the highest, with the cost of membrane being the major contributor. Fig. 7, shows contribution of expenses such as membranes, RED stack without membranes, regeneration system, pumping system, infrastructure and labour to the capital expenses. From Fig. 7, in the *present scenario*, the membrane and RED stack contribute to approximately 80% of CAPEX, this contribution reduces to more than half in the *market* and *future* scenario. The labour cost, which includes civil work associated with site preparation, process equipment building, off site services, contributes to 16% of CAPEX in all the scenarios. Pumping system cost increases from *present scenario* to *future scenario* but has negligible contribution to LCH in all scenarios. The contribution of infrastructure was of low significance (4.4% max. in the *future scenario*).

The maximum limit of c_{mem} to achieve LCH of 3.59 €/kg$_{H_2}$ for *market scenario* (2.86 €/m^2) is a tenth of c_{mem} in the *future scenario*). Compared to the *present* scenario, the contribution of c_{heat} to LCH increased from 3% to 50% and 57% for *market* and *future* scenario respectively. This suggests that as the cost of membrane decreases, and the life of membrane increases, the contribution from c_{heat} to the LCH increases (see Table 7).

In order to improve the accuracy and provide more realistic estimates, the following recommendations are given. The value of the heat of regeneration, q_{th}, was taken from a

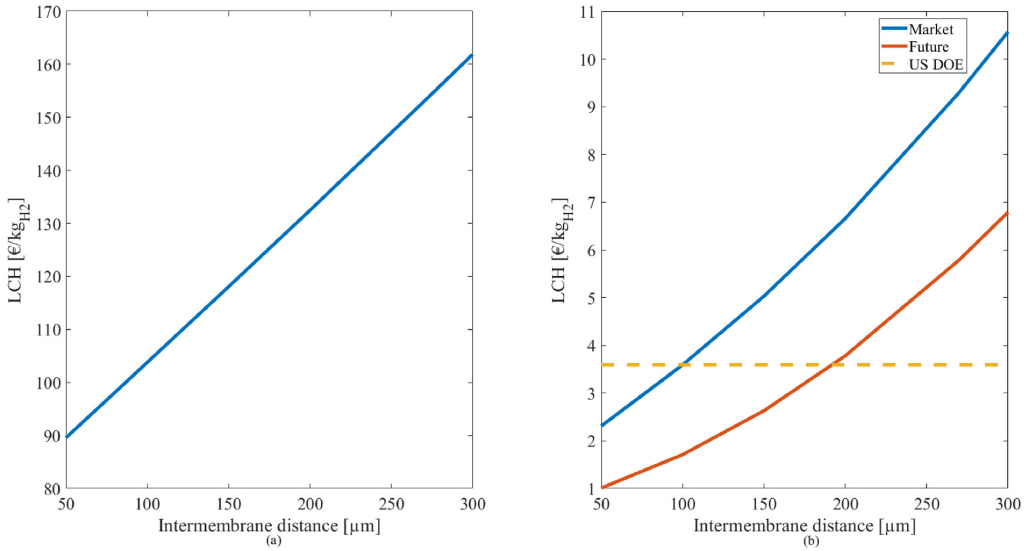

Fig. 5 – a. Influence of inter-membrane distance on LCH for *present* (left) b. *market* and *future* scenario (right).

theoretical study and was not optimized for the present AmB-RED system. Further, to investigate influence of salt type on thermochemical conversion efficiency, η_{th}, modelling and optimization of regeneration system in a process modelling and simulation software is essential. In the economic model, presented simplified LCH method is used to evaluate the specific cost of hydrogen per kg. This method does not include various operational costs and other capital costs such as consultancy and financing costs. Further, the economic model is developed for a standard capacity of 1500 kg_{H_2}/day and hence no upscaling effects were considered. The use of base cost method proposed by Ulrich et al. [30]. includes these costs and upscaling effect, and thus provides more realistic estimates. The cost of other components in a RED stack were assumed to be the same as the cost of membrane. This may not necessarily be true in case of learning rates. Hence individual component cost estimates are needed. The RED model does not include non-ohmic

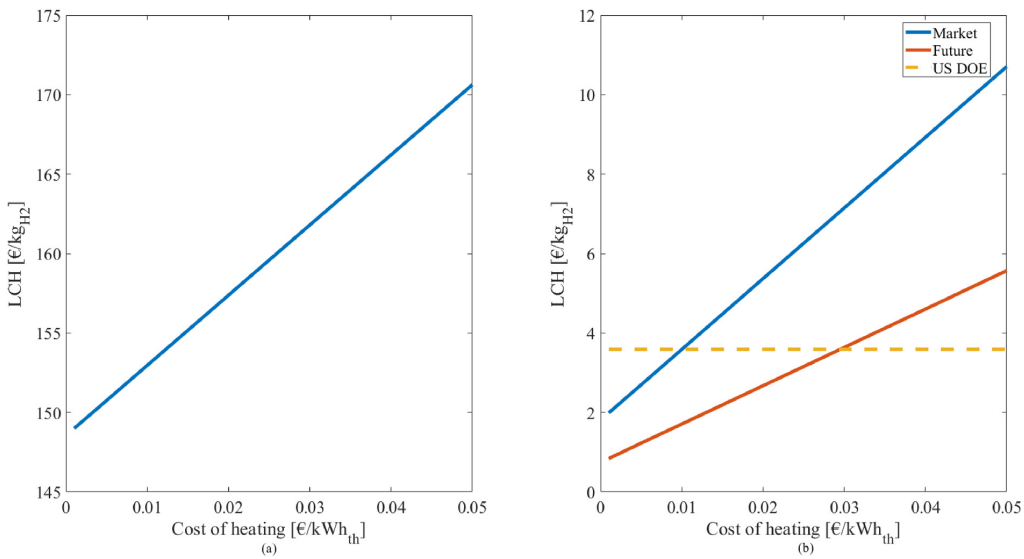

Fig. 6 – a. LCH as a function of cost of heating for *present* (left) b. *market* and *future* scenario (right).

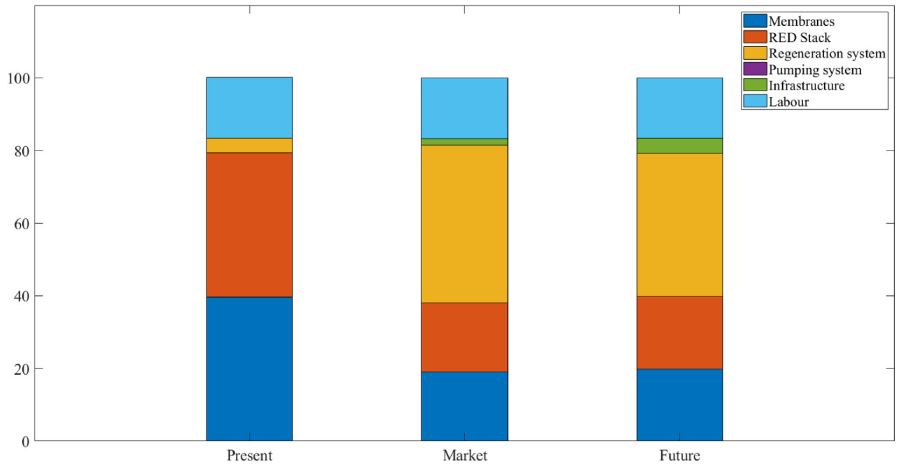

Fig. 7 – Comparison of various system elements in relation to CAPEX in the three scenarios.

Table 7 – Summary of the results from scenario analysis of the techno-economic analysis.

Present Scenario		Market Scenario		Future Scenario	
LCH	152.97 €/kg_{H_2}	LCH	3.59 €/kg_{H_2}	LCH	1.71 €/kg_{H_2}
C_{mem}	150 €/m^2	C_{mem}	2.86 €/m^2	C_{mem}	3.94 €/m^2
t_{mem}	4 yrs	t_{mem}	7 yrs	t_{mem}	10 yrs
$\dot{m}_{H_2}$	0.72 mol/m^2/h	$\dot{m}_{H_2}$	1.19 mol/m/h	$\dot{m}_{H_2}$	3.71 mol/m/h
Waste heat	480 kWh/kg_{H_2}	Waste heat	194 kWh/kg_{H_2}	Waste heat	105 kWh/kg_{H_2}
Re	0.3	Re	0.13	Re	0.16
CAPEX	43%	CAPEX	35%	CAPEX	31%
OPEX	10%	OPEX	8%	OPEX	7%
$C_{mem.re}$	44%	$C_{mem.re}$	7%	$C_{mem.re}$	5%
C_{heat}	3%	C_{heat}	50%	C_{heat}	57%
Profit	−931,378,389 €	Profit	0 €	Profit	11,721,725 €

resistances, they may influence the hydrogen production rate at low Reynolds number [31].

Conclusions

A simplified LCH model is developed for a thermally driven AmB RED system. The model includes capital costs associated with the regeneration system and operation costs for the waste heat. The scenario analysis includes three different cases *present*, *market* and *future*; these scenarios differ in the inlet feed solution concentration, membrane properties, residence time, cost of membrane, membrane lifetime. The scenario analysis demonstrates cost of membrane and membrane lifetime as dictating parameters in *present scenario*; cost of heating and cost of regeneration system, control the levelized cost of hydrogen (LCH) in *market* and *future scenario*. In case of the *present scenario* membrane replacement cost dominates due to high capital cost of membrane (150 €/m^2) and limited membrane life of 4 years. While, in *market* and *future* scenarios cost of regeneration system influences with contribution to CAPEX as high as 40%. Except in the case of the *present scenario*, cost of heating contributes to almost 57% of total expenses, making it a critical parameter that needs to be optimized to further minimize LCH. Parameters such as inter-membrane distance, has a negative effect on the LCH. A decrease in inter-membrane distance increases pumping power but the decrease in heat required to extract salt dominates. The decrease in inter-membrane distance by one fifth of initial value decreases LCH to as low as 1.35 €/kg_{H_2} in the *market* and 0.83 €/kg_{H_2} in the *future* scenario. In future the cost of membrane can reduce to 1.69 €/m^2 with increase in production rate, reduction in production cost, raw material cost, and reduction in membrane thickness. It is clear that AmB RED for hydrogen production has economic potential at membrane cost less than 2.86 €/m^2, and/or, membrane life of 7 years or more. Future efforts must be directed to evaluate performance of potential salts such as lithium bromide that are highly conductive, highly soluble, and may require less heat for recovery. Finally, a thermally driven RED system with membrane cost not exceeding 20 €/m^2; hydrogen production rate of 3.7 mol/m^2/h or higher and cost of heating not more than 0.03 €/kWh can make an economically feasible solution for low grade waste heat to hydrogen production.

Acknowledgement

The authors would like to acknowledge Department of Energy and Process Engineering, Norwegian University of Science and Technology, Norway (Project number 70441041) and ENERSENSE, Norwegian University of Science and Technology, Norway for supporting this research project.

Appendix

Table 8 – Input values for parameters described in equation (20) as a function of inlet solution concentration for stripping column.

Concentration range [M]	a_1	a_2	a_3	a_4	a_5	a_6	a_7
$0.025 \leq C_1 = 0.1$	12.115	0.26	261.787	0.615	297.46	0.252	0.478
$0.1 < C_1 \leq 0.2$	12.836	1.02	258.324	0.612	260	0.165	0.517
$0.2 < C_1 \leq 0.56$	13.195	0.686	60.592	0.667	55.934	0.687	0.212
$0.56 < C_1 \leq 2$	8.714	0.225	35.796	0.656	45.56	0.758	0.045

REFERENCES

[1] Quoilin S, Broek MVD, Declaye S, Dewallef P, Lemort V. Techno-economic survey of organic rankine cycle (ORC) systems. Renew Sustain Energy Rev 2013;22:168–86. https://doi.org/10.1016/j.rser.2013.01.028.

[2] Miró L, Brückner S, Cabeza LF. Mapping and discussing Industrial Waste Heat (IWH) potentials for different countries. Renew Sustain Energy Rev 2015;51:847–55. https://doi.org/10.1016/j.rser.2015.06.035.

[3] Sollesnes G, Helgerud HE. Potensial studie for utnyttelse av spillvarme fra norsk industri. Tech Rep 2009:3–73. Document number 28769.

[4] Forman C, Muritala IK, Pardemann R, Meyer B. Estimating the global waste heat potential. Renew Sustain Energy Rev 2016;57:1568–79. https://doi.org/10.1016/j.rser.2015.12.192.

[5] Kim T, Rahimi M, Logan BE, Gorski CA. Harvesting energy from salinity differences using battery electrodes in a concentration flow cell. Environ Sci Technol 2016;50(17):9791–7. https://doi.org/10.1021/acs.est.6b02554.

[6] Micale G, Cipollina A, Tamburini A. Salinity gradient energy. Elsevier Ltd.; 2016. https://doi.org/10.1016/B978-0-08-100312-1.00001-8.

[7] Weiner AM, McGovern RK, Lienhard JH. A new reverse electrodialysis design strategy which significantly reduces the levelized cost of electricity. J Membr Sci 2015;493:605–14. https://doi.org/10.1016/j.memsci.2015.05.058.

[8] Weiner AM, McGovern RK, Lienhard JH. Increasing the power density and reducing the levelized cost of electricity of a reverse electrodialysis stack through blending. Desalination 2015;369:140–8. https://doi.org/10.1016/j.desal.2015.04.031.

[9] Post JW, Goeting CH, Valk J, Goinga S, Veerman J, Hamelers HVM, et al. Towards implementation of reverse electrodialysis for power generation from salinity gradients. Desalinat Water Treat 2010;16(1–3):182–93. https://doi.org/10.5004/dwt.2010.1093.

[10] Daniilidis A, Herber R, Vermaas DA. Upscale potential and financial feasibility of a reverse electrodialysis power plant. Appl Energy 2014;119:257–65. https://doi.org/10.1016/j.apenergy.2013.12.066.

[11] Turek M, Bandura B. Renewable energy by reverse electrodialysis. Desalination 2007;205(1):67–74. https://doi.org/10.1016/j.desal.2006.04.041.

[12] Bevacqua M, Tamburini A, Papapetrou M, Cipollina A, Micale G, Piacentino A. Reverse electrodialysis with NH4HCO3-water systems for heat-to-power conversion. Energy 2017;137:1293–307. https://doi.org/10.1016/j.energy.2017.07.012.

[13] Veerman J, Vermaas DA. Reverse electrodialysis: fundamentals. Elsevier Ltd.; 2016. https://doi.org/10.1016/B978-0-08-100312-1.00004-3.

[14] Burheim OS, Seland F, Pharoah JG, Kjelstrup S. Improved electrode systems for reverse electro-dialysis and electro-dialysis. Desalination 2012;285:147–52. https://doi.org/10.1016/j.desal.2011.09.048.

[15] McCutcheon JR, McGinnis RL, Elimelech M. A novel ammonia-carbon dioxide forward (direct) osmosis desalination process. Desalination 2005;174(1):1–11. https://doi.org/10.1016/j.desal.2004.11.002.

[16] McGinnis RL, Elimelech M. Energy requirements of ammonia-carbon dioxide forward osmosis desalination. Desalination 2007;207(1–3):370–82. https://doi.org/10.1016/j.desal.2006.08.012.

[17] Luo X, Cao X, Mo Y, Xiao K, Zhang X, Liang P, et al. Power generation by coupling reverse electrodialysis and ammonium bicarbonate: implication for recovery of waste heat. Electrochem Commun 2012;19(1):25–8. https://doi.org/10.1016/j.elecom.2012.03.004.

[18] Cusick RD, Hatzell M, Zhang F, Logan BE. Minimal RED cell pairs markedly improve electrode kinetics and power production in microbial reverse electrodialysis cells. Environ Sci Technol 2013;47(24):14518–24. https://doi.org/10.1021/es4037995.

[19] Bandyopadhyay A. Amine versus ammonia absorption of CO_2 as a measure of reducing GHG emission: a critical analysis. Clean Technol Environ Policy 2011;13(2):269–94. https://doi.org/10.1007/s10098-010-0299-z.

[20] Nazemi M, Zhang J, Hatzell MC. Harvesting natural salinity gradient energy for hydrogen production through reverse electrodialysis power generation. J Electrochem Energy Convers Stor 2017;14(2):020702. https://doi.org/10.1115/1.4035835.

[21] Schoots K, Ferioli F, Kramer GJ, van der Zwaan BC. Learning curves for hydrogen production technology: an assessment of observed cost reductions. Int J Hydrogen Energy 2008;33(11):2630–45. https://doi.org/10.1016/j.ijhydene.2008.03.011.

[22] Kwon K, Park BH, Kim DH, Kim D. Parametric study of reverse electrodialysis using ammonium bicarbonate solution for low-grade waste heat recovery. Energy Convers Manag 2015;103:104–10. https://doi.org/10.1016/j.enconman.2015.06.051.

[23] Naik-Dhungel N. Waste heat to power systems. Tech Rep 2012. https://doi.org/10.1071/EG989133.

[24] Burheim OS. Electrochemical energy storage. In: Engineering energy storage, vol. 1; 2017. p. 1–76. https://doi.org/10.1002/9781118998151.

[25] Veerman J, Post JW, Saakes M, Metz SJ, Harmsen GJ. Reducing power losses caused by ionic shortcut currents in reverse electrodialysis stacks by a validated model. J Membr Sci

2008;310(1–2):418–30. https://doi.org/10.1016/j.memsci.2007.11.032.
[26] Zhu X, He W, Logan BE. Influence of solution concentration and salt types on the performance of reverse electrodialysis cells. J Membr Sci 2015;494:154–60. https://doi.org/10.1016/j.memsci.2015.07.053.
[27] Vermaas DA, Saakes M, Nijmeijer K. Enhanced mixing in the diffusive boundary layer for energy generation in reverse electrodialysis. J Membr Sci 2014;453:312–9. https://doi.org/10.1016/j.memsci.2013.11.005.
[28] Minke C, Turek T. Economics of vanadium redox flow battery membranes. J Power Sources 2015;286:247–57. https://doi.org/10.1016/j.jpowsour.2015.03.144.
[29] Kempener F, Ruud, Neumann. Salinity gradient energy: technology brief. International Renewable Energy Agency (IRENA) (June); 2014. p. 566–71. https://doi.org/10.1109/OCEANS.1979.1151215.
[30] Fischer UR, Krautz HJ, Wenske M, Tannert D, Krüger P, Ziems C. Hydrogen hybrid power plant in prenzlau, brandenburg, hydrogen science and engineering: materials, processes, systems and technology 2016;2:1033–51. https://doi.org/10.1002/9783527674268.ch44 (June 2013).
[31] Jalili Z, Wergeland K, Einarsrud KE, Burheim OS. Energy generation and storage by salinity gradient power : a model-based assessment. J Energy Stor 2019.

Low-Grade Waste Heat to Hydrogen

8

Yash D. Raka, Robert Bock, Jacob J. Lamb, Bruno G. Pollet, and Odne S. Burheim

Y. D. Raka · R. Bock
Department of Energy and Process Engineering, ENERSENSE, Norwegian University of Science and Technology, Trondheim, Norway
e-mail: yash.raka@ntnu.no; robert.bock@ntnu.no

J. J. Lamb (✉)
Department of Electronic Systems, ENERSENSE, Norwegian University of Science and Technology, Trondheim, Norway

Department of Energy and Process Engineering, ENERSENSE, Norwegian University of Science and Technology, Trondheim, Norway
e-mail: jacob.j.lamb@ntnu.no

B. G. Pollet · O. S. Burheim
Department of Energy and Process Engineering, ENERSENSE and NTNU Team Hydrogen, Norwegian University of Science and Technology, Trondheim, Norway
e-mail: bruno.g.pollet@ntnu.no; odne.s.burheim@ntnu.no

J. J. Lamb, B. G. Pollet (eds.), *Micro-Optics and Energy*,
https://doi.org/10.1007/978-3-030-43676-6_8

membranes

Article

The Influence of Concentration and Temperature on the Membrane Resistance of Ion Exchange Membranes and the Levelised Cost of Hydrogen from Reverse Electrodialysis with Ammonium Bicarbonate

Yash Dharmendra Raka [1], Robert Bock [1], Håvard Karoliussen [1], Øivind Wilhelmsen [2] and Odne Stokke Burheim [1,*]

[1] Department of Energy and Process Engineering, Norwegian University of Science and Technology, Kolbjørn Hejes vei 1B, NO-7491 Trondheim, Norway; yash.raka@ntnu.no (Y.D.R.); robert.bock@ntnu.no (R.B.); havard.karoliussen@ntnu.no (H.K.)
[2] SINTEF Energy Research, NO-7465 Trondheim, Norway; oivind.wilhelmsen@sintef.no
* Correspondence: burheim@ntnu.no

Abstract: The ohmic resistances of the anion and cation ion-exchange membranes (IEMs) that constitute a reverse electrodialysis system (RED) are of crucial importance for its performance. In this work, we study the influence of concentration (0.1 M, 0.5 M, 1 M and 2 M) of ammonium bicarbonate solutions on the ohmic resistances of ten commercial IEMs. We also studied the ohmic resistance at elevated temperature 313 K. Measurements have been performed with a direct two-electrode electrochemical impedance spectroscopy (EIS) method. As the ohmic resistance of the IEMs depends linearly on the membrane thickness, we measured the impedance for three different layered thicknesses, and the results were normalised. To gauge the role of the membrane resistances in the use of RED for production of hydrogen by use of waste heat, we used a thermodynamic and an economic model to study the impact of the ohmic resistance of the IEMs on hydrogen production rate, waste heat required, thermochemical conversion efficiency and the levelised cost of hydrogen. The highest performance was achieved with a stack made of FAS30 and CSO Type IEMs, producing hydrogen at 8.48×10^{-7} kg $m_{mem}^{-2} s^{-1}$ with a waste heat requirement of 344 kWh kg^{-1} hydrogen. This yielded an operating efficiency of 9.7% and a levelised cost of 7.80 € $kg_{H_2}^{-1}$.

Keywords: reverse electrodialysis (RED); anion-exchange membrane; cation-exchange membrane; membrane resistance; membrane resistivity; ion-exchange membrane; hydrogen production; ammonium bicarbonate; low-grade waste heat to hydrogen

Citation: Raka, Y.D.; Bock, R.; Karoliussen, H.; Wilhelmsen, Ø.; Stokke Burheim, O. The Influence of Concentration and Temperature on the Membrane Resistance of Ion Exchange Membranes and the Levelised Cost of Hydrogen from Reverse Electrodialysis with Ammonium Bicarbonate. *Membranes* **2021**, *11*, 135. https://doi.org/10.3390/membranes11020135

Academic Editor: Yoshihiko Sano
Received: 16 December 2020
Accepted: 5 February 2021
Published: 16 February 2021

1. Introduction

In the imminent transition needed in our energy economy, shifting from fossils to sustainable, a demand for vast amounts of chemically storable energy for transportation and the chemical process industry is emerging. Our energy economy is transcending from burning chemical energy to generate electricity into an energy economy where electricity is used for producing chemicals and chemical energy. In this emerging energy economy, most of the electrical energy is generated from solar and wind power, likely to an extent where utilising waste heat for electricity production will become much less interesting than what has been suggested so far. Utilising industry waste heat for hydrogen production, however, is far more future-oriented. One of very few techniques that can be employed to achieve this is regenerative reverse electrodialysis electrolysis [1].

In a reverse electrodialysis (RED) system, the concentration gradient of salt solutions across an ion-exchange membrane (IEM) acts as a driving force for ions to diffuse through the membrane to create an ionic flux. This flux can be converted into either electrical current or a gas with an appropriate combination of electrolyte rinse solutions and electrodes.

Typically, seawater and river water salt solutions are used in RED systems today to produce electricity. Due to geographical constraints and biofouling, closed-loop systems have received increasing attention [2–7]. In these systems, the temperatures and pressures of the outlet solutions are modified to restore the initial concentrations [2,8]. Some of these systems use heat to evaporate either the solvent or the solute. The choice of salts in these processes depends on the solubility, the resistivity and the amount of heat required [2]. Ammonium bicarbonate-based reverse electrodialysis (AmB RED) is one such system that has shown potential in developing feasible closed-loop systems [3,9,10]. An example of such an AmB RED system that uses waste heat to generate hydrogen is depicted in Figure 1. This concept will be studied in further detail in this work.

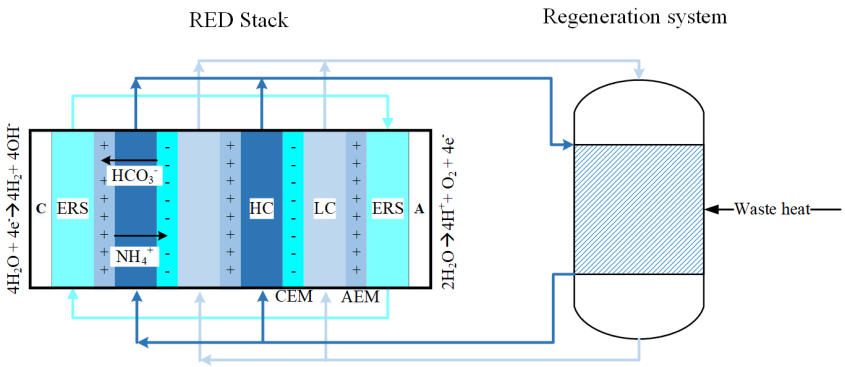

Figure 1. Schematic of an ammonium bicarbonate reverse electrodialysis cell with a thermally regenerative system. Here, C is the cathode where the hydrogen evolution reaction (HER) occurs, A is the anode where water is produced. Both of these electrodes are in contact with electrode rinse solution made of 1 M sodium bicarbonate. The "+" marked symbol denotes anion exchange membrane and "−" marked symbol denotes cation exchange membrane. The concentrate and dilute feed solutions are described as HC and LC, respectively.

As in many electrochemical energy systems, low resistance and high selectivity are key requirements for the membranes used. For an optimal RED system, the membranes must be thin ($\delta_m < 100\,\mu m$), usually without reinforcement (moderate mechanical properties) and with a low electrical resistance ($R_m < 1\,\Omega\,cm^2$) [11]. Determination of the membrane resistance under different working conditions provides insight into loss of efficiency and thus the performance of RED [12]. In this work, we experimentally evaluate the membrane resistance of ten different IEMs. A more thorough introduction and review of methods for measuring the ohmic resistance will be presented in Section 2. The information about the resistance of the IEMs will be used to gauge the influence of the membrane resistance on hydrogen production and waste heat required using a concept similar to the one depicted in Figure 1. Eventually, we will estimate the influence of membrane resistance on the thermodynamic efficiency and levelised cost of hydrogen (LCH).

2. Theory and Background

The performance of a RED system is determined by the maximum power produced per unit membrane area and by its maximum efficiency. The process efficiency of a RED system is a major hurdle, and an increase in membrane resistivity decreases process efficiency. Therefore, to optimise the system, the membrane resistivity is a key parameter [13,14]. The ionic resistance of commercially available ion-exchange membranes is often reported as an area resistance, because this quantity is useful for predicting and comparing the performance of the membranes in many applications [15]. Decreasing the thickness of a polymer film tends to reduce the area resistance [11,15]. The thickness of the membrane is essentially fixed by the manufacturing process. This makes evaluation and comparison of

the intrinsic ion transport properties of polymer films prepared at different film thicknesses difficult [15]. For homogeneous polymer films, such as the membranes considered in this work, the area resistance can be normalised by film thickness to obtain the intrinsic ionic resistance (i.e., resistivity) of the polymer.

The electrical resistivity of an IEM is a function of the concentration of mobile ions in the IEM and of the mobility of the ions in the membrane phase. The membrane phase ion mobility relates to the ion exchange capacity (IEC), water content (V_w) and cross-linkage of the membrane. Typically, an IEM with high IEC, high V_w and low cross-linkage has a low electrical resistivity. This relation is due to the dependence of the electrical resistivity of the ion exchange membrane on the concentration of counterions in the membrane and on Donnan-adsorbed ions. The present work focuses on the use of IEMs for RED working within the typical operating ohmic regime. As this regime is at a relatively low current density, the imposed voltage and current density have a linear relation. Thus, ion depletion in the concentration polarisation boundary layer is not dominant, and a limiting current is not reached. Experimentally, the resistivity of a membrane $\bar{\rho}_{mem}$, is found by measuring the amount of current when a certain potential difference is applied over two electrodes.

$$\bar{\rho}_{mem} = \frac{ASR}{\delta_{mem}} \tag{1}$$

where ASR is the area-specific resistance [Ω-m^2], δ_{mem} is the membrane thickness [μm] and the resistivity is an intensive property. There are various methods to evaluate the membrane resistivity. A flow cell configuration is one such method in which a membrane separates two or more compartments of salt solutions with the same concentration as shown as in Figure 2 left [16]. The cell resistance due to the membrane and due to the ionic solutions between the membranes is measured and defined as the stagnant diffusion layer (SDL) resistance [12]. An illustration of the diffusion boundary layers that can be found in the vicinity of the membrane is provided in Figure 2 right.

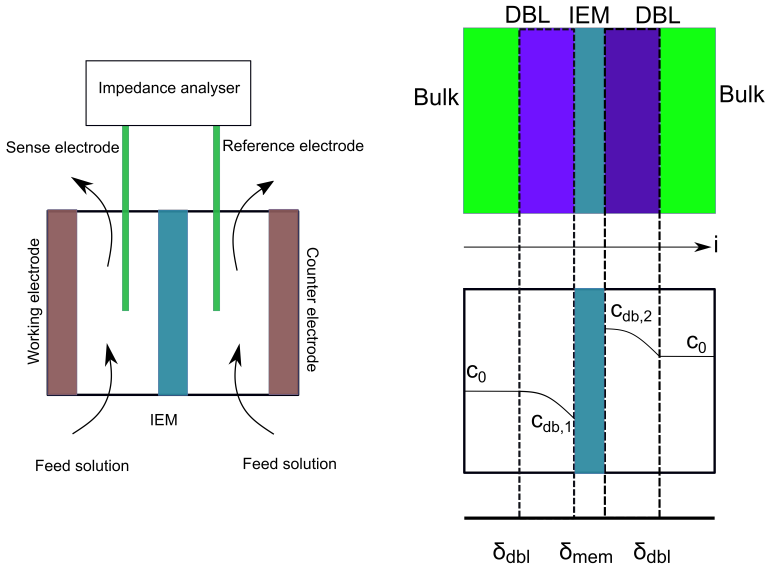

Figure 2. A flow cell configuration measuring membrane resistance using electrochemical impedance spectroscopy (**left**). Diffusion boundary layer (DBL) near the surface of a cation-exchange membrane and the salt concentration distribution in different layers at steady state (**right**). The current direction is to the right.

Another method is a cell configuration in which the membrane is sandwiched between two electrodes with no flow of solution. Here, the ohmic resistance of the electrochemical cell is measured with and without a membrane. The difference between those two values gives the membrane resistance [16]. The resistance measurements can be performed with two, three or four electrodes. In case of two electrodes, one acts as counterelectrode and reference electrode, while the other as working electrode and reference electrode. A three-electrode system includes the working electrode, the counterelectrode and a reference electrode. The potential difference is measured between the reference electrode and the working electrode. In the four-electrode system, there is an additional reference electrode with respect to the three electrode setup. The reference electrodes are connected to a high impedance device, so that in principle there is no current flow through these electrodes. Furthermore, no measurement is needed for the current-generating electrodes [12].

Electrochemical impedance spectroscopy (EIS) gives the frequency-specific impedance of a material. The impedance, Z, is a complex number, defined to be the ratio of the complex potential, E, and the complex current, I. In an EIS measurement, an alternating voltage or alternating current of known frequency and defined amplitude is applied to an electrochemical system. The corresponding response in terms of either current or voltage from the system is measured. When the response to a sinusoidal signal is a sinusoid, the system is said to be a linear system at the same frequency. In case of a complex-valued impedance, the imaginary value is not zero and there will be a phase shift (ϕ).

$$Z = \frac{E(t)}{I(t)} \tag{2}$$

where $E(t)$ and $I(t)$ are voltage [V] and current [A] as a function of time t. The varying voltage and current with time are defined as

$$E(t) = E_0 sin\omega t = E_0 e^{j\omega t} \tag{3}$$

$$I(t) = I_0 sin(\omega t + \phi) = I_0 e^{j(\omega t + \phi)} \tag{4}$$

where E_0 is the voltage in phase, I_0 is the alternating current in phase and j is the imaginary number ($j = \sqrt{-1}$). The ϕ is defined as the tangent of the angle between the real and the imaginary impedance. ω is the circular frequency of alternating current and is given by

$$\omega = 2\pi f \tag{5}$$

where f is the frequency.

By using Euler's formula, the impedance can be defined as

$$Z(\omega) = \frac{E_0 e^{j\omega t}}{I_0 e^{j(\omega t + \phi)}} \tag{6}$$

where the real part and imaginary parts are

$$Re(Z) \equiv Z' = |Z| cos\phi \tag{7}$$

$$Img(Z) \equiv Z'' = |Z| sin\phi \tag{8}$$

If the phase between current and voltage is zero, this implies that there is no capacitive or inductive response of the system and that there is no imaginary part in the impedance. Macdonald et al. were the first to obtain an exact expression for the small signal impedance for the case of no space charge layers in the absence of an applied potential difference [17]. This resulted in exact equivalent electrical circuits including geometric capacity and frequency dependant impedance. Many researchers opt to a graphical representation of a modelled physical and a chemical process analogous to a circuit electrical diagrams [14], as depicted in Figure 3.

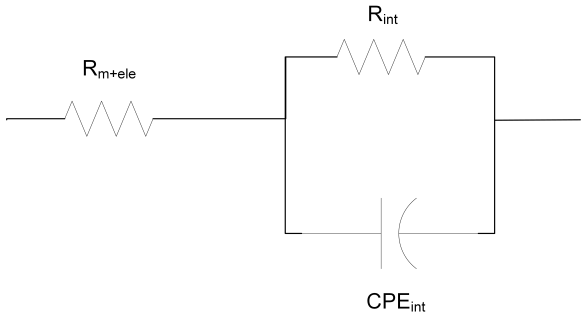

Figure 3. Equivalent circuit used for the fitting of electrochemical impedance spectroscopy (EIS) measurements. The resistance (R_{int}) and constant phase element (C_{int}) represent the interface between electrode and solution layer on the ion-exchange membrane (IEM) (i.e., solution–electrode interface). The ohmic resistance of the IEM and the electrode is represented by R_{m+ele}.

In general, there are three basic elements in such graphical representations: the electrochemical resistor, and the electrical and chemical capacitors. By changing the frequency of the applied AC potential, the resistance of the solution and the electrical double layer (EDL) can be differentiated [12,18–20]. While at low applied AC frequency to the membrane system, the resulting electrical equivalent circuit indicates the effect of the diffusion boundary layer (DBL) and the EDLs, at high frequency, the AC reveals the resistance attributed to the membrane polymer itself. That is, the impedance of the IEM is a real value. The impedance data are interpreted in terms of electrical equivalent circuits (EEC) using simple fitting [14]. When a current pulse is applied to an interface, one part is consumed by the EDL charging and the other is used for an interface electrochemical reaction. Randles and Ershler proposed an EEC for a metal electrode impedance [17]. It is composed of two parallel branches with an EDL capacitance in the first one and a reaction resistance in the second. This means that the total electric current can be separated into faradaic and charging currents. Similar principles are used to describe the impedance of an ion exchange membrane. In this work, we use EIS with a direct difference method and a two electrode setup, primarily because it is simple and robust. In addition, it also avoids electrochemical reactions that may occur during the measurement and is more accurate in differentiating the pure membrane resistance from the DBL and the EDL [12,18,20].

Effect of Solution Concentration, IEM Thickness and Operating Temperature on Membrane Resistance

The membrane resistance depends on the counterion concentration and mobility. IEMs operating at feed concentrations <0.3 M NaCl have displayed significantly increased membrane resistivity. The use of highly concentrated solutions gave a decrease in membrane resistance for an anion-exchange membrane at increasing concentration; the opposite trend was found for a cation-exchange membrane. The difference in the trend was attributed to the density of fixed charge groups and ion exchange capacity, as well as membrane thickness [11,21]. Galama et al. proposed that there are two phases in the membrane: Phase I corresponds to permeation regions with attached fixed charges, where the ionic concentration is determined by electroneutrality and Donnan equilibrium. Phase II corresponds to permeation regions without fixed charges, where the ionic concentration is equal to that in the external bulk solution [12]. The membrane resistance, R_I (Ω cm^2) corresponding to phase I, dominates for concentrations higher than 0.3 M. This is the result of the interaction limiting ion mobility in phase I. The concentration-dependent resistance of phase II, R_{II} (Ω cm^2) dominated for the salt concentration lower than 0.3 M. This behaviour is attributed to a change in the ion concentration in phase II. Kamcev et al. proposed that thin bulk solution layers at the membrane surface contribute to the measured resistance [16]. The membrane resistance is sensitive to the salt identity, for which it depends on the counte-

rion identity. Furthermore, the membrane resistance typically increases with increasing hydration free energy of the counterion in the bulk solution, indicating that steric effects are important determinants of membrane ionic resistance. The membrane resistance has displayed a strong inverse correlation with solution concentration below 0.1 M, and remains approximately constant at higher concentrations. The membrane ionic conductivity increases with increase in salt concentration, which was attributed to increased ion concentrations due to weaker Donnan exclusion. The membrane ionic conductivity for CMX decreases due to osmotic deswelling causing decreased ion diffusion coefficients. The apparent resistance is the actual ohmic resistance from the IEMs introduced in a RED stack in operation and is significantly higher than the value from the standard measurement (with 0.5 M NaCl solution) [22]. This effect needs to be clarified and modelled for an improved representation of the RED stack. Several models have been proposed based on experimental data. Veerman fitted experimental data to an exponential function of the form [23]

$$R_m = A + B \cdot e^{-rC} \tag{9}$$

where A, B and r are all fitting parameters, and C is the solution concentration. Later, Kim et al. pointed out that the membrane resistance is a linear function of the reciprocal of the solution concentration [24]:

$$R_m \propto \frac{1}{C} \tag{10}$$

Guler et al. found that the membrane resistance does not extrapolate to zero when the membrane thickness becomes zero. Galama et.al. proposed the modified relationship as [22]

$$R_m = A + \frac{r}{C} \tag{11}$$

It was found that a route for the fabrication of homogeneous membranes without reinforcement and with reduced thickness yields IEMs with low resistances. Operating at high temperature generally increases the feed resistivity, facilitates ionic mobilities and thus reduces the Ohmic resistance.

3. Materials and Methods

The list of membranes used in the present study is presented in Table 1. The membranes are chosen based on their properties: low membrane resistance and high permselectivity in NaCl solution, or lack of literature data on membrane resistance values for ammonium bicarbonate solution for some membranes. The properties listed are extracted from the manufacturers data sheet and from literature.

Table 1. Overview of the membranes examined in this work. The membrane resistance and permselectivity values extracted from manufacturer's data sheet are tested in 0.5 M NaCl at 298 K and 0.5 M/0.1 M NaCl at 298 K, respectively.

IEM	Type	Thickness µm	Fixed Charge Group	Material	Counter-ion	Permselectivity	Resistance $\times 10^{-4}\ \Omega\ m^2$	IEC meq g^{-1}	SD (wt) meq g^{-1}	Ref
FKE	CEM	28–33	$-SO_3^-$	-	H^+	0.965–0.986	1.6–2.46	1.35–1.36	12–27	[21]
FKSPET	CEM	74–87	$-SO_3^-$	-	H^+	>0.95	2.5	1–1.25	-	*
FAS	AEM	27–33	-	-	Br^-	0.894–0.9	1.03–2	1.1–1.85	8–19	[14,21]
FASPET	AEM	72–85	-	-	Br^-	>0.9	<3	1–1.5	-	*
DSV	AEM	95–121	-		Cl^-	0.899	2.3	1.89	28	[21]
AMV	AEM	110–150	$-N(CH_3)_3^+$	PS/DVB/CMS	Cl^-	0.873–0.96	2.8–3.15	1.78–1.9	17–19.8	[14,21, 25]
CMV	CEM	101–150	-	PS/DVB	Na^+	0.91–0.988	1.03–1.1	2–2.4	20–30	[14,21, 25]
CSO	CEM	100	-	PS/DVB	Na^+	0.923–0.97	2.29–3	1.04	16	[25]
CMF	CEM	440	-	-	H^+	> 0.95	2.5	-	-	*
APS	AEM	138–150	$-N(CH_3)_3^+$	PS/DVB/CMS	SO_4^{2-}	0.884	0.68–0.7	0.29	147	[21,25]

* Manufacturer's data sheet.

3.1. Membrane Resistivity Measurements

3.1.1. Membrane Equilibration

The experimental setup for direct measurement of membrane resistivities is depicted in Figure 4. We shall next describe the details of how the experiments were carried out. First, membranes were cut in a circular shape with a diameter of 2 cm. Each of these membranes were soaked in a bottle with approximately 200 mL of ammonium bicarbonate solution (Merck, Germany, EMPROVE, 99–101%) in an equilibration concentration (0.1 M, 0.5 M, 1 M, 2 M) for at least 48 hrs without refreshing the solution. The membranes were kept at a temperature of 295 ± 2 K and 313 ± 1 K for room and elevated temperature measurements, respectively. The elevated temperature of 313 K was chosen to reflect the RED system's improved performance, the expected maximum operating temperature range of the membranes and the temperature-dependent concentration change of the ammonium bicarbonate solution. The counterions listed in Table 1 were exchanged with ammonium ions for cation-exchange membranes and bicarbonate ions for anion-exchange membranes.

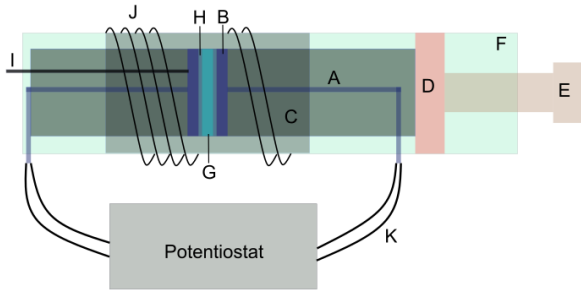

Figure 4. Experimental setup for direct membrane resistance measurement using two electrodes and electrochemical impedance spectroscopy. A. Platinum wire, B. Platinum disc electrode, C. Ceramic casing, D. Stopper, E. Tightening screw, F. Metal casing, G. IEM, H. Solution thin film, I. K-type thermocouple, J. Heating coil, K. Cables.

3.1.2. Electrode Preparation

The membrane resistance was measured using platinum disc electrodes. The disc electrodes were polarised for uniform surfaces using cyclic voltammetry using the reversible hydrogen electrodes (RHE) prepared in the lab. RHE were prepared in a glass tube with a 0.5 mm diameter platinum wire. An air-tight glass flask of 1200 mL filled with 200 mL of 99 % concentrated H_2SO_4 diluted in 1000 mL of DI water was used to prepare RHE and disc electrodes using chronoamperometry and cyclic voltammetry. A glass tube was filled with the same solution and then a two-electrode setup was used to produce hydrogen with chronoamperometry using a Gamry 5000 E interface. The experimental settings for this procedure are provided in Table 2.

The chronoamperometry was performed until the tube was 50% filled with H_2 gas. The disc electrodes used to measure membrane resistance were made of platinum with an active area of 3.14 cm^2 and a thickness of 1 mm. These electrodes were polarised using cyclic voltammetry (CV) under the following conditions the initial and final potential was 0 V. The scan limit, rate and step size were 1.6 V, 20 mV s^{-1} and 0.5 mV, respectively. The experiment was performed for 60 cycles at maximum current limit of 20 mA.

The CVs were performed with a three-electrode setup with the RHE (explained above) as the reference. Ten to fifteen cycles were performed to have a stable voltammogram which corresponds to a uniform surface. Insulated platinum/copper wires were used to connect the platinum disc electrodes to the potentiostat. The disc electrodes were enclosed in a ceramic hollow cylinder and kept in a thick rectangular metal box. A screw was used to clamp the ceramic cylinder and metal box. A clamping torque of 2 Nm was set for all experiments.

Table 2. Parameters for the chronoamperometry procedure.

Parameter	Value	Unit
Electrode Area	3.14	cm^2
Pre-step Voltage	0 vs. E_{ref}	V
Pre-step Delay Time	0.5	s
Step 1 Voltage	−2.5	V
Step 1 Time	200	s
Step 2 Voltage	0.1	V
Step 2 Time	5	s
Max Current	200	mA
Limit I	200	mA cm^{-2}
Equil. Time	5	s

Electrochemical impedance spectroscopy was used to measure the ohmic resistance of the membranes. A set of three measurements were performed for a stack of 1, 3 and 5 membrane layers. The settings for the measurements are as follows: the initial frequency: -10^6 Hz; final frequency: −10 Hz, points/decade-15; AC Voltage: −10 mV; Area: −3.14 cm^2; and initial delay of 60 s.

Furthermore, a blank cell measurement was performed after every set. In the case of a high-temperature measurement, the setup was kept in a heating oven. For boosting the temperature of the membrane and disc electrodes, an external heating coil was wound along the length on the hollow ceramic cylinder as shown in Figure 4. One of the electrodes was connected to a thermocouple (type K) to measure the temperature of the disc electrode. The measurements were analysed using an equivalent circuit model. The ohmic resistance of the membrane plus the electrodes was then estimated. These resistances were plotted as functions of the membrane thickness. The intercept was treated as the ohmic resistance of the blank cell.

3.2. Thermodynamic Model for the RED System

To assess the significance of the measurement results and the resistance of the IEMs, a thermodynamic model for a thermally driven AmB RED based on a closed loop regenerative system developed by Raka et al. was used [26]. For details on the thermodynamic model, we refer to the work in [26]. The performance was evaluated in terms of hydrogen produced and waste heat required for restoring the concentrations.

The unit cell open circuit potential ($E^{oc}_{u.c}$) is the electromotive force driven by concentration difference across an ion exchange membrane with no losses considered. The open circuit potential of an IEM pair placed between two different concentration solutions can be described using the modified Nernst equation:

$$E^{oc}_{u.c} = (\alpha_{aem} + \alpha_{cem}) \frac{RT}{F} \ln\left(\frac{\gamma_c m_c}{\gamma_d m_d}\right) \quad (12)$$

where α is the permselectivity of IEMs measured at concentration m_c and m_d at a constant temperature of 298 K for a specific membrane. Here, we assume the same α for both membranes. In the above equation, F is the Faraday constant, T is the room temperature and R is the universal gas constant. The activity coefficient of solutions (γ) is a measure of the deviation from ideal solution. The activity coefficients depend on molal salt concentration. There is an internal loss in the RED cell due to its components and operating parameters. This internal resistance consists of ohmic and non-ohmic resistances. The ohmic resistance for a unit cell [$\Omega\ m^2$] is the cumulative sum of membrane and channel (concentrate and dilute) resistances.

$$R_{u.c} = R_{ch,d} + R_{ch,c} + R_{m,aem} + R_{m,cem} \quad (13)$$

The channel ohmic resistance (R_{ch}) is the resistance ($\Omega\ m^2$) due to the conductivity of the feed solution in the channel and spacer geometry. It depends on concentration and is

calculated using the molar conductivity of the salt. The actual unit cell potential ($E_{u.c}^{act}$) is the potential across the RED unit cell. The potential drops due to ohmic resistances in the RED unit cell:

$$E_{u.c}^{act} = E_{u.c}^{oc} - R_{u.c} j_{u.c}^{pp} \quad (14)$$

where the peak power current density ($j_{u.c}^{pp}$) [A m_{mem}^{-2}] is calculated using the following equation based on Ohm's law:

$$j_{u.c}^{pp} = \frac{E_{u.c}^{oc}}{2R_{u.c}} \quad (15)$$

3.2.1. Hydrogen Production

The theoretical amount of hydrogen produced per unit time in the compartment with electrode–electrolyte rinse solution is the hydrogen production rate ($\dot{n}_{H_2}$) [moles $m_{mem}^{-2} h^{-1}$], which can be calculated from

$$\dot{n}_{H_2} = \frac{j_{u.c}^{pp} 3600}{zF} \eta_F. \quad (16)$$

Here, z = 2 is the ion valence per mole of hydrogen gas, η_F is the faradaic efficiency. The η_F considers hydrogen gas losses and signifies that the current density generated is not fully converted to produce hydrogen gas due to various system related losses such as undesired reactions or loss in the form of heat [27]. In a RED system, the loss in faradaic efficiency is due to back diffusion of ions, transport of co-ions and osmosis (i.e., closely related to membrane permselectivity), and ionic short-circuiting in the feed and drain channels. This loss in faradaic efficiency can be as high as 50% in a typical closed loop RED system in comparison with alkaline water electrolysers where the faradaic efficiency ranges from 5 to 25% due to other reasons. Assuming a nearly ideal membrane, the faradaic efficiency is assumed to be 0.90. From Equations (15) and (16), we see that the resistance of the membrane is inversely proportional to hydrogen production rate at peak power.

3.2.2. Waste Heat/Regeneration System

The regeneration system restores the outlet concentration of the concentrate and dilute solutions to the corresponding inlet concentrations. It includes a stripping and an absorption process. The air-stripping column decomposes the outlet solution from the dilute compartment to a mixture of ammonia and carbon dioxide gas at 333 K. The absorption unit dissolves the decomposed gases at 293 K at the outlet of the concentrate channel. The heat required for restoring the concentrations to their original concentration is the regeneration heat (q_{reg}). The total amount of thermal power required to strip a volume flow rate of Q_{lc} [$m^3\ s^{-1}$] per unit membrane area of ammonium bicarbonate salt from the dilute solution channel is computed from

$$Q_{reg} = q_{AmB} Q_{lc}\ A_{mem}^{tot} \times 3600, \quad (17)$$

where q_{AmB} is the specific thermal duty [kWh m^{-3}] required to decompose ammonium bicarbonate solution into its components $NH_{4,(g)}$ and $CO_{2,(g)}$. The value was estimated using the relation from Bevacqua et al. with inlet and outlet concentration C_1 and C_2 from the stripping column, respectively:

$$q_{AmB} = a_1 e^{a_2 \cdot C_1} - a_3 C_2^{a_4} + a_5 C_1^{a_6} C_2^{a_7} \quad (18)$$

Here, a_1 to a_7 are fitting parameters that are functions of C_1 [10] .

3.2.3. Levelised Cost of Hydrogen

The model used to estimate the levelised cost of hydrogen (LCH) for the proposed system was developed previously by Raka et al. [26]. The parameters that have been changed for the present study are stated below, and we refer to Raka et al for further details [26]. Parameters used for this study are as follows: C_{mem} is cost of membrane,

5–150 € m^{-2}; C_{heat} is cost of waste heat, 0.01 € kWh^{-1}; η_{ele} is electrolysis efficiency, 0.9; and t_{mem} is membrane life, 10 years.

4. Results and Discussion

The membrane area resistances were estimated using equivalent circuit modelling of the data from the impedance measurement using a simple equivalent circuit as shown in Figure 3. The resistance in series (R_{m+ele}) is associated with the ohmic resistance from the membrane and the electrode. A blank cell measurement was performed to estimate the electrode resistance. This value was subtracted from R_{m+ele} to estimate the membrane resistance values. In the following section, the measured values for R_{mem} will be reported and discussed.

4.1. Influence of Thickness on Membrane Resistance and Membrane Resistance at Elevated Temperature

The membrane resistance is not only a material property, it is a ratio between the membrane thickness and its conductivity. With increasing membrane thickness, the length of transport pathway increases, and the membrane resistance increases proportionally. For all of the IEMs considered in this study, we observe a linear relationship between the membrane resistance and the membrane thickness. This has been shown for anion-exchange membranes (AEMs) at 295 ± 2 K and 313 ± 1 K in Figures 5 and 6, and for the cation-exchange membranes (CEMs) at the same temperatures in Figures 7 and 8. The membrane resistance is here found to increase with increasing thickness. A linear regression was used to fit the resistance as a function of thickness, and the coefficients of these polynomials and their uncertainties are provided in the Appendix A in Tables A1–A4. Though the linear equation describes the effect of thickness on the resistance reasonably well, we observe that there is a high double standard deviation in the resistivity (the slope of the equation). This is likely to be associated with the high variation in the IEM thickness, which is difficult to measure for swollen membranes, especially for the APS type (AEM). The increase in resistance due to increase in thickness is because an ion has to traverse further through the tortuous path inside of the membrane. Even though the AEMs are thinner compared to CEMs, in general, the CEM have lower resistances compared to the AEM. This may be due to the mobility of NH_4^+ ions, which is very high compared to the mobility of HCO_3^- ions, as shown in Table 3.

Table 3. Properties of the ions considered in this study.

Ion	NH_4^+	HCO_3^-
Hydrated radius [nm]	0.331	0.439
Charge density [mC cm^{-3}]	1.05	0.45
Average polarisability [a.u]	7.91	23.7
Ionic mobility [$cm^2V^{-1}s^{-1}$]	7.71×10^{-4}	4.59×10^{-4}

The Fumasep membranes with reinforcement—FASPET and FKSPET—have higher resistances compared to FAS and FKE. The increased resistance can be explained from the increased thickness (polyester reinforcement). FAS and FASPET follow a similar trend when it comes to the resistance as a function of the thickness. From Figures 5–8, it is difficult to evaluate the membranes based on their thickness normalised membrane conductivity or membrane ohmic resistance, as they give a different prioritisation of which membranes should be preferred. Although a thinner membrane may show lower conductivity at different concentrations, the measured membrane resistance of the thinner membranes can be lower than the thicker membranes with highest conductivity. This is because the conductive membrane is thicker.

In general, the membrane resistance decreases with increasing temperature. This can be explained on the basis of the increase in ionic mobility through the membrane which increases with temperature.

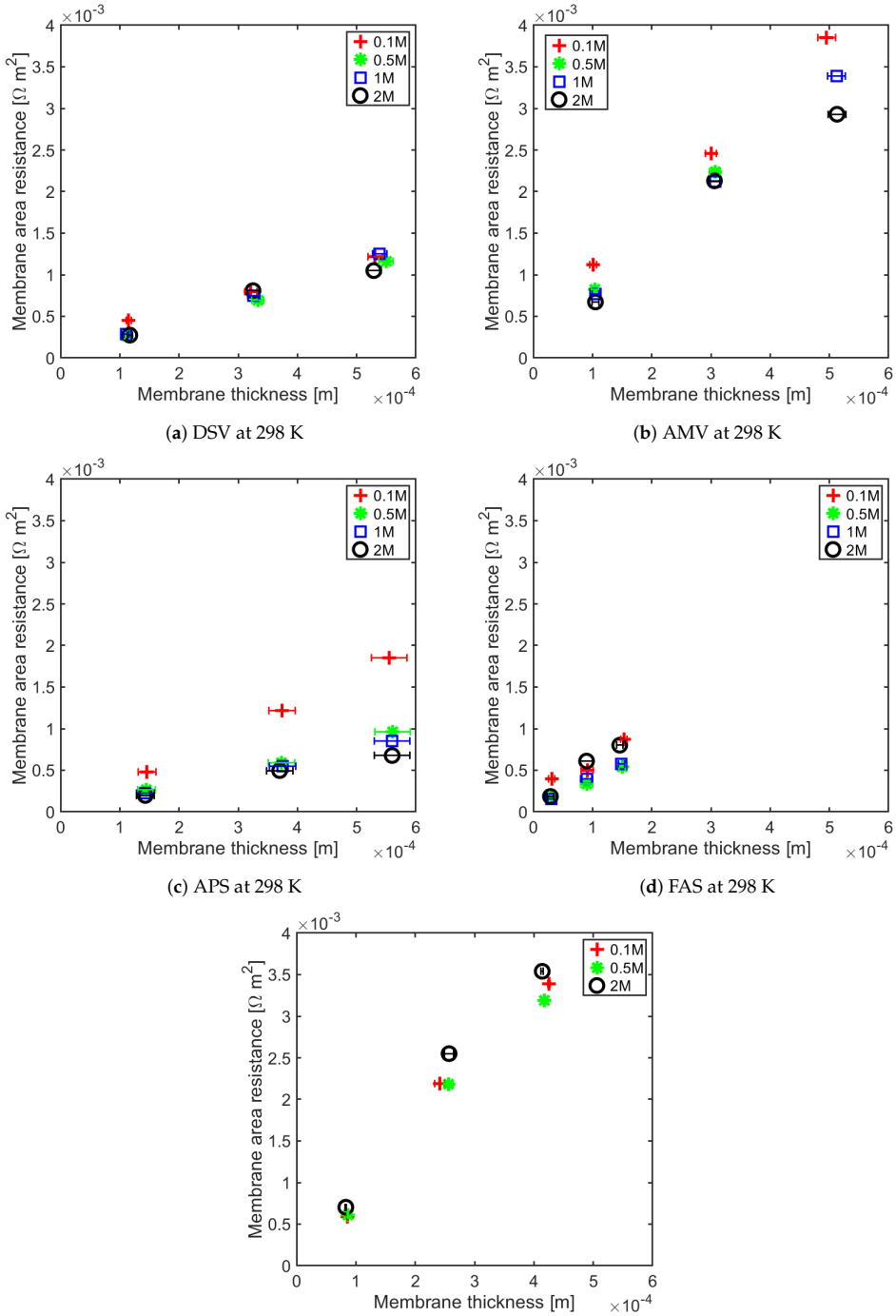

(**a**) DSV at 298 K

(**b**) AMV at 298 K

(**c**) APS at 298 K

(**d**) FAS at 298 K

(**e**) FASPET at 298 K

Figure 5. Anion exchange membrane (AEM) resistance as a function of thickness for different concentrations at 298 K.

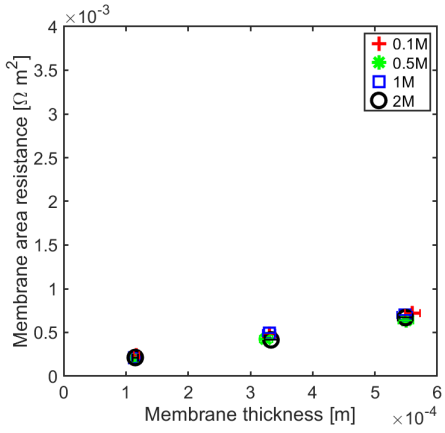

(**a**) DSV at 313 K

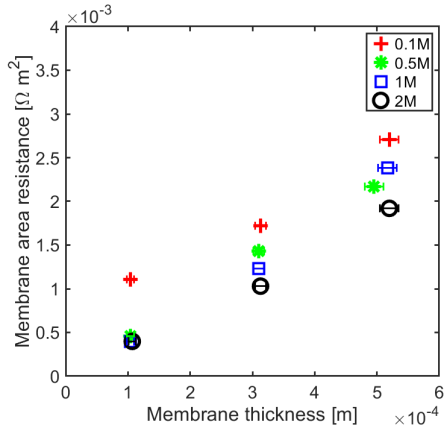

(**b**) AMV at 313 K

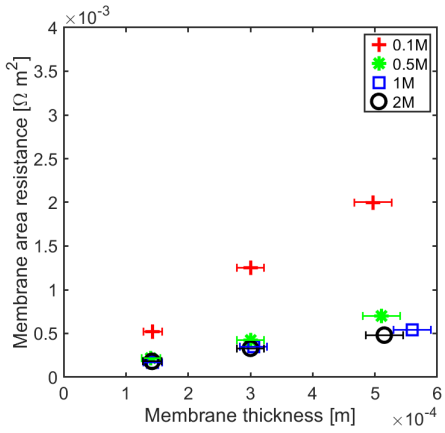

(**c**) APS at 313 K

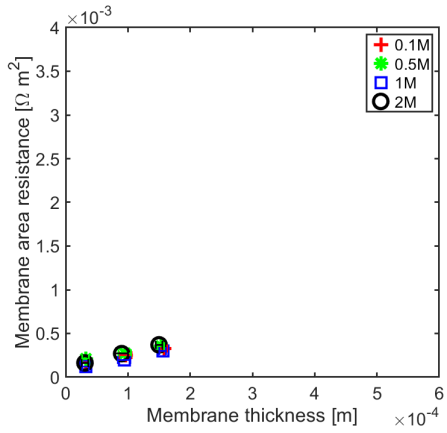

(**d**) FAS at 313 K

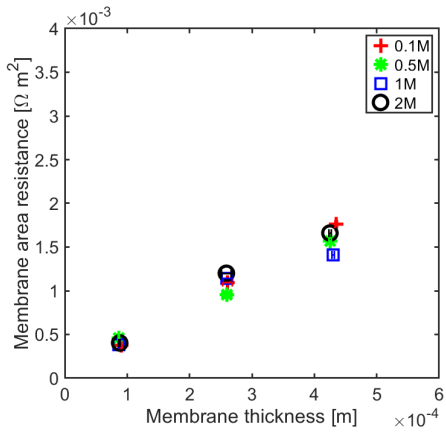

(**e**) FASPET at 313 K

Figure 6. AEM resistance as a function of thickness for different concentrations at 313 K.

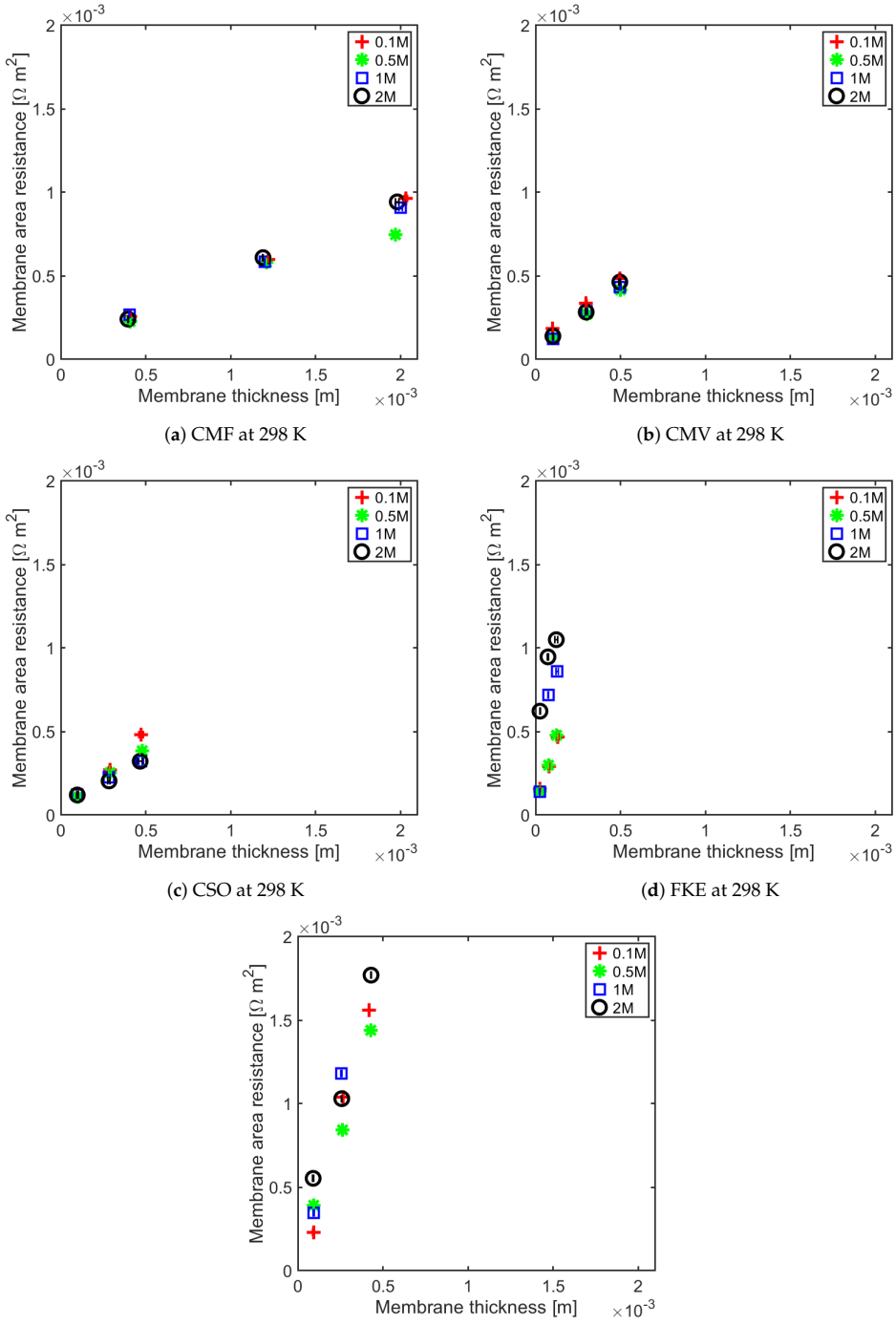

(**a**) CMF at 298 K

(**b**) CMV at 298 K

(**c**) CSO at 298 K

(**d**) FKE at 298 K

(**e**) FKSPET at 298 K

Figure 7. Cation exchange membrane (CEM) resistance as a function of thickness for different concentrations at 298 K.

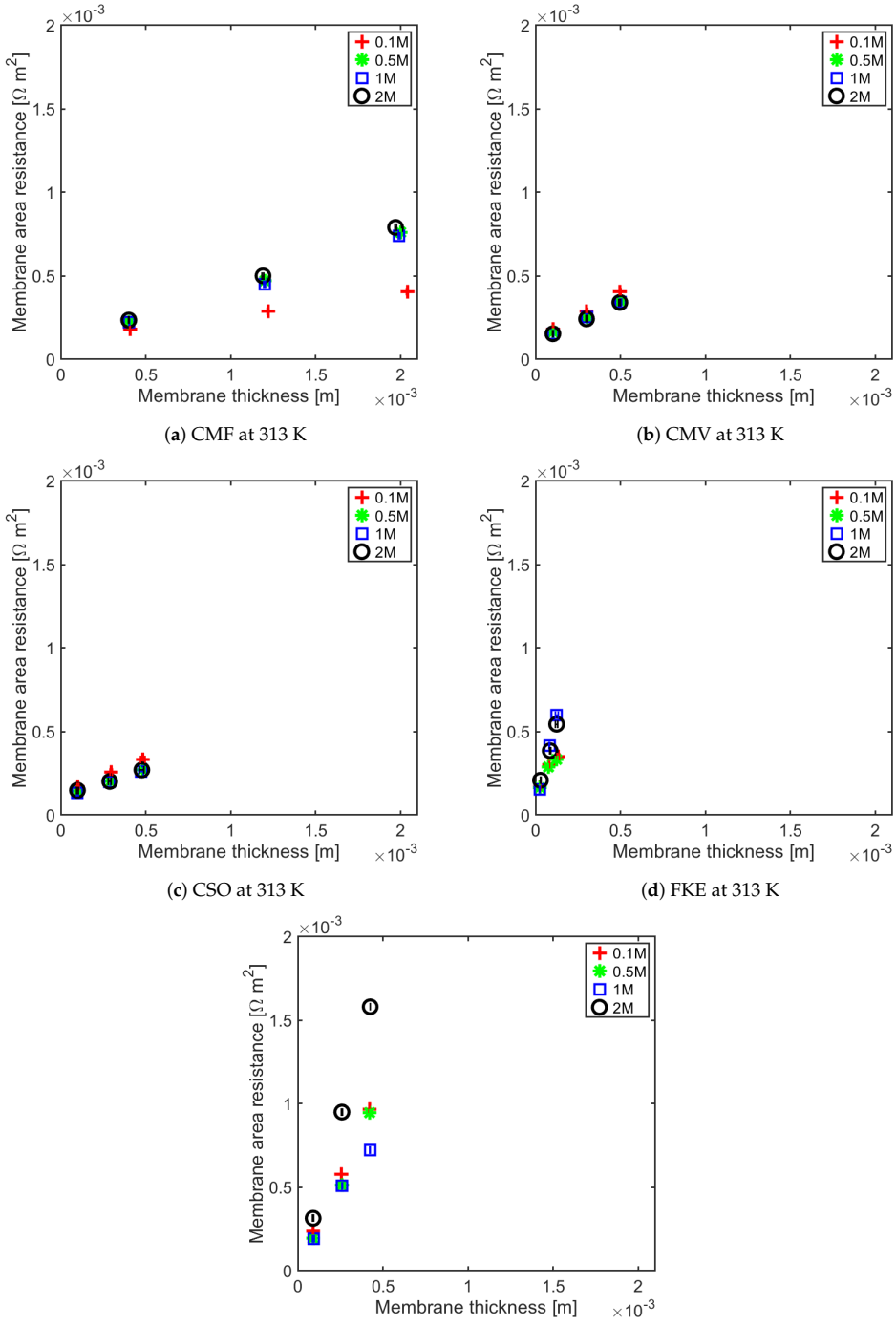

(**a**) CMF at 313 K

(**b**) CMV at 313 K

(**c**) CSO at 313 K

(**d**) FKE at 313 K

(**e**) FKSPET at 313 K

Figure 8. CEM resistance as a function of thickness for different concentrations at 313 K.

4.2. Influence of Concentration on Membrane Conductivity

Figure 9 shows how the conductivities of the different AEMs and CEMs change with concentration. The first conclusion that can be made on the basis of these results is that the conductivities of the CEMs are typically significantly higher than those of the AEMs. The mobility ratio of ammonium ions to bicarbonate ions is 1.67, this may explain higher conductivities in CEM membrane compared to AEM.

The electrolyte concentration influences the various IEMs differently. In the case of the CEMs, CMF and CSO exhibit the highest conductivities of all the membranes at both temperatures examined. For the AEMs, APS and DSV have the highest conductivities at both temperatures. APS and CSO display a clear trend, where the conductivity increases with increasing concentration.

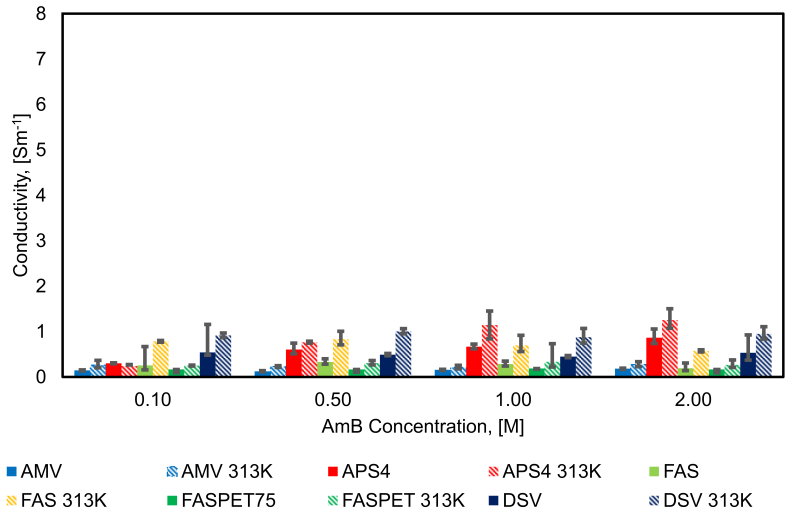

(**a**) AEM

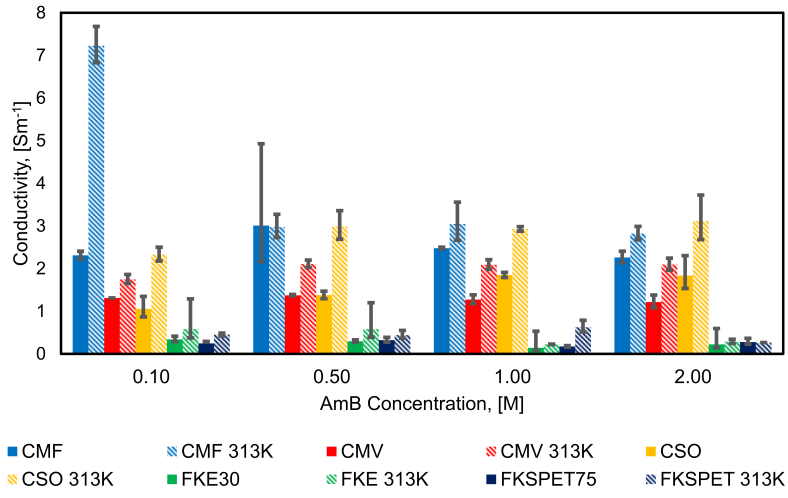

(**b**) CEM

Figure 9. Effect of the solution concentration on the IEM conductivity.

AMV, DSV and FKE have the lowest conductivities at 0.5 M and 1 M, respectively, and the conductivities increase/remain constant with further increase in concentration. This may be due to loss of water through the IEM or shrinkage, causing loss of conduction paths. In case of FAS, FASPET and CMV, the conductivity decreases with increase in concentration above 0.5 M, and it is lowest at 2 M. CMF shows almost constant conductivity with increase in concentration. The exact values of the mean conductivities of the membranes are reported in the Appendix A in Tables A5 and A6.

4.3. Influence of Membrane Resistance on H_2 Production rate and Specific Waste Heat Required Q_{req}

After the membrane characteristics have been determined experimentally, it is of interest to study how they influence the performance of a RED stack for generation of hydrogen by use of waste heat. Based on the measured values, we find that a lower ohmic resistance for the membranes gives higher hydrogen production rate and lower waste heat required per kg of hydrogen. The article compares the hydrogen production rate and specific waste heat required for membranes with the highest conductivity (APS and CMF) with the least resistance (FAS and CSO). The highest conductivity was found for a stack made with APS and CMF for 2 M/0.1 M feed solutions concentration. The hydrogen production rate and specific waste heat required based on APS and CMF membranes were found to be $6.51 \times 10^{-7}\,\mathrm{kg\,m^{-2}s^{-1}}$ and $419\,\mathrm{kWh\,kg_{H_2}^{-1}}$, respectively. For a stack made of FAS30 and CSO membranes as AEM and CEM with the least area specific resistance ($\Omega\,\mathrm{m^2}$) for 2 M/0.1 M feed solutions concentration at room temperature, the corresponding hydrogen production rate and specific waste heat required is $8.48 \times 10^{-7}\,\mathrm{kg\,m^{-2}s^{-1}}$ and $344\,\mathrm{kWh\,kg_{H_2}^{-1}}$. The hydrogen production from a RED stack with NaCl solution operating at sea water/river water concentration of 0.6 M/0.0015 M was theoretically estimated to be $9.64 \times 10^{-7}\,\mathrm{kg\,m^{-2}s^{-1}}$ and artificial NaCl solution with concentrations 4 M/0.017 M was experimentally found to be $4.94 \times 10^{-8}\,\mathrm{kg\,m_{ele}^{-2}s^{-1}}$ [27,28]. Compared with the proposed system, the reasons for low hydrogen production rate can be low permselectivity, high area-specific membrane resistance, high overpotentials and effect of activity coefficients. In comparison, the conventional electrolysis such as alkaline electrolysers operating at atmospheric conditions the hydrogen production rate was found to be $2 \times 10^{-4}\,\mathrm{kg\,m^{-2}s^{-1}}$ [29,30]. Therefore, an increase in the membrane resistance decreases the electrochemical potential of the stack, and thus the resulting peak power current density decreases. This decrease in current density decreases the number of hydrogen moles produced due to electrolysis of water as well. From the previous sections, it is clear that a thinner membrane can have low area-specific resistance but can be relatively less conducive, for example, FKE. On the other hand, a thicker membrane can have more resistance but can be relatively highly conductive, for example, CMF. The results signify that the membrane's thickness plays a vital role in improving the hydrogen production rate. In the thermodynamic model to calculate the peak power density produced, we consider area-specific resistance, and we emphasise ohmic resistance rather than conductivity. Therefore, a stack made of CMF/APS has a higher area-specific resistance compared to CSO/FAS and was not chosen as optimum. Furthermore, the decrease in the operating current density causes a decrease in the amount of salt transported through a membrane due to electro-migration, and decreases the amount of water dragged along due to electro-osmosis. As the salt flux decreases, the concentration of dilute solution at the outlet decreases. The decrease in the dilute solution concentration decreases the waste heat required per unit volume of dilute solution (q_{th} [$\mathrm{kWh\ m^{-3}}$]). However, the total waste heat required per kg of hydrogen produced increases as the volume of the dilute solution at reduced current densities increases due to a increased number of unit cells required to develop the potential in a stack required for electrolysis of water.

4.4. Influence of R on η and LCH

An increase in the membrane resistance decreases the thermodynamic efficiency, η, and increases the levelised cost of hydrogen (LCH) as shown in the Figure 10. For a stack made of FAS30 and CSO membranes as AEM and CEM with the least area specific resistance ($\Omega\,m^2$) for 2 M/0.1 M feed solutions concentration at room temperature, the thermochemical conversion efficiency was found to be 9.7% and the LCH was estimated to be 7.80 € $kg_{H_2}^{-1}$. The highest conductivity was found for a stack made with APS and CMF for 2 M/0.1 M feed solutions concentration. The corresponding thermodynamic efficiency and LCH estimated were 8.00% and 9.99 € $kg_{H_2}^{-1}$, respectively. The membranes with a lower resistance give a higher thermochemical conversion efficiency, lower waste heat required per kg of hydrogen and lower levelised cost of hydrogen. Thus, with an increase in membrane resistance, the thermochemical conversion efficiency decreases and the LCH increases significantly.

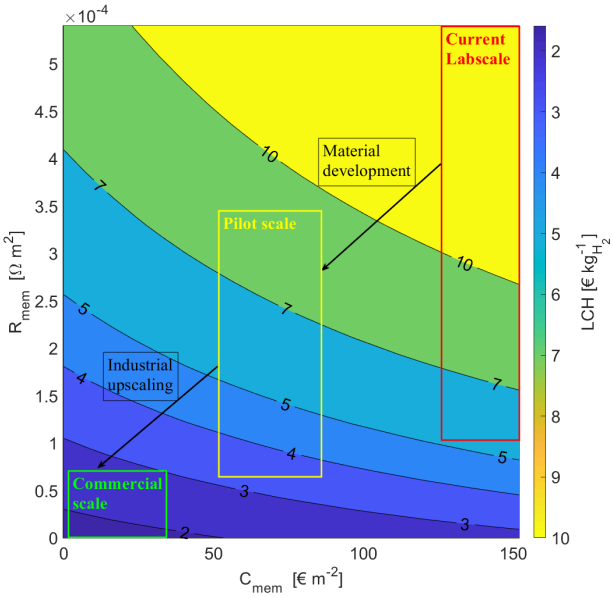

Figure 10. Levelised cost of hydrogen (LCH) as a function of membrane resistance for different membrane cost. Here, we assume the membrane resistances $R_{aem} = R_{cem}$. CSO and FAS30 permselectivities were measured and used as input. The membrane cost range assumed for lab, pilot and commercial scale is 130–150, 50–80 and less than 30 € m^{-2}, respectively. The cost of heating is assumed to be 0.005 € kWh^{-1} [26]. We assume for the pilot scale, that the material development will lead to cheaper and less resistive membranes, i.e., SPEEK or carbon-based membranes, and that for the commercial scale these membranes will be produced at large scale (60×10^8 m^2 per year) and reduced thickness (25 µm and maintaining the mechanical strength) which will in turn reduce the cost and resistance further [26,31,32].

The increase in membrane resistance decreases the performance of the cell by decreasing operating potential and peak power current density. Furthermore, with an increase in membrane resistance, the amount of heat required to restore the concentrations to original increases due to the increased amount of solution from the stack needed for same amount of hydrogen production capacity. Therefore, a decrease in efficiency can be observed. In the case of LCH, the number of membranes required increases with an increase in the membrane resistance and thus the investment cost and membrane replacement cost increases. Moreover, an increase in the volume of the outlet solutions increases the capacity of the

regeneration system, which in turn increases the cost. All these factors cause an increase in LCH.

5. Conclusions

In the present work, the membrane resistance/conductivity were estimated for membranes soaked in a ammonium bicarbonate salt solution at various concentrations and different temperatures. It was found that cation exchange membranes (CEMs) have higher conductivities than anion exchange membranes (AEM) for nearly all of the concentrations examined (0.1 M, 0.5 M, 1 M and 2 M). For use in combination with reverse electrodialysis, the highest thickness normalised conductivity was found for a stack consisting of the APS type AEM and the CMF type of CEM.

In a closed loop ammonium bicarbonate reverse electrodialysis system that uses these type of membranes in combination with waste heat to generate hydrogen, the hydrogen production rate and specific waste heat required based were estimated to be $6.51 \times 10^{-7}\,\mathrm{kg\,m^{-2}s^{-1}}$ and $413\,\mathrm{kWh\,kg_{H_2}^{-1}}$. This resulted in a thermodynamic efficiency of 8.00% and an estimated levelised cost of hydrogen of $9.99\,€\mathrm{kg_{H_2}^{-1}}$. Of the membranes examined in this work, the FAS30 type of AEM and the CSO type of CEM were found to have the smallest area specific resistance. With a closed loop reverse electrodialysis system with these membranes, the hydrogen production rate and specific waste heat required are estimated to be $8.48 \times 10^{-7}\,\mathrm{kg\,m^{-2}s^{-1}}$ and $344\,\mathrm{kWh\,kg_{H_2}^{-1}}$, respectively. This resulted in a thermodynamic efficiency of 9.7% and an estimated levelised cost of the hydrogen of $7.80\,€\,\mathrm{kg_{H_2}^{-1}}$.

Author Contributions: Conceptualisation, O.S.B. and Y.D.R.; Methodology, O.S.B. and Y.D.R.; Software, Y.D.R.; Validation, Y.D.R., O.S.B. and R.B.; Formal Analysis, Y.D.R.; Investigation, Y.D.R.; Resources, R.B. and O.S.B.; Data Curation, Y.D.R.; Writing—Original Draft Preparation, Y.D.R.; Writing—Review and Editing, R.B., O.S.B. and Ø.W.; Visualisation, Y.D.R.; Supervision, O.S.B. and H.K.; Project Administration, O.S.B.; Funding Acquisition, O.S.B. All authors have read and agreed to the published version of the manuscript.

Funding: The project is funded by the Department of Energy and Process Technology at the Norwegian University of Science and Technology under the project number 70441041.

Data Availability Statement: The data presented in this study are available in Appendix A.

Acknowledgments: This material is based upon work supported in part by the Department of Energy and Process Technology under the project number 70441041. The authors thank the research framework ENERSENSE at the Norwegian University of Science and Technology. We would also like to thank Martin Nord Flote for his help in conducting the experiments.

Conflicts of Interest: The authors declare no conflicts of interest.

Appendix A. The Regression Coefficients

Tables A1–A4 present the regression equations for the resistances as a function of membrane thickness for the anion-exchange membranes (AEMs) and cation-exchange membranes (CEMs) as described in Equation (A1). The regression equation is expressed as

$$R = a \cdot x + b \tag{A1}$$

where R is the area specific resistance of an IEM [$\Omega\,\mathrm{m^2}$], x is the thickness of the IEM [m] and a,b are the fitting parameters.

Table A1. AEMs at 298 K.

IEM	Concentration (M)	Regression (R = a· Thickness + b)
DSV	0.1	$(1.85 \pm 0.22) \times +2.26 \times 10^{-4} \pm 8.26 \times 10^{-5}$
	0.5	$(2.04 \pm 0.10) \times +2.92 \times 10^{-5} \pm 4.04 \times 10^{-5}$
	1	$(2.24 \pm 0.12) \times +2.91 \times 10^{-5} \pm 4.30 \times 10^{-5}$
	2	$(1.89 \pm 0.80) \times +1.01 \times 10^{-4} \pm 2.94 \times 10^{-4}$
AMV	0.1	$(6.94 \pm 0.2) \times +4.04 \times 10^{-4} \pm 6.79 \times 10^{-4}$
	0.5	$(7.98 \pm 1.06) \times -7.64 \times 10^{-5} \pm 4.06 \times 10^{-4}$
	1	$(6.45 \pm 0.28) \times +1.07 \times 10^{-4} \pm 3.06 \times 10^{-4}$
	2	$(5.52 \pm 0.36) \times +2.10 \times 10^{-4} \pm 2.54 \times 10^{-4}$
APS	0.1	$(3.34 \pm 0.12) \times +1.55 \times 10^{-4} \pm 1.56 \times 10^{-4}$
	0.5	$(1.52 \pm 0.12) \times +4.05 \times 10^{-5} \pm 4.68 \times 10^{-5}$
	1	$(1.50 \pm 0.12) \times +1.19 \times 10^{-6} \pm 4.82 \times 10^{-5}$
	2	$(1.10 \pm 0.14) \times +6.98 \times 10^{-5} \pm 5.70 \times 10^{-5}$
FAS30	0.1	$(3.96 \pm 2.46) \times +2.27 \times 10^{-4} \pm 2.56 \times 10^{-4}$
	0.5	$(3.01 \pm 0.52) \times +8.04 \times 10^{-5} \pm 5.32 \times 10^{-5}$
	1	$(3.54 \pm 0.66) \times +5.74 \times 10^{-5} \pm 6.70 \times 10^{-5}$
	2	$(5.29 \pm 2.04) \times +6.54 \times 10^{-5} \pm 2.06 \times 10^{-4}$
FASPET	0.1	$(8.23 \pm 2.14) \times -5.79 \times 10^{-6} \pm 6.14 \times 10^{-4}$
	0.5	$(7.81 \pm 1.74) \times +1.10 \times 10^{-5} \pm 4.98 \times 10^{-4}$
	1	$(5.69 \pm 0.28) \times +1.02 \times 10^{-6} \pm 8.14 \times 10^{-5}$
	2	$(8.45 \pm 0.90) \times -4.28 \times 10^{-5} \pm 2.76 \times 10^{-4}$

Table A2. CEMs at 298 K.

IEM	Concentration (M)	Regression (R = a· Thickness + b)
CMV	0.1	$(0.76 \pm 0.00) \times +1.09 \times 10^{-4} \pm 5.64 \times 10^{-7}$
	0.5	$(0.73 \pm 0.00) \times +5.07 \times 10^{-5} \pm 3.32 \times 10^{-6}$
	1	$(0.79 \pm 0.06) \times +4.66 \times 10^{-5} \pm 2.16 \times 10^{-5}$
	2	$(0.82 \pm 0.10) \times +4.90 \times 10^{-5} \pm 3.34 \times 10^{-5}$
CMF	0.1	$(0.43 \pm 0.02) \times +8.07 \times 10^{-5} \pm 2.44 \times 10^{-5}$
	0.5	$(0.43 \pm 0.01) \times +5.20 \times 10^{-5} \pm 1.47 \times 10^{-5}$
	1	$(0.40 \pm 0.00) \times +1.02 \times 10^{-5} \pm 4.88 \times 10^{-6}$
	2	$(0.44 \pm 0.02) \times +7.25 \times 10^{-5} \pm 3.58 \times 10^{-5}$
CSO	0.1	$(0.95 \pm 0.20) \times +2.15 \times 10^{-5} \pm 6.72 \times 10^{-5}$
	0.5	$(0.73 \pm 0.04) \times +3.81 \times 10^{-5} \pm 1.50 \times 10^{-5}$
	1	$(0.54 \pm 0.02) \times +7.02 \times 10^{-5} \pm 5.72 \times 10^{-6}$
	2	$(0.54 \pm 0.10) \times +6.18 \times 10^{-5} \pm 3.50 \times 10^{-5}$
FKE	0.1	$(2.93 \pm 0.52) \times +7.47 \times 10^{-5} \pm 4.64 \times 10^{-5}$
	0.5	$(3.36 \pm 0.32) \times +5.58 \times 10^{-5} \pm 2.80 \times 10^{-5}$
	1	$(7.02 \pm 5.06) \times +4.18 \times 10^{-5} \pm 4.46 \times 10^{-4}$
	2	$(4.45 \pm 2.76) \times +5.45 \times 10^{-4} \pm 2.32 \times 10^{-4}$
FKSPET	0.1	$(4.66 \pm 0.00) \times -1.98 \times 10^{-4} \pm 0.00$
	0.5	$(3.11 \pm 0.54) \times +7.76 \times 10^{-5} \pm 1.60 \times 10^{-4}$
	1	$(5.70 \pm 0.58) \times -2.18 \times 10^{-4} \pm 1.68 \times 10^{-4}$
	2	$(3.57 \pm 0.86) \times +1.89 \times 10^{-4} \pm 2.52 \times 10^{-4}$

Table A3. AEMs at 313 K.

IEM	Concentration (M)	Regression (R = a· Thickness + b)
DSV	0.1	$(1.10 \pm 0.06) \times +1.15 \times 10^{-4} \pm 2.36 \times 10^{-5}$
	0.5	$(1.00 \pm 0.06) \times +9.51 \times 10^{-5} \pm 2.04 \times 10^{-5}$
	1	$(1.14 \pm 0.20) \times +9.04 \times 10^{-5} \pm 7.68 \times 10^{-5}$
	2	$(1.05 \pm 0.14) \times +8.30 \times 10^{-5} \pm 5.64 \times 10^{-5}$
AMV	0.1	$(3.85 \pm 1.12) \times +6.46 \times 10^{-4} \pm 3.98 \times 10^{-4}$
	0.5	$(5.34 \pm 1.06) \times -1.33 \times 10^{-5} \pm 3.24 \times 10^{-4}$
	1	$(4.79 \pm 0.86) \times -1.52 \times 10^{-4} \pm 3.06 \times 10^{-4}$
	2	$(3.69 \pm 0.72) \times -3.94 \times 10^{-4} \pm 2.54 \times 10^{-4}$,
APS	0.1	$(3.75 \pm 0.06) \times +1.30 \times 10^{-4} \pm 1.80 \times 10^{-5}$
	0.5	$(1.15 \pm 0.02) \times +7.86 \times 10^{-5} \pm 8.68 \times 10^{-6}$
	1	$(1.15 \pm 0.16) \times +3.79 \times 10^{-5} \pm 6.12 \times 10^{-5}$
	2	$(0.86 \pm 0.08) \times +8.04 \times 10^{-5} \pm 2.86 \times 10^{-5}$
FAS30	0.1	$(1.28 \pm 0.04) \times +1.28 \times 10^{-4} \pm 3.40 \times 10^{-6}$
	0.5	$(1.21 \pm 0.22) \times +1.65 \times 10^{-4} \pm 2.24 \times 10^{-5}$
	1	$(1.44 \pm 0.34) \times +7.11 \times 10^{-5} \pm 3.70 \times 10^{-5}$
	2	$(1.74 \pm 0.06) \times +1.10 \times 10^{-4} \pm 6.82 \times 10^{-6}$
FASPET	0.1	$(4.01 \pm 0.18) \times -2.56 \times 10^{-5} \pm 5.10 \times 10^{-5}$
	0.5	$(3.29 \pm 0.52) \times +1.49 \times 10^{-4} \pm 1.50 \times 10^{-4}$
	1	$(2.99 \pm 1.62) \times +2.05 \times 10^{-4} \pm 4.78 \times 10^{-4}$
	2	$(3.75 \pm 1.06) \times -1.24 \times 10^{-4} \pm 3.12 \times 10^{-4}$

Table A4. CEMs at 313 K.

IEM	Concentration (M)	Regression (R = a· Thickness + b)
CMV	0.1	$(0.57 \pm 0.04) \times +1.20 \times 10^{-4} \pm 1.07 \times 10^{-5}$
	0.5	$(0.47 \pm 0.02) \times +1.13 \times 10^{-4} \pm 6.84 \times 10^{-6}$
	1	$(0.48 \pm 0.02) \times +1.06 \times 10^{-4} \pm 8.76 \times 10^{-6}$
	2	$(0.48 \pm 0.04) \times +1.02 \times 10^{-4} \pm 1.09 \times 10^{-5}$
CMF	0.1	$(0.14 \pm 0.00) \times +1.23 \times 10^{-4} \pm 1.03 \times 10^{-5}$
	0.5	$(0.34 \pm 0.04) \times +8.09 \times 10^{-5} \pm 4.20 \times 10^{-5}$
	1	$(0.33 \pm 0.04) \times +7.76 \times 10^{-5} \pm 6.42 \times 10^{-5}$
	2	$(0.35 \pm 0.02) \times +8.92 \times 10^{-5} \pm 2.66 \times 10^{-5}$
CSO	0.1	$(0.43 \pm 0.02) \times +1.27 \times 10^{-4} \pm 4.97 \times 10^{-6}$
	0.5	$(0.33 \pm 0.04) \times +1.08 \times 10^{-4} \pm 1.23 \times 10^{-5}$
	1	$(0.34 \pm 0.00) \times +9.98 \times 10^{-5} \pm 2.04 \times 10^{-6}$
	2	$(0.32 \pm 0.06) \times +1.14 \times 10^{-4} \pm 1.71 \times 10^{-5}$
FKE	0.1	$(1.72 \pm 0.94) \times +1.34 \times 10^{-4} \pm 8.64 \times 10^{-5}$
	0.5	$(1.71 \pm 0.88) \times +1.34 \times 10^{-4} \pm 7.44 \times 10^{-5}$
	1	$(4.47 \pm 0.14) \times +4.30 \times 10^{-5} \pm 1.26 \times 10^{-5}$
	2	$(3.51 \pm 0.60) \times +9.97 \times 10^{-5} \pm 5.26 \times 10^{-5}$
FKSPET	0.1	$(0.79 \pm 0.44) \times -2.03 \times 10^{-4} \pm 4.84 \times 10^{-5}$
	0.5	$(2.27 \pm 0.46) \times -3.25 \times 10^{-5} \pm 1.32 \times 10^{-4}$
	1	$(1.60 \pm 0.34) \times +6.02 \times 10^{-5} \pm 9.74 \times 10^{-5}$
	2	$(3.79 \pm 0.04) \times -2.85 \times 10^{-4} \pm 1.05 \times 10^{-5}$

Table A5. Mean IEM conductivities [Sm^{-1}] at 298 K.

IEM at 298 K	Concentration [M] 0.10	0.50	1.00	2.00
AMV	0.14	0.13	0.16	0.18
APS	0.30	0.61	0.67	0.87
FAS	0.25	0.33	0.28	0.19
FASPET	0.16	0.16	0.18	0.16
DSV	0.54	0.49	0.45	0.53
CMF	2.31	3.01	2.48	2.26
CMV	1.31	1.37	1.27	1.21
CSO	1.06	1.38	1.85	1.84
FKE	0.34	0.30	0.14	0.22
FKSPET	0.24	0.32	0.18	0.28

Table A6. Mean IEM conductivities [Sm^{-1}] at 313 K.

IEM at 313 K	Concentration [M] 0.10	0.50	1.00	2.00
AMV	0.26	0.23	0.21	0.27
APS	0.24	0.76	1.14	1.25
FAS	0.78	0.83	0.69	0.57
FASPET	0.25	0.30	0.33	0.27
DSV	0.91	1.00	0.88	0.95
CMF	7.23	2.98	3.05	2.82
CMV	1.75	2.11	2.09	2.09
CSO	2.33	2.99	2.93	3.12
FKE	0.58	0.59	0.22	0.29
FKSPET	0.45	0.44	0.62	0.26

References

1. Burheim, O. *Engineering Energy Storage*; Academic Press: Cambridge, MA, USA, 2017.
2. Giacalone, F.; Vassallo, F.; Griffin, L.; Ferrari, M.C.; Micale, G.; Scargiali, F.; Tamburini, A.; Cipollina, A. Thermolytic reverse electrodialysis heat engine: model development, integration and performance analysis. *Energy Convers. Manag.* **2019**, *189*, 1–13. [CrossRef]
3. Luo, Y.; Guo, J.; Wang, C.; Chu, D. Fuel cell durability enhancement by crosslinking alkaline anion exchange membrane electrolyte. *Electrochem. Commun.* **2012**, *16*, 65–68. [CrossRef]
4. Nam, J.Y.; Cusick, R.D.; Kim, Y.; Logan, B.E. Hydrogen generation in microbial reverse-electrodialysis electrolysis cells using a heat-regenerated salt solution. *Environ. Sci. Technol.* **2012**, *46*, 5240–5246. [CrossRef]
5. Kwon, K.; Park, B.H.; Kim, D.H.; Kim, D. Parametric study of reverse electrodialysis using ammonium bicarbonate solution for low-grade waste heat recovery. *Energy Convers. Manag.* **2015**, *103*, 104–110. [CrossRef]
6. Cusick, R.D.; Kim, Y.; Logan, B.E. Energy Capture fromThermolytic Solutions in Microbial Reverse-Electrodialysis Cells. *Science* **2012**, *335*, 1474–1478. [CrossRef]
7. Logan, B.E.; Elimelech, M. Membrane-based processes for sustainable power generation using water. *Nature* **2012**, *488*, 313–319. [CrossRef] [PubMed]
8. Micari, M.; Cipollina, A.; Giacalone, F.; Kosmadakis, G.; Papapetrou, M.; Zaragoza, G.; Micale, G.; Tamburini, A. Towards the first proof of the concept of a Reverse ElectroDialysis—Membrane Distillation Heat Engine. *Desalination* **2019**, *453*, 77–88. [CrossRef]
9. Kwon, K.; Park, B.H.; Kim, D.H.; Kim, D. Comparison of spacer-less and spacer-filled reverse electrodialysis. *J. Renew. Sustain. Energy* **2017**, *9*, 044502. [CrossRef]
10. Bevacqua, M.; Tamburini, A.; Papapetrou, M.; Cipollina, A.; Micale, G.; Piacentino, A. Reverse electrodialysis with NH4HCO3-water systems for heat-to-power conversion. *Energy* **2017**, *137*, 1293–1307. [CrossRef]
11. Güler, E.; Elizen, R.; Vermaas, D.a.; Saakes, M.; Nijmeijer, K. Performance-determining membrane properties in reverse electrodialysis. *J. Membr. Sci.* **2013**, *446*, 266–276. [CrossRef]
12. Galama, A.H.; Hoog, N.A.; Yntema, D.R. Method for determining ion exchange membrane resistance for electrodialysis systems. *Desalination* **2016**, *380*, 1–11. [CrossRef]
13. Geise, G.M.; Hickner, M.A.; Logan, B.E. Ammonium Bicorbonate Transport in anion exchange membranes for salinity gradient energy. *ACS Macro Lett.* **2013**, *2*, 814–817. [CrossRef]
14. Hong, J.G.; Zhang, B.; Glabman, S.; Uzal, N.; Dou, X.; Zhang, H.; Wei, X.; Chen, Y. Potential ion exchange membranes and system performance in reverse electrodialysis for power generation: A review. *J. Membr. Sci.* **2015**, *486*, 71–88. [CrossRef]

15. Geise, G.M.; Hickner, M.A.; Logan, B.E. Ionic resistance and permselectivity tradeoffs in anion exchange membranes. *ACS Appl. Mater. Interfaces* **2013**, *5*, 10294–10301. [CrossRef]
16. Kamcev, J.; Sujanani, R.; Jang, E.S.; Yan, N.; Moe, N.; Paul, D.R.; Freeman, B.D. Salt concentration dependence of ionic conductivity in ion exchange membranes. *J. Membr. Sci.* **2018**, *547*, 123–133. [CrossRef]
17. Nikonenko, V.V.; Kozmai, A.E. Electrical equivalent circuit of an ion-exchange membrane system. *Electrochim. Acta* **2011**, *56*, 1262–1269. [CrossRef]
18. Park, J.S.; Choi, J.H.; Woo, J.J.; Moon, S.H. An electrical impedance spectroscopic (EIS) study on transport characteristics of ion-exchange membrane systems. *J. Colloid Interface Sci.* **2006**, *300*, 655–662. [CrossRef]
19. Długołęcki, P.; Ogonowski, P.; Metz, S.J.; Saakes, M.; Nijmeijer, K.; Wessling, M. On the resistances of membrane, diffusion boundary layer and double layer in ion exchange membrane transport. *J. Membr. Sci.* **2010**, *349*, 369–379. [CrossRef]
20. Zhang, W.; Ma, J.; Wang, P.; Wang, Z.; Shi, F.; Liu, H. Investigations on the interfacial capacitance and the diffusion boundary layer thickness of ion exchange membrane using electrochemical impedance spectroscopy. *J. Membr. Sci.* **2016**, *502*, 37–47. [CrossRef]
21. Tufa, R.A.; Pawlowski, S.; Veerman, J.; Bouzek, K.; Fontananova, E.; di Profio, G.; Velizarov, S.; Goulão Crespo, J.; Nijmeijer, K.; Curcio, E. Progress and prospects in reverse electrodialysis for salinity gradient energy conversion and storage. *Appl. Energy* **2018**, *225*, 290–331. [CrossRef]
22. Galama, A.H.; Vermaas, D.A.; Veerman, J.; Saakes, M.; Rijnaarts, H.H.; Post, J.W.; Nijmeijer, K. Membrane resistance: The effect of salinity gradients over a cation exchange membrane. *J. Membr. Sci.* **2014**, *467*, 279–291. [CrossRef]
23. Veerman, J.; Saakes, M.; Metz, S.J.; Harmsen, G.J. Reverse electrodialysis: Performance of a stack with 50 cells on the mixing of sea and river water. *J. Membr. Sci.* **2009**, *327*, 136–144. [CrossRef]
24. Kim, K.S.; Ryoo, W.; Chun, M.S.; Chung, G.Y. Simulation of enhanced power generation by reverse electrodialysis stack module in serial configuration. *Desalination* **2013**, *318*, 79–87. [CrossRef]
25. Mei, Y.; Tang, C.Y. Recent developments and future perspectives of reverse electrodialysis technology: A review. *Desalination* **2017**, *425*, 156–174. [CrossRef]
26. Raka, Y.D.; Karoliussen, H.; Lien, K.M.; Odne Stokke Burheim. Opportunities and challenges for thermally driven hydrogen production using reverse electrodialysis system. *Int. J. Hydrog. Energy* **2020**, *5*, 1212–1225. [CrossRef]
27. Nazemi, M.; Zhang, J.; Hatzell, M.C. Harvesting Natural Salinity Gradient Energy for Hydrogen Production Through Reverse Electrodialysis Power Generation. *J. Electrochem. Energy Convers. Storage* **2017**, *14*, 020702 [CrossRef]
28. Chen, X.; Jiang, C.; Zhang, Y.; Wang, Y.; Xu, T. Storable hydrogen production by Reverse Electro-Electrodialysis (REED). *J. Membr. Sci.* **2017**, *544*, 397–405. [CrossRef]
29. Millet, P.; Grigoriev, S. Water Electrolysis Technologies. In *Renewable Hydrogen Technologies: Production, Purification, Storage, Applications and Safety*; Elsevier Science: Amsterdam, The Netherlands, 2013; pp. 19–41.
30. Buttler, A.; Spliethoff, H. Current status of water electrolysis for energy storage, grid balancing and sector coupling via power-to-gas and power-to-liquids: A review. *Renew. Sustain. Energy Rev.* **2018**, *82*, 2440–2454. [CrossRef]
31. Minke, C.; Turek, T. Economics of vanadium redox flow battery membranes. *J. Power Sources* **2015**, *286*, 247–257. [CrossRef]
32. Krakhella, K.W.; Morales, M.; Bock, R.; Seland, F.; Burheim, O.S.; Einarsrud, K.E. Electrodialytic energy storage system: Permselectivity, stack measurements and life-cycle analysis. *Energies* **2020**, *13*, 1247. [CrossRef]

Permselectivity of Ion Exchange Membranes for ammonium bicarbonate - influence of junction potentials and reference electrodes

Yash Dharmendra Raka, Simon Birger Byremo Solberg, Robert Bock, Øivind Wilhelmsen, Håvard Karoliussen, Odne Stokke Burheim*

[a] *Norwegian University of Science and Technology, Department of Energy and Process Engineering, Kolbjørn Hejes vei 1B, NO-7491 Trondheim, Norway*
[b] *SINTEF Energy Research, NO-7465 Trondheim, Norway*

Abstract

The open circuit potential of a reverse electrodialysis cell depends mainly on the membrane permselectivity of the anion and cation exchange membranes and the concentration gradient. The membrane permselectivity, α, is the ability of the material to selectively permeate counter-ions and to exclude co-ions through the membrane. In this article we investigate the influence of the concentration of ammonium bicarbonate on the α-value of cation and anion exchange membranes. We determine the permselectivity of the cation exchange membrane of type CSO and anion exchange membrane of type FAS30 for the concentrations 0.5 M/0.1 M, 1 M/0.1 M and 2 M/0.1 M and find that the permselectivity of the membranes decreases with increasing concentration. The α-value of the cation exchange membrane, CSO was higher compared to the anion exchange membrane, FAS30. The junction potentials influence the open circuit membrane potential measurements. We propose a method to reduce the influence of junction potential by introducing salt bridges. We find that the concentration of ammonium bicarbonate solutions in the salt bridge influences the junction potential measurements, but without any clear trend. To gauge the role of the permselectivities in the use of reverse electrodialysis for production of hydrogen by use of waste heat, we use a thermodynamic and an economic model to study the impact on the hydrogen production rate, waste heat required, thermochemical conversion efficiency and the levelised cost of hydrogen. The models show that an increase in permselectivity increases the hydrogen production rate and the thermochemical conversion efficiency. It also decreases the heat required per kg of hydrogen to restore the concentrations of the effluent solutions to original and reduce the levelised cost of hydrogen. The estimated values for hydrogen production rate, thermodynamic efficiency, specific waste heat and the levelised cost of hydrogen are $8.05{\cdot}10^{-7}\,\mathrm{kg\,m^{-2}s^{-1}}$, 9.1%, $365.87\,\mathrm{kWh\,kg_{H_2}^{-1}}$, $10.132\,€\,\mathrm{kg^{-1}}$ H_2 respectively.

Keywords: Reverse electrodialysis (RED), permselectivity, membrane resistance, membrane conductivity, ion exchange membrane, hydrogen production, ammonium bicarbonate, low grade waste heat to hydrogen.